Detection and Channel Estimation for Channels with Heavy Interference

---

A DISSERTATION

SUBMITTED TO THE FACULTY OF THE GRADUATE SCHOOL

OF THE UNIVERSITY OF MINNESOTA

BY

Daejung Yoon

IN PARTIAL FULFILLMENT OF THE REQUIREMENTS

FOR THE DEGREE OF

DOCTOR OF PHILOSOPHY

Professor Jaekyun Moon, Advisor

October, 2011

Acknowledgements

This thesis is by far the most significant accomplishment in my life, and it would not have been impossible without people who supported me and believed in me. Most of all I would like to express my sincere gratitude to my advisor, Professor Jaekyun Moon, for his professional advice and guidance throughout my studies at University of Minnesota at Minneapolis. The experiences in the Communication and Data Storage Laboratory (CDS) under Professor Jaekyun Moon are the most valuable times in my career and life.

I would like to be very grateful to my lovely wife, Rami, and lovely daughter, Haejin, for their endless patience and great devotion. Without their patience and sacrifice, I could have never made this. Finally, I cannot complete these acknowledgements without expressing how appreciative I am of all the love and affection that my parents have provided throughout my life. This thesis is dedicated to them.

I also express my sincere gratitude to Prof. Zhi-Quan (Tom) Luo, Prof. Emad S. Ebbini from the Department of Electrical and Computer Engineering and Prof. Tian He from the Department of Computer Science and Engineering for serving as the committee members in my final oral exam. I wish to thanks my friends, Jihoon, Hakim, Jaewook and Seongwook in the CDS lab for helpful discussions and exchanging many ideas.

To my parents, wife Rami and a little angel Haejin

Abstract

Iterative decision-directed (DD) channel estimation (CE) and detection algorithms for multiple-input multiple-output (MIMO) orthogonal frequency division multiplexing (OFDM) systems are investigated. A main strength of the MIMO-OFDM is a potential capability to support high data rates. However, interference between MIMO antennas has been a serious obstacle to high data rate communication. Accurate channel state information (CSI) is critical to reduce antenna interference and improve throughput performance of the MIMO-OFDM communication systems. First, we develop soft-decision-driven sequential CE algorithms specific to turbo equalization for the MIMO communication. Two kinds of channel estimators are proposed: an optimal Kalman-based channel estimator geared to the pipelined turbo equalizer and a low-complexity estimator design for practical implementation. An effective strategy is established for the channel estimators dealing with different qualities of feedback decisions from the turbo equalizer. The proposed CE algorithms employ puncturing on observation samples to effectively deal with the inherent correlated error input that cannot easily be removed by the traditional innovations approach. Performance of the optimal estimator is excellent at compensating loss due to imperfect CSI; however, computational complexity of the MIMO CE becomes a challenge as the number of MIMO antenna links increases in practical systems. The proposed low-complexity algorithm resolves the MIMO channel estimation problem into a single-input single-output CE form to avoid heavy computation load associated with matrix operations. Also, in order to reduce packet losses due to the inherent correlated error, a novel packet recovery scheme is introduced that reprocesses failed packets by innovating on the inaccurate CSI. The recovery scheme detects erroneous OFDM-symbol locations by comparing extrinsic (EXT) information from the turbo equalizer. For the error correction, it applies additional turbo iterations to the erroneous OFDM symbols with the innovated CSI. In demonstrating the viability of the proposed schemes, a MIMO-OFDM communication system is constructed to comply with the IEEE 802.11n WLAN standard.

Contents

Acknowledgments **i**

Abstract **iii**

List of Tables **vii**

List of Figures **viii**

Acronyms **xi**

1 Introduction **1**

1.1 Motivation 1

1.2 Thesis Outline 4

2 Introduction to the MIMO-OFDM systems **7**

2.1 Turbo receiver for the SM-MIMO-OFDM communication system 7

2.2 MIMO channel interference due to the channel estimation error 10

3 Soft-Decision-Driven Channel Estimation for Pipelined Turbo Receivers **13**

3.1 Overview 13

3.2 Channel and System Model 14

3.3 Sequential and Soft-Decision-Directed Channel Estimation 18

3.3.1 Initial Channel Estimation Based on Training Symbols 18

3.3.2 Derivation of the Kalman-Based Sequential Channel Estimation Algorithm . . . 19
3.3.3 Kalman-Based Sequential Channel Estimation Algorithm with Punctured Innovation Sequence . . . 25
3.3.4 Noise Variance Update for the Soft Detectors . . . 28
3.4 Mean Squared Error (MSE) Analysis . . . 30
3.5 Performance Evaluation . . . 39
3.5.1 EXIT and PER Performance Comparisons . . . 39
3.6 Discussions . . . 47

4 Low-Complexity Iterative Channel Estimation for Turbo Receivers 48
4.1 Overview . . . 48
4.2 Low-Complexity Kalman-Based Channel Estimation . . . 49
4.2.1 Linear Successive Interference Cancellation Based on Soft Decisions 49
4.2.2 Soft-Decision-Directed Kalman Channel Estimator . . . 53
4.3 Performance evaluation . . . 57
4.3.1 Complexity Comparison with Existing Channel Estimators . . . 57
4.3.2 PER Simulation Results . . . 60
4.4 Discussions . . . 62

5 Packet Recovery Algorithm using Turbo Equalization 64
5.1 Overview . . . 64
5.2 System Model . . . 65
5.3 Packet Recovery Algorithm . . . 70
5.3.1 Erroneous OFDM symbol detection . . . 70
5.3.2 Error Recovery Scheme with IDD . . . 72
5.4 Analysis on soft-symbol distance . . . 75
5.5 Performance Evaluation . . . 80

5.6 Discussions 84

6 Conclusion and Future Work **87**

6.1 Concluding Remarks 87

6.2 Future Research Directions 90

6.2.1 Detection algorithm to prevent error propagation 90

6.2.2 Packet recovery algorithm using an inner ECC 91

Bibliography **93**

List of Tables

3.1 Complexity comparison : the number of multipliers used in the proposed Kalman-based CE, Song's CE and the EM-DD CE 47

4.1 Complexity comparison ; the number of a multiplier used in the proposed low-complexity CE, the optimal Kalman-based CE and EM-based CE. . . . 58

List of Figures

2.1 MIMO communication system 8
2.2 IEEE 802.11n transmitter block diagram 9
2.3 MIMO-OFDM turbo receiver block diagram 11

3.1 Block diagram of the turbo receiver and the soft-decision-directed channel estimator 15
3.2 OFDM-symbol processing procedure in the pipelined IDD 16
3.3 Block diagram of the proposed optimum channel estimation algorithm geared to the pipelined IDD 17
3.4 Correlations in the 'innovation' sequence: (a) $E[\mathbf{x}_{n-2}\mathbf{x}_n^H]$ (b) $E[\mathbf{y}_{n-2}\mathbf{y}_n^H]$, $c = 0.8$ (normalized by $E[|y_n[0]|^2]$, averaging 50 erroneous packets) 22
3.5 Threshold parameter c optimization for the optimal Kalman-based channel estimator 34
3.6 Open-loop channel estimation MSE for different values of σ_s^2 ($N_d = 12$) . . 37
3.7 Open-loop channel estimation MSE depending on different values of N_d ($\sigma_s^2 = 0.1$) 38
3.8 EXIT chart analysis on the proposed Kalman-based CE and conventional CEs in the 2×2 SM-MIMO-OFDM turbo receiver 40
3.9 PER simulations of the proposed Kalman-based CE and conventional CEs in the 2x2 SM-MIMO-OFDM system(7 iterations) 42

3.10 PER simulations of the proposed Kalman-based CE and conventional CEs in the 3x3 SM-MIMO-OFDM system(9 iterations) 44
3.11 PER simulations of the proposed Kalman-based CE and conventional CEs in the 4x4 SM-MIMO-OFDM system (9 iterations) 45
3.12 Complexity comparison : the number of multipliers used in the proposed Kalman-based CE, Song's CE and the EM-DD CE 46

4.1 Block diagram of the turbo receiver and the soft-decision-directed channel estimator 50
4.2 OFDM-symbol processing procedure in IDD 52
4.3 Threshold parameter c optimization for the low-complexity Kalman-based channel estimator 56
4.4 Complexity comparison ; the number of a multiplier used in the proposed low-complexity CE, the optimal Kalman-based CE and EM-based CE.($N_r = 4, N_b = 4$) 59
4.5 PER simulations of the low-complexity CE and the conventional CEs in the 3×3 SM-MIMO-OFDM turbo receiver (7 iterations, $c = 2$) 61
4.6 PER simulations of the low-complexity CE and the conventional CEs in the 4×4 SM-MIMO-OFDM turbo receiver (9 iterations, $c = 2.5$) 63

5.1 Turbo equalizer block diagram with the error monitoring scheme 66
5.2 Block diagram of the packet recovery process 68
5.3 Packet processing timing diagram with the packet recovery 69
5.4 16QAM constellation of soft symbols in error packets (a) SISO demapper EXT in (b) SISO decoder EXT 81
5.5 MSE analysis : channel estimate quality depending on min and max D_n . . 82
5.6 Histogram of the number of error OFDM-symbols in invalid packets (a) IDD without the recovery algorithm (b) IDD using the recovery algorithm . 83

5.7 PER simulation with the recovery algorithm in the 2×2 MIMO-OFDM . . 85

6.1 Conception diagram of error propagation problem in decision feedback estimation manners 91

Acronyms

AWGN	Additive White Gaussian Noise
BICM	Bit-Interleaved Coded Modulation
CE	Channel Estimation
CRC	Cyclic Redundancy Code
CSD	Cyclic Shift Delay
CSI	Channel State Information
DD	Decision-Directed
DFT	Discrete Fourier Transform
DFT	Fast Fourier Transform
ECC	Error Control Code
ELLR	Extrinsic Log Likelihood Ratio
EM	Expectation Maximization
EXIT	Extrinsic Information Transfer
EXT	Extrinsic
HT-LTF	High Throughput Long Training Field
IDD	Iterative Detection and Decoding
ISI	Inter-Symbol Interference
LDPC	Low Density Parity Check
LLR	Log Likelihood Ratio
LMMSE	Linear Minimum Mean Squared Error
LS	Least Square

MAP	Maximum A posteriori Probability
MI	Mutual Information
MIMO	Multiple Input Multiple Output
MISO	Multiple Input Single Output
ML	Maximum Likelihood
MMSE	Minimum Mean Squared Error
M-QAM	M-ary Quadrature Amplitude Modulation
MSE	Mean Squared Error
OFDM	Orthogonal Frequency Division Multiplexing
PD	Perfect decision
PDF	Probability Density Function
PER	Packet Error Rate
PHY	Physical
PSD	Power Spectrum Density
RX	Receiver
SIC	Successive Interference Cancellation
SISO	Soft In Soft Out
SM	Spatial Multiplexing
SNR	Signal to Noise Ratio
SOVA	Soft output Viterbi Algorithm
TX	Transmitter
WLAN	Wireless Local Area Network
ZF	Zero Forcing

Chapter 1

Introduction

1.1 Motivation

Combining the multiple-input multiple-output (MIMO) antenna method with orthogonal frequency division multiplexing (OFDM) and spatial multiplexing is a well-established wireless communication technique. Bit-interleaved coded modulation (BICM) [1] used in conjunction with MIMO-OFDM and spatial multiplexing (SM) is particularly effective in exploring both spatial diversity and frequency selectivity without significant design efforts on specialized codes [2, 3]. Turbo equalization [4], also known as iterative detection and decoding (IDD) in wireless applications [5], is well-suited for BICM-MIMO-OFDM for high data rate transmission with impressive performance potentials [5, 6].

A critical issue in realizing the full performance potential of a MIMO-OFDM system is significant performance degradation due to imperfect channel state information (CSI). The detrimental impact of imperfect CSI on MIMO detection is well known [7,8] and continues to be a great challenge in wireless communication system design. Previous works have identified desirable training patterns or pilot tones for estimating channel responses for MIMO systems [9–13]. However, with these methods the achievable data rate is inevitably reduced, especially when the number of channel parameters to be estimated increases (e.g.,

caused by an increased number of antennas).

Decision-directed (DD) channel estimation algorithms can be applied to turbo receivers to improve channel estimation accuracy [14–17]. However, inaccurate feedback decisions degrade the estimation performance [5]. Maximum-a-posteriori (MAP)-based DD algorithms discussed in [14, 15] can improve the estimation accuracy, but they require additional information such as the channel probability density function. The DD iterative channel estimation algorithms with IDD been actively researched [19–23]. Among the existing research works, several papers have been devoted to iterative expectation maximization (EM) channel estimation algorithms using extrinsic or a posteriori information fed back from the outer decoder [19–21]. Although the traditional EM-based estimation algorithms typically have outstanding performance, the heavy computation load and iteration latency can be problematic for many practical applications. While an approximation scheme as discussed in [20] can reduce complexity, the performance of these approaches degrade as the number of antennas increases [19]. Also, the EM estimation algorithms need to be aided by pilot-based EM algorithms to guarantee good performance [20, 21].

As an alternative approach to iterative EM channel estimation, Kalman-based channel estimators have been developed that are effective against error propagation [22, 23]. The authors of [22, 23] have introduced a soft-input channel estimator that adaptively updates the channel estimates based on feedback decision quality. The decision quality is important for the decision-directed estimation due to error propagation. The soft-input channel estimator of [22] evaluates the feedback decision quality by tracking the noise variance associated with the soft-decision error in efforts to realize a robust updating process for the Kalman-filter.

The conventional iterative channel estimation designs are typically employed based on the EM or the Kalman-filter theories [20, 22]. However, their practical applications combined with the IDD scheme may not maintain their optimal performance. In fact, because the inherent correlated error exists among successive feedback IDD decisions, assumptions

in the construction of the optimal estimators may not hold in practical applications.

The first objective of our research is development of a robust iterative channel estimation algorithm that deals with the inherent correlated error in the channel estimator input. In order for the channel estimators to function as optimal algorithms, correlated error mixed in the estimator input must be suppressed. Practically, we propose an innovation scheme that can puncture out such problematic inputs by monitoring the error correlation. Secondly, we have interest in a low-complexity design of the Kalman-based MIMO channel estimator maintaining its optimality. A high computation requirement of the conventional MIMO channel estimators usually becomes a major issue when attempting circuit implementation. Moreover, the implementation of the MIMO channel estimator becomes more challenging as the number of wireless antenna links increases. This research proposes a solution of the low-complexity design when the number of the MIMO channel links increases.

The last objective of our research is to invent a packet recovery algorithm that recovers from loss of packets due to error propagation. When a packet transmission fails, the transmitter attempts to retransmit the same packet, which degrades the transmission throughput. Accordingly, the transmitter needs to reduce the number of retransmissions by exploiting stronger transmitting schemes such as strong ECC or QAM techniques [38–40]. However, those approaches also sacrifice important communication resources such as power and data rate. So, if the error recovery is performed without any redundant parity information, it can help to reduce the number of packet retransmission without network overload. Based on the statistic analysis of error propagation, our goal is to design a packet recovery algorithm using the turbo equalizer that corrects the major error upon completing the default receiving processes.

1.2 Thesis Outline

The introduction to MIMO-OFDM systems is presented in Chapter 2. For practical application, the SM-MIMO-OFDM system is constructed to comply with the packet structure and the channel tone allocations of the IEEE 802.11n high speed WLAN standard [27]. The basic transmitter blocks are explained in this chapter. Based on the given transmitter, the MIMO turbo receiver is implemented. Fundamental issues of the MIMO turbo receiver are also discussed in Chapter 2.

An optimal Kalman-based channel estimator geared to a pipelined turbo equalizer architecture is developed in Chapter 3. The proposed algorithm performs iterative channel estimation using soft-decisions feedback from the pipelined IDD. The resulting algorithm is essentially is a Kalman-based linear sequential estimation algorithm, however the main feature is that the proposed algorithm employs puncturing on observation samples to effectively deal with the inherent correlation among the multiple demapper/decoder module outputs that cannot easily be removed by the traditional innovations approach. Specifically, the proposed channel estimator is designed for the pipelined turbo equalizer receiver architecture. A critical issue in the original turbo receiver design is long processing latency due to inherent iterative processing of information. The pipelined architecture is adopted to reduce the latency and improve processing throughput in turbo receivers as a result it is the prevailing approach to implementation architecture [24, 26]. One interesting feature of the pipelined turbo equalizer is that multiple sets of soft-decisions become available at various processing stages. One difficulty is that these multiple decisions from different pipeline stages have varying levels of reliability as well as correlated error. Therefore, a special optimization strategy is required for monitoring and filtering out poor decisions. We propose a method which weights the estimated channel responses according to the reliability level of the multiple decisions.

In Chapter 4, we focus on a low-complexity algorithm for the Kalman-based MIMO channel estimation. The proposed estimator relies on soft-feedback-decision-based cance-

lation of interferences from adjacent antennas, just as in [35]. Our focus in this research is low-complexity MIMO channel estimation that can handle varying amounts of interference depending on the decision and channel estimate quality. Setting up a Kalman-based estimator requires care, as the residual interference after cancellation contains correlated error as well as the varying amounts of interference. The proposed estimator continuously monitors the level of potential residual interference by assessing the quality of the soft decisions and channel estimates utilized in SIC; if the selected soft decision is deemed unreliable, then an appropriate penalty is applied to it by temporarily raising the variance of the noise-plus-interference signal in the Kalman-based channel estimation process. In addition, to address the inherent correlation that exists between successive inputs to the channel estimator, we adopt the refined innovation method of [33, 34] via irregular puncturing of the channel estimator input sequence. We discuss the trade-off between complexity and performance loss and show that the proposed channel estimation algorithm can dramatically reduce computational loads while maintaining robust receiving performances.

Finally, in Chapter 5, we consider a reprocessing algorithm to recover broken packets. A packet recovery scheme is developed utilizing turbo equalization which does not cause significant reprocessing latency nor reduce the data rate. Error detection and correction are performed utilizing bit-reliability information from turbo equalization. Suspected errors among received OFDM symbols are detected and flagged by comparing extrinsic (EXT) information from the soft detector and the soft decoder. Once a packet is declared failed by a cyclic redundancy code (CRC) check, additional IDD iterations are applied to the flagged OFDM symbols. Once the feedback decisions have significant error, error propagation cannot be avoided in the DD estimation process. A root cause of the error propagation involves correlated errors circulating between IDD blocks and a channel estimator. The error recovery scheme utilizes a whitening filter to prevent this correlated error circulation. Also, the channel estimates in the recovery mode are provided from a buffer that captures the most reliable channel estimates updated over a packet. Accordingly, error recovery can

be performed by the additional IDD iterations using enhanced CSI.

To demonstrate the benefits of the proposed schemes, we compare the receiving performance of the proposed channel estimator to conventional iterative channel estimators such as the Kalman-based estimators and the EM-based estimator. To evaluate performance, the packet error rate (PER) of the proposed and compared channel estimation algorithms is compared. Also, mean-squared-error (MSE) and extrinsic information transfer (EXIT) charts analysis are performed, validating the improved estimation performance of the proposed scheme.

Chapter 2

Introduction to the MIMO-OFDM systems

2.1 Turbo receiver for the SM-MIMO-OFDM communication system

The MIMO technologies have attracted attention in wireless communications, because they offer significant increases in data throughput without additional bandwidth or transmit power. The MIMO communication system yields a substantial improvement in the throughput performance by transmitting information through multiple parallel channels. Fig.2.1 shows an MIMO communication system between N_t transmitter (TX) antennas and N_r receiver (RX) antennas. The MIMO communication is an important part of modern wireless communication standards such as WiFi, Long Term Evolution, WiMAX systems. For a basic system of our channel estimation researches, we adopt the transmitter of the IEEE 802.11n which fully supports SM-MIMO-OFDM techniques [27]. The basic block diagram of the SM-MIMO-OFDM transmitter described in the IEEE 802.11n specifications is illustrated in Fig.2.2.

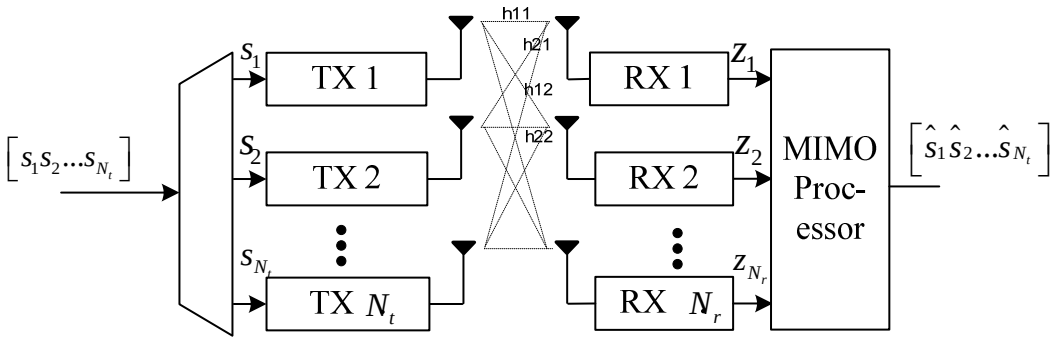

Figure 2.1: MIMO communication system

The IEEE 802.11n system normally uses a 20MHz bandwidth but can extend it to 40MHz as an option. A user frequency channel has 64 subcarriers. Among 64 sub-carriers, four subcarriers in each side are used for guard bands to prevent interference from neighbor channels. Accordingly, the receiver is required to estimate the channel transfer matrix for 56 subcarriers out of the 64 subcarriers. The 56 subcarriers are again divided into 52 subcarriers and 4 pilot carries. Each of data subcarriers can be modulated BPSK, QPSK, 16-QAM or 64-QAM. An OFDM-symbol duration is 4 microseconds with a guard interval of 0.8 microseconds.

We assume a SM-MIMO-OFDM transmitter where a data bit sequence is encoded by a convolutional channel encoder, and the encoded bit stream is divided into N_t spatial streams by a serial-to-parallel demultiplexer. Each spatial stream is interleaved separately, and the interleaved streams are modulated using an M-ary quadrature amplitude modulation (M-QAM) symbol set $\mathcal{A}$ based on the Gray mapping. Since Q binary bits form an M-QAM symbol, a binary vector $\mathbf{b} = [b_0, b_1, \cdots, b_{QN_t-1}]^T$ is mapped to a transmitted symbol vector $\mathbf{s} = [s_1, s_2, \cdots, s_{N_t}]^T$ (with $s_i \in \mathcal{A}$), taken from the set $\mathcal{A}^{Nt}$, a Cartesian product of M-QAM constellations. The M-QAM symbol sequence in each spatial stream is transmitted by an OFDM transmitter utilizing a fixed number of frequency subcarriers. The cyclic shift delay (CSD) block in Fig.2.2 prevents unintentional beamforming and the high peak-to-average power ratio problem.

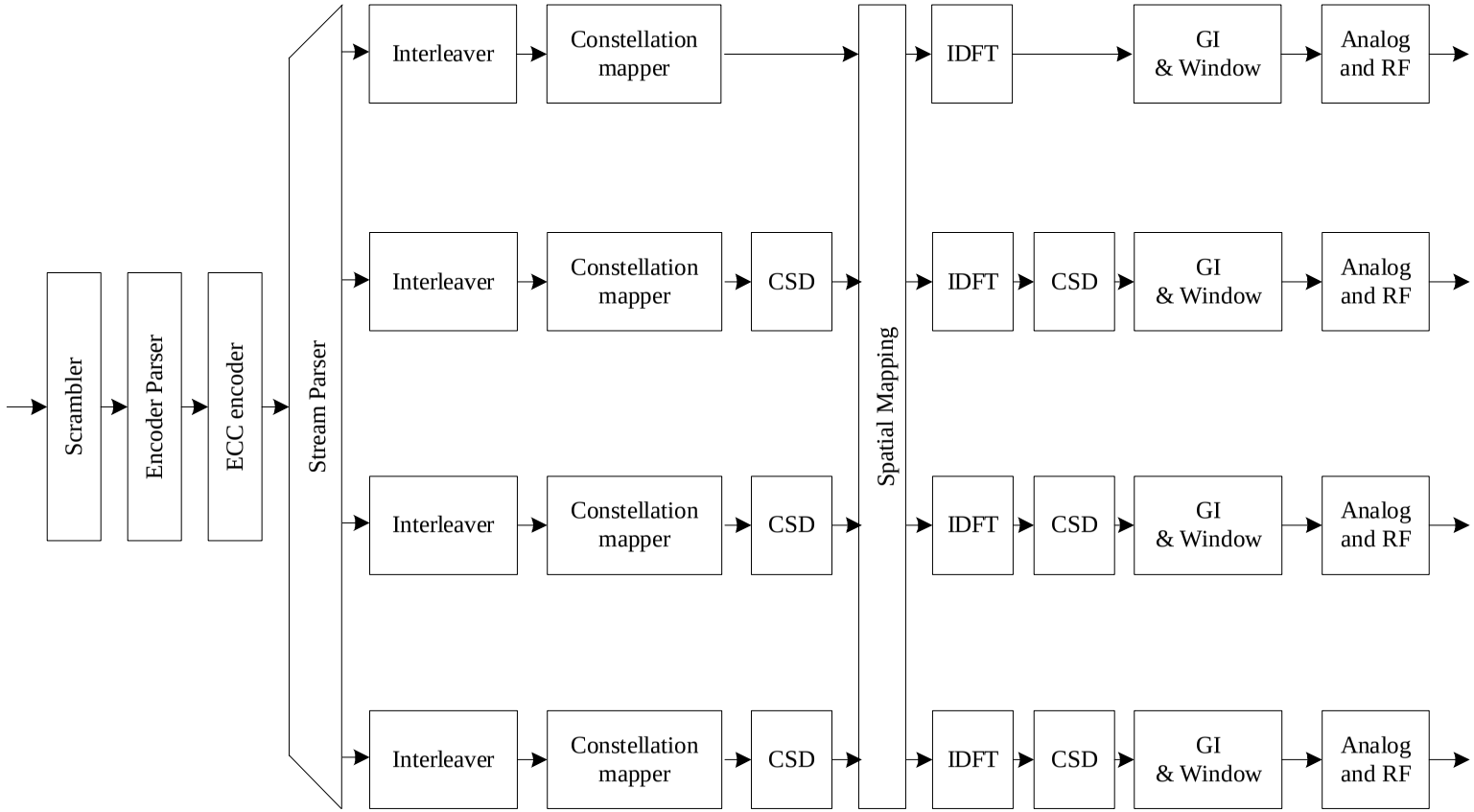

Figure 2.2: IEEE 802.11n transmitter block diagram

In the frequency domain, the MIMO communication process is expressed as

$$\mathbf{z}_n = \mathbf{H}\mathbf{s}_n + \mathbf{n}_n, \tag{2.1}$$

where $\mathbf{H}$ is a $N_r \times N_t$ channel matrix for a subcarrier known to the receiver, $\mathbf{s}$ is a $N_t \times 1$ transmit signal vector, $\mathbf{z}$ is a $N_r \times 1$ receive signal vector, and $\mathbf{n}$ is a $N_r \times 1$ complex AWGN noise vector with zero mean and variance N_o.

In the receiver side, the turbo equalizer is implemented as described in [29]. The turbo-equalization strategy iterates soft information between the SISO demapper and the SISO outer decoder. The demapper performs equalization that detects the transmitted QAM symbols from the received signal. As shown in Fig. 2.3, soft bit information are exchanged in a form of log-likelihood ratio (LLR) between the SISO decoder and SISO demapper [5]. The input and output of the SISO demapper and decoder are named as *a priori* and extrinsic information. We adopt the optimal maximum a posteriori (MAP) soft-demapping scheme [5]. The MAP demapper takes advantage of reliable soft symbol information that is available from the outer SISO decoder. Soft output Viterbi algorithm (SOVA) is used for SISO decoder implementation [30]. Fig. 2.3 shows the IDD process with the soft demapper and soft decoder, and let's call the one demapping-decoding process 'one iteration,' and the extrinsic LLR (ELLR) information of the soft demapper and the soft decoder outputs are improved through the IDD iterations.

2.2 MIMO channel interference due to the channel estimation error

Performance of the MIMO detector (also called a MIMO demapper) is significantly affected by channel estimation error. Here, we review a simple example of its impact. Consider a zero-forcing (ZF) detection for the received signal in (2.1). The ZF detector makes

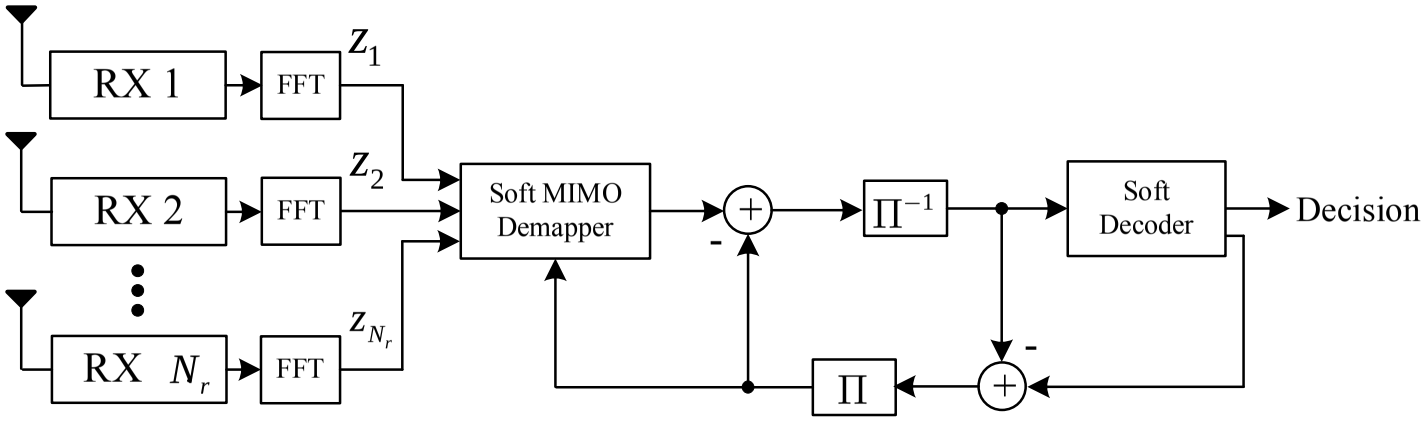

Figure 2.3: MIMO-OFDM turbo receiver block diagram

hard decisions $\widehat{\mathbf{s}}$ as

$$\widehat{\mathbf{s}}_n = \min_{\mathbf{s}_i \in \mathcal{A}^{Nt}} ||\tilde{\mathbf{s}}_n - \mathbf{s}_i||^2 \quad \text{where} \quad \tilde{\mathbf{s}}_n = \widehat{\mathbf{H}}^{-1}\mathbf{z}_n \tag{2.2}$$

An issue of the detection in (2.2) is that the CSI is imperfect in a receiver side due to estimation error. An ideal case would be $\widehat{\mathbf{H}}^{-1}\mathbf{H} = \mathbf{I}$ in the ZF detection process, however the actual detection is made as

$$\widetilde{\mathbf{s}}_n = \mathbf{s}_n + \underbrace{(\mathbf{H} - \widehat{\mathbf{H}})\mathbf{s}_n}_{\text{antenna interference}} + \widehat{\mathbf{H}}^{-1}\mathbf{n}_n. \tag{2.3}$$

As a result, the MIMO demapper cannot remove the interference completely due to the channel estimation error. Then, the symbol transmitted from the ith TX antenna is detected as

$$\widetilde{s}_i = s_i + \sum_{k=1, k\neq i}^{N_t} f(\hat{h}_k, h_k, s_k) + n, \tag{2.4}$$

The MIMO interference from unintentional TX antennas and symbols in (2.4) degrades the detector performance. Eq. (2.4) is a simple example of the ZF detector, the soft-demapper in the IDD is iteratively affected by the correlated channel estimation error, which is a root cause of the error propagation. Therefore, the interference should be processed properly based on the investigation of error correlation characteristics.

Chapter 3

Soft-Decision-Driven Channel Estimation for Pipelined Turbo Receivers

3.1 Overview

We consider channel estimation specific to turbo equalization for MIMO wireless communication. We develop a soft-decision-driven sequential algorithm geared to the pipelined turbo equalizer architecture operating on OFDM symbols. One interesting feature of the pipelined turbo equalizer is that multiple soft-decisions become available at various processing stages. A tricky issue is that these multiple decisions from different pipeline stages have varying levels of reliability. This paper establishes an effective strategy for the channel estimator to track the target channel, while dealing with observation sets with different qualities. The resulting algorithm is basically a linear sequential estimation algorithm and, as such, is Kalman-based in nature. The main difference here, however, is that the proposed algorithm employs puncturing on observation samples to effectively deal with the inherent correlation among the multiple demapper/decoder module outputs that cannot easily be

removed by the traditional innovations approach. The proposed algorithm continuously monitors the quality of the feedback decisions and incorporates it in the channel estimation process. The proposed channel estimation scheme shows clear performance advantages relative to existing channel estimation techniques. This chapter is based on the published papers in [33, 34].

3.2 Channel and System Model

We assume the SM-MIMO-OFDM system discussed in Chapter 2.1. For a particular subcarrier for the n^{th} OFDM symbol, the received signal at the discrete Fourier transform (DFT) output can be written as

$$\mathbf{z}_n = \mathbf{H}\mathbf{s}_n + \mathbf{n}_n \ , \tag{3.1}$$

where $\mathbf{z}_n = [z_1(n), z_2(n), \cdots, z_{N_r}(n)]^T$ is the received signal vector observed at N_r receive antennas, and $\mathbf{H}$ is the channel response matrix associated with all the wireless links connecting N_t transmit antennas with N_r receive antennas antennas, and $\mathbf{n}_n$ is a vector of uncorrelated, zero-mean additive white Gaussian noise (AWGN) samples of equal variance set to $\mathcal{N}_o$. The IDD technique of [6] that performs turbo equalization for MIMO systems is assumed at the receiver. The extrinsic information on the coded-bit stream is exchanged in the form of log-likelihood ratio (LLR) between the soft-input soft-output (SISO) decoder and the SISO demapper as shown in Fig. 3.1. The demapper takes advantage of the reliable soft-symbol information made available by the outer SISO decoder. A soft-output Viterbi algorithm (SOVA) is used for the SISO decoder implementation [30]. Each data packet transmitted typically contains many OFDM symbols, and they are processed sequentially by the demapper and the decoder as they arrive at the receiver. The feedback decisions used for channel estimation must be interleaved coded-bit decisions. The extrinsic information from the demapper are rearranged accordingly and made available to the channel estimation block. The pipelined architecture is adopted to reduce the iteration latency [24, 26].

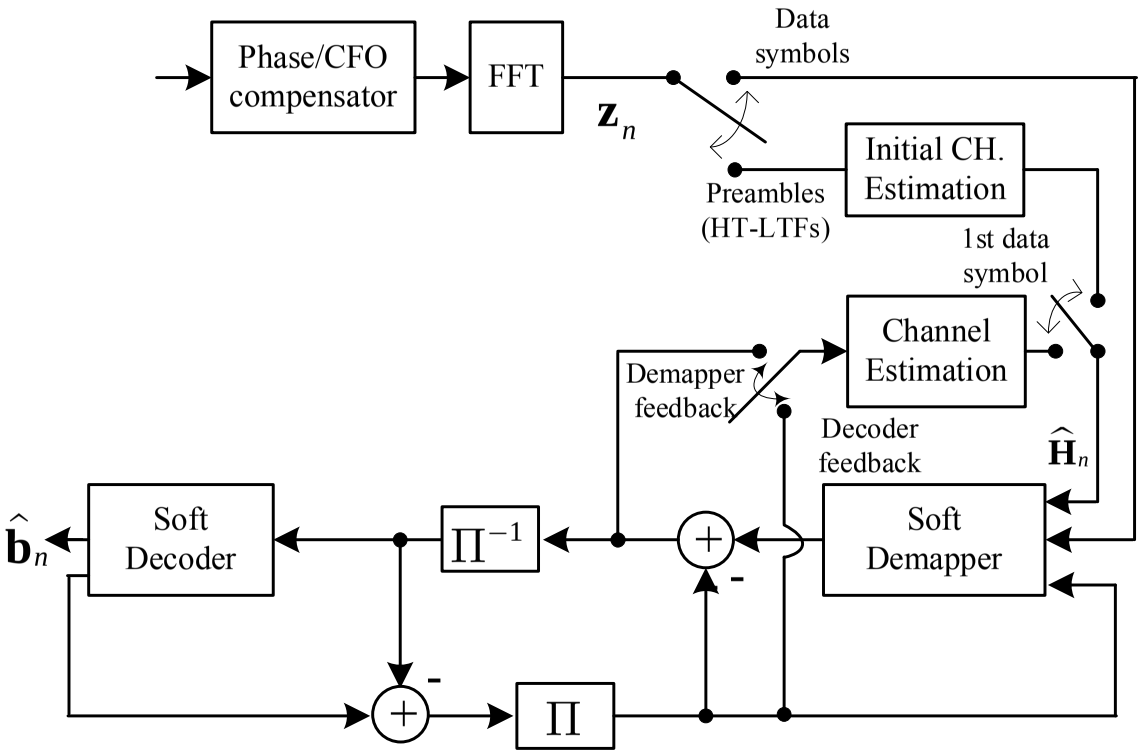

Figure 3.1: Block diagram of the turbo receiver and the soft-decision-directed channel estimator

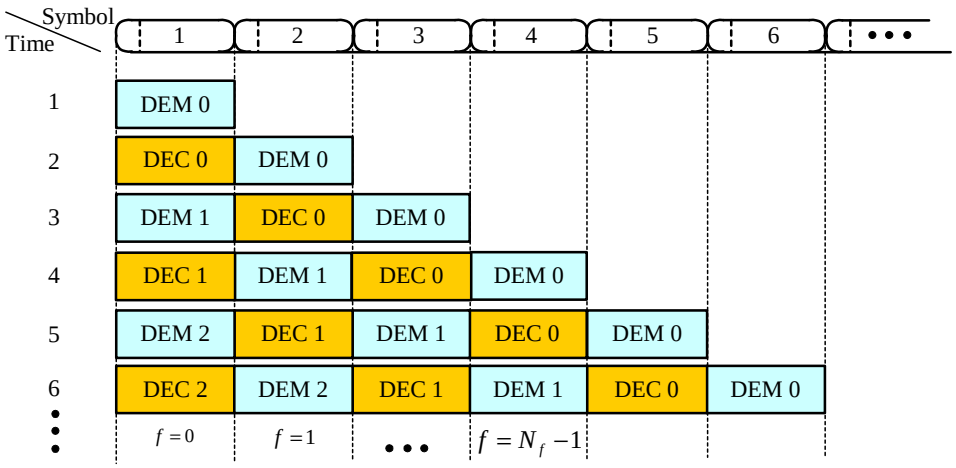

Figure 3.2: OFDM-symbol processing procedure in the pipelined IDD

Fig. 3.2 illustrates OFDM symbols processed in the pipelined IDD, and Fig. 3.3 shows the structure of the pipelined IDD receiver and its interface with the channel estimator. Multiple demapper-decoder pairs process multiple OFDM symbols at different iteration stages. Let N_{itr} denote the number of the IDD iterations required to achieve satisfactory error rate performance. The N_{itr}-stage pipelined IDD receiver is equipped with N_{itr} demappers and N_{itr} decoders that are serially connected as in Fig. 3.3. The decoder forwards its extrinsic information output to the demapper in the next iteration stage. Simultaneously, the demapper and the decoder in the previous iteration stage start to process a new OFDM symbol. The pipelined IDD operation is functionally equivalent to the original IDD scheme [24]. The extrinsic LLRs released from the pipelined demappers and decoders are utilized for the channel estimation. Let N_{sym} denote the number of the total OFDM symbols in a packet and N_f the number of the feedback symbols available for channel estimation. Note, however, that not all of N_f symbols are used for the estimation. If the receiver requires N_{itr} IDD iterations, then a maximum of $2N_{itr}$ OFDM symbols are processed in the pipelined IDD receiver as illustrated in Fig. 3.3. Because the LLR outputs from the initial demapper and decoder have low reliability, they are not used for the channel estimation. Let index n indicate the time. In this pipelined IDD setup, when $2 \leq n \leq 2N_{itr}$, the channel es-

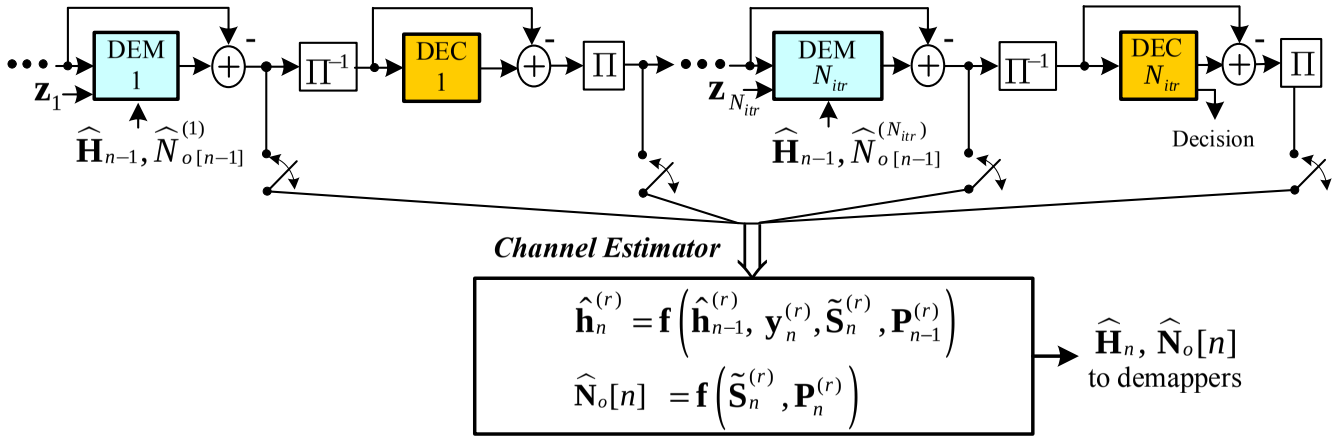

Figure 3.3: Block diagram of the proposed optimum channel estimation algorithm geared to the pipelined IDD

timator can get $(n-2)$ feedback decisions (i.e. $N_f = n-2$). When the number of the processed symbols increases to $2N_{itr}$ ($2N_{itr} \leq n \leq N_{sym}$), N_f is equal to $2N_{itr}-2$. After all the OFDM symbols in the packet have arrived at the receiver front-end, it will take sometimes until all symbols will clear out of the pipeline. For $n \geq N_{sym}$, N_f is equal to $N_{sym}+2N_{itr}-n$.

3.3 Sequential and Soft-Decision-Directed Channel Estimation

First, we make a brief review on the initial channel estimation method based on preambles of an IEEE 802.11n WLAN packet, and discuss the proposed sequential channel estimation algorithms.

3.3.1 Initial Channel Estimation Based on Training Symbols

The IEEE 802.11n standard specification provides a special training sequence named high-throughput long training fields (HT-LTFs) for the initial channel estimation purposes [27]. These HT-LTFs are inserted before the data fields in each packet. The transmitter sends an orthogonal symbol matrix $\mathbf{S}_{tr}$ representing the HT-LTFs sequence. A MIMO transmitter sends $\mathbf{S}_{tr}$ through a MIMO channel and the receiver observes a signal $\mathbf{Z}_{tr}$ as given in (5.1). The initially estimated $N_r \times N_t$ channel matrix can be performed by the least square method as

$$\begin{aligned} \widehat{\mathbf{H}}_{init} &= \mathbf{Z}_{tr}\mathbf{S}_{tr}^{T}\left(\mathbf{S}_{tr}\mathbf{S}_{tr}^{T}\right)^{-1} \\ &= \frac{1}{N_{tr}}\mathbf{Z}_{tr}\mathbf{S}_{tr}^{T}, \end{aligned} \tag{3.2}$$

where N_{tr} is the number of training symbols. The need for direct matrix inversion is avoided due to the orthogonal constraint imposed on $\mathbf{S}_{tr}$ (i.e. $\mathbf{S}_{tr}\mathbf{S}_{tr}^{T} = N_{tr}\mathbf{I}_{N_t}$). Using (3.2), the initial channel state information is obtained for each frequency tone.

3.3.2 Derivation of the Kalman-Based Sequential Channel Estimation Algorithm

The sequential form of the estimator is useful in improving the quality of the channel estimate as the observed symbols arrive in a sequential fashion, as OFDM symbols do in the system of our interest. It is assumed that the channel is quasi-static over N_f OFDM symbol periods. For the pipelined IDD receiver at hand, the observation equation is set up at the r^{th} receiver (RX) antenna as

$$\mathbf{z}_n^{(r)} = \mathbf{S}_n \mathbf{h}^{(r)} + \mathbf{n}_n^{(r)}, \tag{3.3}$$

where $\mathbf{z}_n^{(r)}$ is the received signal vector $[z_0^{(r)}(n), ..., z_{N_f-1}^{(r)}(n)]^{\mathrm{T}}$, $\mathbf{S}_n$ is a $N_f \times N_t$ matrix, $\mathbf{h}^{(r)}$ is a $N_t \times 1$ vector that is a multi-input-single-output (MISO) channel vector specific to the r^{th} RX antenna. The goal is to do a sequential estimation of $\mathbf{h}^{(r)}$ as n progresses. The estimation process is done in parallel to obtain channel estimates for all N_r RX antennas. With an understanding that we focus on a specific RX antenna, the RX antenna index r is dropped to reduce notation cluttering.

A mean symbol decision $\tilde{s}$ is defined as the average of the constellation symbols according $\tilde{s} = \sum_{s_i \in \mathcal{A}} s_i P(s_i)$, where $P(s_i)$ is the "extrinsic probability" obtained from a direct conversion of the available extrinsic LLR.

Innovation Sequence Setup

The pipeline architecture can be viewed as a buffer large enough to accommodate N_f OFDM symbols, but we take into account in our channel estimator design the different levels of reliability for the soft decisions coming out of the demapper or decoder modules at different iteration stages. First, defining the soft decision error $\mathbf{E} \triangleq \mathbf{S} - \widetilde{\mathbf{S}}$, (3.3) can be rewritten as

$$\mathbf{z}_n = \{\widetilde{\mathbf{S}}_n + \mathbf{E}_n\}\mathbf{h} + \mathbf{n}_n. \tag{3.4}$$

Note that this type of soft decision representation has been used previously [22]. We emphasize, however, that unlike in [22], our derivation of a linear sequential estimator is based on the attempt to explicitly generate the innovation sequence. As will be clear in the sequel, this approach has led us to a realization that the standard steps taken to generate the innovations do not work in our set up; this in turn allowed us to devise corrective measures. Let us first see if we can find $\mathbf{x}_n$, the innovations of $\mathbf{z}_n$ (i.e., the whitened sequence that is a causal, as well as a casually invertible, linear transformation of $\mathbf{z}_n$). We write:

$$\begin{aligned} \mathbf{x}_n &\stackrel{\Delta}{=} \mathbf{z}_n - \widetilde{\mathbf{S}}_n \hat{\mathbf{h}}_{n-1} && (3.5) \\ &= \widetilde{\mathbf{S}}_n(\mathbf{h} - \hat{\mathbf{h}}_{n-1}) + \mathbf{E}_n \mathbf{h} + \mathbf{n}_n. && (3.6) \end{aligned}$$

Ideally, the vector sequence $\mathbf{x}_n$ would represent an innovation sequence in the sense that any given component of the vector $\mathbf{x}_{n-k}$ is orthogonal to any component of $\mathbf{x}_n$ as long as $k \neq 0$. The correlation of $\mathbf{x}_n$ over time is solved as

$$\begin{aligned} & E \left[\mathbf{x}_{n-k}\mathbf{x}_n^H\right] \\ = \; & E\left[\mathbf{x}_{n-k}\left\{\left(\mathbf{h} - \widehat{\mathbf{h}}_{n-1}\right)^H \widetilde{\mathbf{S}}_n^H\right\}\right] + E\left[\mathbf{x}_{n-k}\mathbf{h}^H\mathbf{E}_n^H\right] + E\left[\mathbf{x}_{n-k}\mathbf{n}_n^H\right] \\ = \; & E\left[\mathbf{x}_{n-k}\mathbf{h}^H\mathbf{E}_n^H + \mathbf{n}_{n-k}\mathbf{n}_n^H\right] \\ = \; & E\left[\mathbf{E}_{n-k}\widehat{\mathbf{h}}_{n-k-1}\mathbf{h}^H\mathbf{E}_n^H + \mathbf{n}_{n-k}\mathbf{n}_n^H\right]. \end{aligned} \tag{3.7}$$

In this scenario we would have

$$\begin{aligned} E\left[x_{n-k}[i]x_n^*[j]\right] &= E\left[\mathbf{e}_{n-k}[i]\widehat{\mathbf{h}}_{n-k-1}\mathbf{h}^H\mathbf{e}_n^H[j]\right] + E\left[n_{n-k}[i]n_n^*[j]\right] \\ &= \begin{cases} \sum_{t=1}^{N_t}\hat{\rho}_{n-1}^{(t)}\sigma_s^2[t,i] + \mathcal{N}_o & \text{when } k=0 \text{ and } i=j \\ \epsilon(\approx 0) & \text{otherwise,} \end{cases} \end{aligned} \tag{3.8}$$

where $\mathbf{e}_n[i]$ indicates the i^{th} row vector $\mathbf{E}_n$, $\hat{\rho}_{n-1}^{(t)} \stackrel{\Delta}{=} E[\hat{h}_{n-1}^{(t)}h^{*(t)}]$ and $\sigma_s^2 \stackrel{\Delta}{=} E[|s-\tilde{s}|^2]$, the symbol decision error variance. The superscript 'H' and the symbol '$*$' denote the Hermitian transpose and the complex-conjugate, respectively. In deriving (3.8), we assumed: $E[x_{n-k}[i](\mathbf{h} - \widehat{\mathbf{h}}_{n-1})^H] = \mathbf{0}$, $E[s[i]\,e^*[j]] = 0$ for any k, i and j. In order for this to be true, though, the following must hold:

(1) Links in the MISO channel are uncorrelated.

(2) The channel estimate and decision error are independent.

(3) The decision errors are uncorrelated.
(i.e. $E[e_{n-k}[i]e_n^*[j]] = \epsilon, k \neq 0$ or $i \neq j$)

Under these three assumptions, the vector $\mathbf{x}_n$ reasonably represents an innovation sequence.

Innovation Sequence with Punctured Feedback

Assumption (1) is reasonable, if the RX antennas maintain reasonable physical separation. However, assumptions (2) and (3) are not convincing. A poor channel estimate generates a poor decision, which in turn affects the ability to make reliable channel estimation. This makes both assumptions (2) and (3) invalid. As such, the Kalman filter is not optimum any more, and the correlated error circulates in the IDD and channel estimator loop. Our goal here is to provide a refined innovation sequence to reduce this error propagation. First, we observe that there is no significant correlation between the decision errors of the demapper and decoder thanks to the interleaver/deinterleaver. An issue is the demapper-demapper or decoder-decoder output correlations for a given received signal (OFDM symbol), especially when a packet is bad (i.e., certain tones cause errors despite persistent IDD efforts). In the pipelined IDD setup, it takes $n = 2$ time steps for a demapper decision to shift to the next-stage demapper, and likewise for the decoder outputs. Consequently, components in observation vectors with even time difference has correlation, as seen in Fig.3.4 (a) between $\mathbf{x}_n$ and $\mathbf{x}_{n-2}$. In addition, we cannot assume that the noise is random as long as identical observations are reused during the iterative channel estimation.

This correlation in $\mathbf{x}_n$ is definitely problematic for any Kalman estimator design. Imagine removing correlation in $\mathbf{x}_n$ using the Gram-Schmidt procedure:

$$x_n^{'}[f] = x_n[f] - \frac{\langle x_n[f],\ \ x_{n-2}[f-2] \rangle}{|x_{n-2}[f-2]|^2} x_{n-2}[f-2] \tag{3.9}$$

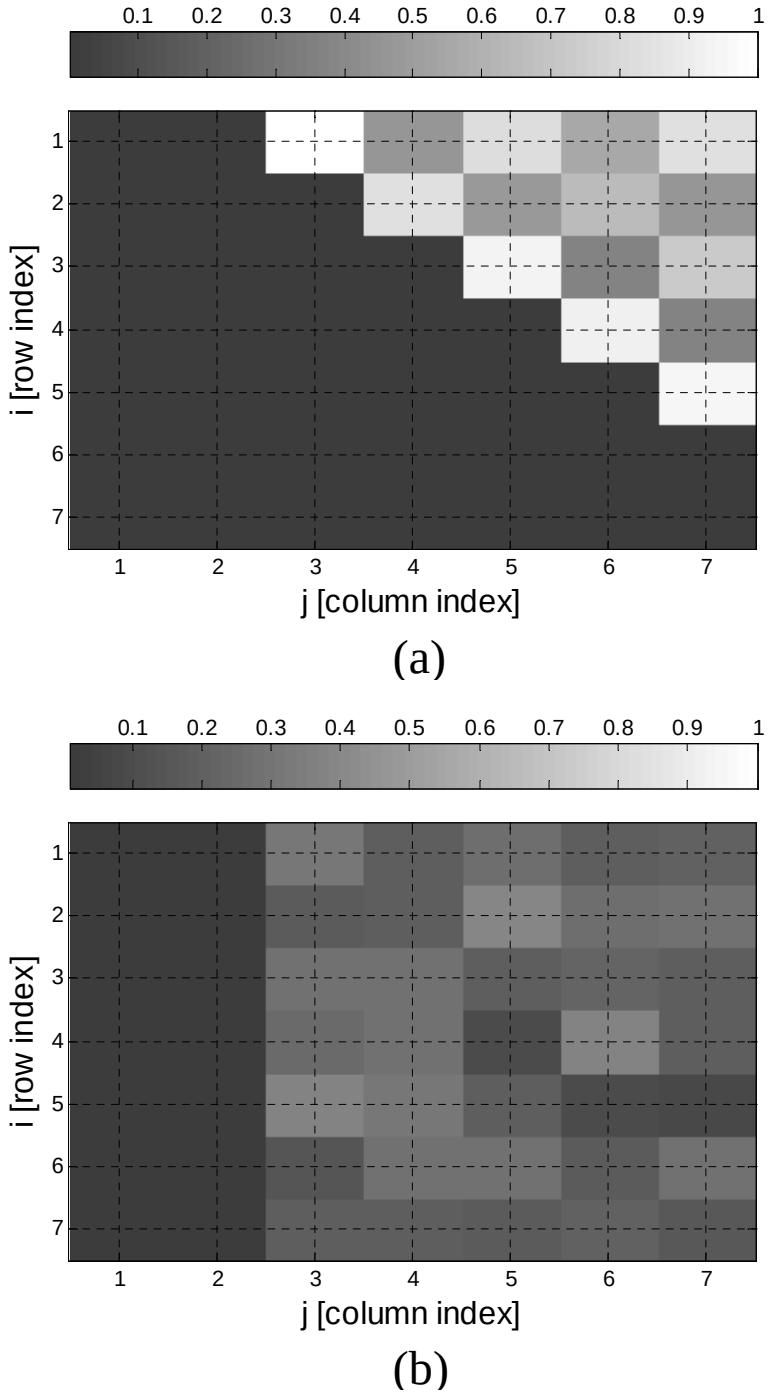

Figure 3.4: Correlations in the 'innovation' sequence: (a) $E[\mathbf{x}_{n-2}\mathbf{x}_n^H]$ (b) $E[\mathbf{y}_{n-2}\mathbf{y}_n^H]$, $c = 0.8$ (normalized by $E[|y_n[0]|^2]$, averaging 50 erroneous packets)

where $< a, b >$ denotes the inner product: $< a, b >= Re(a)Re(b) + Im(a)Im(b)$. Now, (3.8) can be rewritten (for $k = 2$ and dropping indices to simplify notation) as

$$\begin{aligned} E\left[x_{n-2}\, x_n^*\right] &= E\left[x_{n-2}\, x_n^{'*}\right] + E\left[\left|x_{n-2}\right|^2 \frac{\langle x_n, x_{n-2}\rangle}{\left|x_{n-2}\right|^2}\right] \\ &= E\left[\langle x_n,\, x_{n-2}\rangle\right] \end{aligned} \tag{3.10}$$

which suggests that using only those samples of x_n for which $\langle x_n,\ \ x_{n-2}\,\rangle \leq \epsilon$, where ϵ is an adjustable threshold, we can limit the amount of correlation in the overall observation samples utilized.

Before delving into the proposed "puncturing" process, we note that the amount of puncturing needs be decided judiciously, as removing observation samples also tends to "harden" the decisions, making the overall system approach one of hard decision feedback, a situation we need to avoid. Also, one may be tempted to use a more conceptually straightforward approach of subtracting out the correlated component as suggested by (3.9) or its generalized version including subtraction of less correlated components, but we had no meaningful success in reducing correlated errors with approaches along this direction.

Equation (3.10) suggests the following as a measure of correlation between the previous demapper and current demapper outputs (or between the previous decoder and current decoder outputs):

$$\beta_n(f) \triangleq \langle x_{n-2}[f-2],\ \ x_n[f]\,\rangle\,. \tag{3.11}$$

Now redefine N_d as the number of components among $x_n(f)$'s satisfying a threshold condition of

$$|\beta_n(f)| \ \leq\ c\mathcal{N}_o. \tag{3.12}$$

With this condition, let index d now denote the number of selected components among N_f feedback symbols (i.e. $d = 0, ..., N_d - 1$). The constant c (≥ 0) is an important parameter that controls the puncturing threshold. An improved innovation sequence $\mathbf{y}_n$ can be written

as

$$\mathbf{y}_n = \mathbf{G}_n \mathbf{x}_n, \tag{3.13}$$

where $\mathbf{G}_n$ is defined as a $N_d \times N_f$ puncturing matrix. For the d^{th} row vector $\mathbf{g}_n^{(d)}$ of the puncturing matrix, elements are given as

$$g_n^{(d)}[f] = \begin{cases} 1, & if\, \beta_n(f) \leq c\mathcal{N}_o \, or \, d = f = 0 \, or \, d = f = 1 \\ 0, & \text{otherwise.} \end{cases} \tag{3.14}$$

Note $x_n[0]$ and $x_n[1]$ are new input elements from the first demapper and decoder outputs, which are automatically included in the refined innovation vector. As long as the observations are reused during the iterative process, the noise correlation is also problematic in the channel estimation. To resolve this issue, a scaled noise variance is adopted as a threshold criterion to judge minimum correlation, because the noise variance term in (3.8) is inevitable. Highly correlated signal and noise components are punctured out depending on the constant c.

It is insightful to consider a simple argument based on random puncturing. Suppose the observation samples are dropped in a random fashion. Then, the element $x_{n-2}[f-2]$ can of course be excluded from $\mathbf{y}_{n-2}$ by puncturing, and so can $x_n[f]$ from $\mathbf{y}_n$. With random puncturing, the innovation process on each element can be analyzed as (dropping index f)

$$\begin{aligned} E \quad & [y_{n-2} y_n^* \,] = E\left[g_{n-2} x_{n-2} x_n^* g_n\right] \\ = \quad & P\left(g_{n-2} = 1\right) E\left[x_{n-2} x_n^*\right] P\left(g_n = 1\right) \\ = \quad & \frac{N_d^{(n-2)} N_d^{(n)} E\left[x_{n-2} x_n^*\right]}{\left(N_f^{(n-2)} - N_d^{(n-2)} + 1\right)\left(N_f^{(n)} - N_d^{(n)} + 1\right)}, \end{aligned} \tag{3.15}$$

where $P(g_n = 1)$ is the probability that the corresponding component x_n exists in $\mathbf{y}_n$. As N_f increases and/or N_d decreases in (3.16), the correlation $E\left[y_{n-2} y_n^*\right]$ decreases (likewise for the variance-normalized correlation). The same is true for the noise correlation.

Fig. 3.4 shows the example of correlation in the innovation sequence before and after the refinement through puncturing: $E[\mathbf{x}_{n-2}\mathbf{x}_n^H]$ vs $E[\mathbf{y}_{n-2}\mathbf{y}_n^H]$. The sequence $\mathbf{y}_n$ may have

a smaller number of observation samples, but its correlation is low as seen in Fig.3.4 (b), which is useful to maintain the optimality of the Kalman filter. The parameter c controls trade-off : if c is large, the number of observation increases, which can be beneficial for ML estimation. However a large c can feed biased decision errors to the Kalman-based estimator.

Note that the actual puncturing process is not fully random as our assumption made in (3.16). However, the puncturing happens irregularly, and an interesting observation we make is that irregular puncturing activity become more pronounced in broken (bad) packets. Once the decisions are incorrect, correlation between the components of $\mathbf{x}_n$ appears, and puncturing becomes active. In order to salvage a bad packet from biased errors, the puncturing attempts to "innovate" the sequence $\mathbf{x}_n$. Moreover, in high SNR, random puncturing is not necessary to produce reliable decisions, because the signal term itself in (3.6) (without the noise and estimation error terms) is an innovation sequence. Also, the puncturing process in this context can also be viewed as an effort to prevent redundant information from circulating in the iterative signal processing. We observe that although the puncturing cannot completely remove the correlated errors, a significant portion of the biased-errors gets eliminated before the channel estimation step resumes.

3.3.3 Kalman-Based Sequential Channel Estimation Algorithm with Punctured Innovation Sequence

Once the punctured innovation sequence $\mathbf{y}_n$ is generated, a linear channel estimator can be specified as a matrix $\mathbf{A}$, that is, $\hat{\mathbf{h}} = \mathbf{A}\mathbf{y}_n$. The Kalman estimator is now derived as

$$\begin{aligned}
\hat{\mathbf{h}}_n &= \widehat{E}[\mathbf{h}|\mathbf{y}_1, \mathbf{y}_2, ..., \mathbf{y}_n] \\
&= \widehat{E}[\mathbf{h}|\mathbf{y}_1, \mathbf{y}_2, ..., \mathbf{y}_{n-1}] + \widehat{E}[\mathbf{h}|\mathbf{y}_n] \\
&= \hat{\mathbf{h}}_{n-1} + \mathbf{A}_n\mathbf{y}_n \\
&= (\mathbf{I}_{N_t} - \mathbf{A}_n\widetilde{\mathbf{S}}_n)\hat{\mathbf{h}}_{n-1} + \mathbf{A}_n\mathbf{z}_n
\end{aligned} \tag{3.16}$$

where $\widehat{E}[\mathbf{a}|\mathbf{b}]$ denotes the optimal linear estimator of $\mathbf{a}$ given $\mathbf{b}$.

To find the linear estimator matrix $\mathbf{A}_n$, the orthogonality principle is applied:

$$\begin{aligned}\overline{(\mathbf{h}-\mathbf{A}_n\mathbf{y}_n)\,\mathbf{y}_n^H} &= \mathbf{0}\\ \mathbf{A}_n\overline{\mathbf{y}_n\mathbf{y}_n^H} &= \overline{\mathbf{h}\mathbf{y}_n^H},\end{aligned} \tag{3.17}$$

where an overbar also indicates statistical expectation. The right-hand-side of the last line in (3.17) is given by

$$\overline{\mathbf{h}\mathbf{y}_n^H} = \underbrace{\overline{(\mathbf{h}-\hat{\mathbf{h}}_{n-1})(\mathbf{h}-\hat{\mathbf{h}}_{n-1})^H}}_{\triangleq\mathbf{P}_{n-1}}\,\widetilde{\mathbf{S}}_n^H, \tag{3.18}$$

where $\mathbf{P}_{n-1}$ is defined as the channel estimation error variance matrix, and the term $\overline{\mathbf{y}_n\mathbf{y}_n^H}$ in (3.17) can be written as

$$\begin{aligned}\overline{\mathbf{y}_n\mathbf{y}_n^H} &= \widetilde{\mathbf{S}}_n\overline{(\mathbf{h}-\hat{\mathbf{h}}_{n-1})(\mathbf{h}-\hat{\mathbf{h}}_{n-1})^H}\,\widetilde{\mathbf{S}}_n^H\\ &\quad+\underbrace{\overline{\mathbf{E}_n\mathbf{h}\mathbf{h}^H\mathbf{E}_n^H}}_{\triangleq\mathbf{Q}_n}+\mathcal{N}_o\mathbf{I}_{N_d}.\end{aligned} \tag{3.19}$$

Now using (3.17), (3.18) and (3.19), the matrix $\mathbf{A}_n$ is obtained as

$$\begin{aligned}\mathbf{A}_n &= \overline{\mathbf{h}\mathbf{y}_n^H}(\overline{\mathbf{y}_n\mathbf{y}_n^H})^{-1}\\ &= \mathbf{P}_{n-1}\widetilde{\mathbf{S}}_n^H(\widetilde{\mathbf{S}}_n\mathbf{P}_{n-1}\widetilde{\mathbf{S}}^H+\mathbf{Q}_n+\mathcal{N}_o\mathbf{I}_{N_d})^{-1}\\ &= \left(\widetilde{\mathbf{S}}_n^H\,(\mathbf{Q}_n+\mathcal{N}_o\mathbf{I}_{N_d})^{-1}\,\widetilde{\mathbf{S}}_n+\mathbf{P}_{n-1}^{-1}\right)^{-1}\widetilde{\mathbf{S}}_n^H\,(\mathbf{Q}_n+\mathcal{N}_o\mathbf{I}_{N_d})^{-1}\end{aligned} \tag{3.20}$$

The next steps to complete the derivation process are to express $\mathbf{P}_{n-1}$ and $\mathbf{Q}_n$ in a recursive fashion. Noticing $(\mathbf{h}-\hat{\mathbf{h}}_n) = \mathbf{h}-(\hat{\mathbf{h}}_{n-1}+\mathbf{A}_n\mathbf{y}_n)$ from (3.16), the channel estimation error variance at time n can be rewritten as

$$\begin{aligned}\mathbf{P}_n &= \overline{\{\mathbf{h}-(\hat{\mathbf{h}}_{n-1}+\mathbf{A}_n\mathbf{y}_n)\}\{\mathbf{h}-(\hat{\mathbf{h}}_{n-1}+\mathbf{A}_n\mathbf{y}_n)\}^H}\\ &= \overline{(\mathbf{h}-\hat{\mathbf{h}}_{n-1})(\mathbf{h}-\hat{\mathbf{h}}_{n-1})^H}-\overline{(\mathbf{h}-\hat{\mathbf{h}}_{n-1})\mathbf{y}_n^H}\mathbf{A}_n^H\\ &\quad-\mathbf{A}_n\overline{\mathbf{y}_n(\mathbf{h}-\hat{\mathbf{h}}_{n-1})^H}+\mathbf{A}_n\overline{\mathbf{y}_n\mathbf{y}_n^H}\mathbf{A}_n^H\\ &= \mathbf{P}_{n-1}-\mathbf{A}_n\widetilde{\mathbf{S}}_n\mathbf{P}_{n-1}^H\\ &= (\mathbf{I}_{N_t}-\mathbf{A}_n\widetilde{\mathbf{S}}_n)\mathbf{P}_{n-1}\end{aligned} \tag{3.21}$$

where we utilized the relation $\overline{\mathbf{y}_n\mathbf{y}_n^H}\mathbf{A}_n^H = \widetilde{\mathbf{S}}_n\mathbf{P}_{n-1}^H$ which is obvious from (3.17) and (3.18). Also note $\mathbf{P}_n$ is a symmetric matrix of which pivot has non-negative real values.

Finally, $\mathbf{Q}_n$ needs to be found. The symbol decision error variance $\sigma_s^2 = E[|s-\tilde{s}|^2]$ can be found by using the extrinsic probabilities (i.e. $\sigma_s^2 = \sum_{s_i\in\mathcal{A}}|s_i-\tilde{s}|^2P(s_i)$). Under the reasonable assumption of $\overline{(s_j-\tilde{s}_j)(s_i-\tilde{s}_i)^*} = 0$ when $i \neq j$, the $N_d \times N_d$ diagonal matrix $\mathbf{Q}_n$ is given as

$$\overline{\mathbf{E}_n\mathbf{h}\mathbf{h}^H\mathbf{E}_n^H} = \text{diag}\left[\sum_{t=1}^{N_t}\rho^{(t)}\sigma_s^2(n,0,t),\ ...,\sum_{t=1}^{N_t}\rho^{(t)}\sigma_s^2(n,N_d-1,t)\right]_{N_d\times N_d} \quad (3.22)$$

where $\rho^{(t)} \triangleq |h^{(t)}|^2$. However, finding $\rho^{(t)}$ is a bit tricky as the channel state information is unknown to the receiver. The channel correlation matrix $\mathbf{h}\mathbf{h}^H$, on the other hand, can be found from $\overline{\mathbf{h}\mathbf{h}^H} = \overline{\{(\mathbf{h}-\hat{\mathbf{h}}_n)+\hat{\mathbf{h}}_n\}\{(\mathbf{h}-\hat{\mathbf{h}}_n)+\hat{\mathbf{h}}_n\}^H}$, which reduces to $\mathbf{P}_n + \hat{\mathbf{h}}_n\hat{\mathbf{h}}_n^H$. Utilizing this expression, we can write

$$\begin{aligned}\mathbf{Q}_n &= \overline{\mathbf{E}_n\left(\mathbf{P}_n + \hat{\mathbf{h}}\hat{\mathbf{h}}_n^H\right)\mathbf{E}_n^H} \\ &= \text{diag}\left[\sum_{t=1}^{N_t}\left(p_n(t,t)+|\hat{h}_{n-1}^{(t)}|^2\right)\sigma_s^2(n,0,t),\ ...,\right. \\ &\qquad \left.\sum_{t=1}^{N_t}\left(p_n(t,t)+\hat{h}_{n-1}^{(t)}|^2\right)\sigma_s^2(n,N_d-1,t)\right] \end{aligned} \quad (3.23)$$

where $\hat{h}_t[n-1]$ is from the previous estimate $\hat{\mathbf{h}}_{n-1}$, $p_n(t,t)$ is the t^{th} diagonal element of $\mathbf{P}_{n-1}$, and $\sigma_s^2(n,j,t)$ is the decision error variance of the (j,t) element of $\widetilde{\mathbf{S}}_n$.

Putting it all together, for the receive antenna r, the proposed estimator is summarized

as a set of equations :

$$\mathbf{Q}_n^{(r)} = \mathrm{diag}\left[\sum_{t=1}^{N_t}\left(p_n(t,t)+|\hat{h}_{n-1}^{(t)}|^2\right)\sigma_s^2(n,0,t),\cdots,\right.$$
$$\left.\sum_{t=1}^{N_t}\left(p_n(t,t)+|\hat{h}_{n-1}^{(t)}|^2\right)\sigma_s^2(n,N_d-1,t)\right]_{N_d\times N_d} \quad (3.24)$$

$$\mathbf{A}_n^{(r)} = \left(\widetilde{\mathbf{S}}_n^H\left(\mathbf{Q}_n^{(r)}+\mathcal{N}_o\mathbf{I}_{N_d}\right)^{-1}\widetilde{\mathbf{S}}_n+\mathbf{P}_{n-1}^{(r)-1}\right)^{-1}\widetilde{\mathbf{S}}_n^H\left(\mathbf{Q}_n^{(r)}+\mathcal{N}_o\mathbf{I}_{N_d}\right)^{-1} \quad (3.25)$$

$$\mathbf{P}_n^{(r)} = (\mathbf{I}_{N_t}-\mathbf{A}_n^{(r)}\widetilde{\mathbf{S}}_n)\mathbf{P}_{n-1}^{(r)} \quad (3.26)$$

$$\hat{\mathbf{h}}_n^{(r)} = \hat{\mathbf{h}}_{n-1}+\mathbf{A}_n\mathbf{y}_n, \quad (3.27)$$

where $\hat{\mathbf{h}}_{-1}$ corresponding to the initial time $n=0$ can be given by an initial channel estimator based on the use of known preambles. Also the initial matrix $\mathbf{P}_{-1}^{(r)}$ can be derived from the MMSE analysis [31] as $\mathbf{P}_{-1}^{(r)} = \mathrm{diag}[|\hat{\mathrm{h}}_{-1}^{(\mathrm{r,t})}|^2/(\gamma|\hat{\mathrm{h}}_{-1}^{(\mathrm{r,t})}|^2+1)]$ for $t=1,..,N_t$ where $\gamma = E_s/(N_t\mathcal{N}_o)$. We note that the channel estimation algorithm summarized in (3.24)-(3.27) takes into account the quality of the soft decisions that are generated at various stages in the pipeline for a given processing time n. When t=1, the resulting algorithm becomes very similar to the one presented in [22] for the inter-symbol interference channel, as the gist of the algorithm of [22] is in incorporating the quality of the soft decisions as part of effective noise in a Kalman sequential updating process. The difference, however, is that in our algorithm, we do not assume that the operation of $\mathbf{z}_n-\widetilde{\mathbf{S}}_n\hat{\mathbf{h}}_{n-1}$ makes the observation sequence automatically white, which, as argued above, would be faulty. Also, in our algorithm, varying qualities of the decisions generated from different processing modules at *a given time* are taken into account in the update process. More specifically, the effective noise covariance matrix of (3.24) is a function not only of n but also of N_d which itself is a growing function of n initially (up to $2N_{itr}$).

3.3.4 Noise Variance Update for the Soft Detectors

A Kalman-based estimation algorithm, as the one proposed here, has the advantage (compared with, e.g., EM-like algorithms) that the channel estimation error variance is available

for free and it is continually updated as a part of the recursive process. Realizing that the channel estimation error variance is a reasonable measure of how accurate the channel estimate is, this information somehow should play a beneficial role in the detection (or demapping) process.

As the first step in utilizing the available channel estimation error variance, the observation equation of (5.1) is recast with the channel estimation error shown explicitly:

$$\mathbf{z}_n^{(k)} = \widehat{\mathbf{H}}\mathbf{s}_n^{(k)} + \underbrace{\left(\mathbf{H} - \widehat{\mathbf{H}}_n\right)\mathbf{s}_n^{(k)}}_{\triangleq \mathbf{a}_n^{(k)}} + \mathbf{n}_n^{(k)}, \tag{3.28}$$

where superscript k points to a specific demapper out of the N_{itr} demappers operating in the pipeline stages ($k = 1, .., N_{itr}$). Accordingly, $\mathbf{s}_n^{(k)}$ here corresponds to each odd row of $\mathbf{S}_n$ in (3.3). For the k^{th} demapper in the pipeline, the noise variance is updated to include the channel estimation error:

$$\begin{aligned} \widehat{\mathbf{N}}_o^{(k)}[n] &= E\left\{ \left\| \mathbf{s}_n^{(k)}(\mathbf{H} - \widehat{\mathbf{H}}_n) + \mathbf{n}^{(k)} \right\|^2 \right\} \\ &= \mathbf{Cov}(\mathbf{a}_n^{(k)}, \mathbf{a}_n^{(k)}) + \mathcal{N}_o \mathbf{I}_{N_r}, \end{aligned} \tag{3.29}$$

where $\| \ \|$ indicates vector norm operation. The $N_r \times N_r$ covariance matrix $\mathbf{Cov}(\mathbf{a}_n^{(k)}, \mathbf{a}_n^{(k)})$ can be obtained (with an understanding we are focusing on the k^{th} demapper in the pipeline at time n, drop the indices k and n to simplify notation) as

$$\begin{aligned} &\mathbf{Cov}(\mathbf{a}, \mathbf{a}) = E\left\{ (\mathbf{H} - \widehat{\mathbf{H}})^H \mathbf{s}^H \mathbf{s} (\mathbf{H} - \widehat{\mathbf{H}}) \right\} \\ &\approx \mathrm{diag}\left[\sum_{t=1}^{N_t} p^{(1)}(t,t) |\widetilde{s}^{(t)}|^2, .., \sum_{t=1}^{N_t} p^{(N_r)}(t,t) |\widetilde{s}^{(t)}|^2 \right] \end{aligned} \tag{3.30}$$

where the approximation is due to the assumption that channel estimation errors and transmitted symbols are independent and that $E[\mathbf{s}_n^H \mathbf{s}_n] \approx E[\widetilde{\mathbf{s}}_n^H \widetilde{\mathbf{s}}_n]$. Note that the updated noise variance is specified in matrix form because different RX antennas are subject to different channel estimate errors in the Kalman estimator. This is the same as saying each RX antenna is subject to a different amount of observation noise. Therefore, the demapper algorithm must properly be optimized for the given equivalent noise covariance matrix.

The demappers in the pipeline utilize (3.28). An M-QAM symbol vector transmitted from N_t-TX streams is demapped to one binary vector $\mathbf{b} = [b_0, b_1, \cdots, b_{QN_t-1}]^T$. Using the updated noise variance, the likelihood function of the MIMO demapper is given as

$$\begin{aligned} P(\mathbf{z}|\mathbf{s}) &= \prod_{r=1}^{N_r} \frac{1}{\sqrt{2\pi\widehat{\mathcal{N}}_o^{(r)}}} \exp\left(-\frac{|z^{(r)} - \widehat{\mathbf{h}}^{(r)}\mathbf{s}|^2}{\widehat{\mathcal{N}}_o^{(r)}}\right) \\ &= \frac{1}{\left(\sqrt{2\pi}\right)^{N_r} \prod_{r=1}^{N_r} \widehat{\mathcal{N}}_o^{(r)}} \exp\left(-\sum_{r=1}^{N_r} \frac{|z^{(r)} - \widehat{\mathbf{h}}^{(r)}\mathbf{s}|^2}{\widehat{\mathcal{N}}_o^{(r)}}\right) \end{aligned} \tag{3.31}$$

where $\widehat{\mathcal{N}}_o^{(r)}$ is the noise variance corresponding to $z^{(r)}$, that is, the (r, r) diagonal element of matrix $\widehat{\mathbf{N}}_o$. The k^{th} soft MAP demapper in the pipeline directly gives out the posteriori LLR output L_P:

$$\begin{aligned} L_P(b_i) &= \ln \frac{P(b_i = 1|\mathbf{z})}{P(b_i = 0|\mathbf{z})} \\ &= \ln \frac{\sum\limits_{\mathbf{s}\in\mathcal{A}^{Nt}|b_i=1} P(\mathbf{z}|\mathbf{s}) \prod\limits_{j\neq i} P(b_j)}{\sum\limits_{\mathbf{s}\in\mathcal{A}^{Nt}|b_i=0} P(\mathbf{z}|\mathbf{s}) \prod\limits_{j\neq i} P(b_j)} + \ln \frac{P(b_i = 1)}{P(b_i = 0)}, \end{aligned} \tag{3.32}$$

where $i = 0, ..., QN_t - 1$ for the individual bits in the transmitted symbol vector.

The MMSE demapper solution can also be derived from the modified observation equation (3.28). The MMSE demapper can be shown to yield

$$\begin{aligned} \widehat{\mathbf{s}} \;=\; & E[\mathbf{s}] + \mathbf{\Sigma_s}\widehat{\mathbf{H}}^H \left(\widehat{\mathbf{H}}\mathbf{\Sigma_s}\widehat{\mathbf{H}}^H + \mathbf{Cov}(\mathbf{a}, \mathbf{a}) + \mathcal{N}_o\mathbf{I}\right)^{-1} \\ & \cdot \left(\mathbf{z} - \widehat{\mathbf{H}}E[\mathbf{s}]\right), \end{aligned} \tag{3.33}$$

where $E[\mathbf{s}]$ is a mean-symbol vector based on the $apriori$ probabilities, and $\mathbf{\Sigma_s}$ is given as $\mathrm{diag}[\sigma^2_{s_0}, \ldots, \sigma^2_{s_{N_t-1}}]$.

3.4 Mean Squared Error (MSE) Analysis

In the MSE analysis, we try to understand 1) the impact of biased soft decision errors, and 2) when the soft decision error is unbiased, the performance impact of mismatching the soft

decision error variance in the estimation channel process. Through the MSE analysis, we also investigate the impacts of the number and quality of decisions used in the estimation process.

The soft decisions fed back from the detectors and decoders are assumed to have potential errors and are written as

$$\tilde{s}[d,n] = s[d,n] + e[d,n], \tag{3.34}$$

where $d = 0,..,N_d - 1$. As discussed in Section 4.2.2, the fed-back soft-decisions may contain biased decision errors. So the decision error e_d is modeled as

$$e[d,n] = m[n] + q[d,n], \tag{3.35}$$

where m is a non-zero-mean random variable, and q is a white Gaussian noise with zero mean and variance σ_q^2. Also, denote $\sigma_s^2 = E[|e|^2]$. For both biased and unbiased cases, assume that the total decision error power σ_s^2 is identical. Also assume correlations of the bias mean with the symbol as well as with the channel are zero (i.e. $E[s\,m] = 0$ and $E[h\,m] = 0$).

The proposed estimator is designed based on the linear MMSE (LMMSE) criterion. For the MISO communication channel of (3.3), the LMMSE estimator is expressed as

$$\begin{aligned} \hat{\mathbf{h}}_n^{(r)} &= \mathbf{A}_n^{(r)} \mathbf{z}_n^{(r)} \\ \mathbf{A}_n^{(r)} &= \mathbf{R}_h^{(r)} \widetilde{\mathbf{S}}_n^H \left(\widetilde{\mathbf{S}}_n \mathbf{R}_h^{(r)} \widetilde{\mathbf{S}}_n^H + \mathbf{V}_n^{(r)} \right)^{-1} \\ &= \underbrace{\left(\widetilde{\mathbf{S}}_n^H \widetilde{\mathbf{S}}_n + v_n^{(r)} \mathbf{R}_h^{(r)-1} \right)^{-1}}_{\triangleq \mathbf{\Psi}^{-1}} \widetilde{\mathbf{S}}_n^H, \end{aligned} \tag{3.36}$$

where $\mathbf{V}_n^{(r)} = v_n^{(r)} \mathbf{I}_{N_d}$ with $v_n^{(r)} = (\sigma_{s,n}^2 \sum_{t=1}^{N_t} \rho^{(r,t)} + \mathcal{N}_o)$, and $\mathbf{R}_h^{(r)-1} = E\left\{ \mathbf{h}^{(r)} \mathbf{h}^{(r)H} \right\}$. Also, denote $\mathbf{\Psi} \triangleq \widetilde{\mathbf{S}}_n^H \widetilde{\mathbf{S}}_n + v_n \mathbf{R}_h^{(r)-1}$. The estimator of (3.36) is optimum under unbiased decision errors ($m = 0$), and the minimum estimation error variance of the MIMO LMMSE

estimator is obtained as

$$\begin{aligned}\varepsilon^2_{unbiased}[n] &= \sum_{r=1}^{N_r} E\left\{\|\mathbf{h}^{(r)} - \hat{\mathbf{h}}_n^{(r)}\|^2\right\} \\ &= \sum_{r=1}^{N_r} \mathbf{tr}\left\{\left(\widetilde{\mathbf{S}}_n^H \mathbf{V}_n^{(r)-1}\widetilde{\mathbf{S}}_n + \mathbf{R}_h^{(r)-1}\right)^{-1}\right\},\end{aligned} \tag{3.37}$$

where $\varepsilon^2_{unbiased}$ is the estimation error variance of the optimum MMSE estimator (3.36). As N_d increases, it is reasonable to write $\widetilde{\mathbf{S}}^H\widetilde{\mathbf{S}} = N_d E\{\widetilde{\mathbf{S}}^H\widetilde{\mathbf{S}}\} = N_d(E_s+\sigma_s^2)\mathbf{I}_{N_t}$. Accordingly, we have

$$\varepsilon^2_{opt} = \varepsilon^2_{unbiased} = \sum_{r=1}^{N_r}\sum_{t=1}^{N_t} \frac{1}{N_d(E_s+\sigma_s^2)/v^{(r)} + 1/\rho^{(r,t)}}. \tag{3.38}$$

Meanwhile, when $m \neq 0$ with the same decision error power σ_s^2, the MSE with the biased decision error is calculated as

$$\varepsilon^2_{biased} = \sum_{r=1}^{N_r} E\left\{||h^{(r)} - \widehat{\mathbf{h}}^{(r)}_{biased}||^2\right\}, \tag{3.39}$$

where $\widehat{\mathbf{h}}_{biased} = \mathbf{A}_{biased}\mathbf{z}$ and $\mathbf{A}_{biased} = (\widetilde{\mathbf{S}}^H_{biased}\widetilde{\mathbf{S}}_{biased} + v\mathbf{R}_h^{-1})^{-1}\widetilde{\mathbf{S}}^H_{biased}$ that utilizes soft-decisions with correlated error. Note that the correlation matrix of decision errors is $E[\mathbf{E}^H\mathbf{E}] = N_d\sigma_s^2\,\mathbf{I}_{Nt} + N_d\mathbf{\Phi}_{N_t}$, where $\mathbf{\Phi}_{N_t}$ is a matrix with all diagonal elements set to zeros and all non-diagonal elements to $|m|^2$. Assuming a very large N_d and applying a matrix lemma $(\mathbf{X}+\mathbf{Y})^{-1} = \mathbf{X}^{-1} - \mathbf{X}^{-1}(\mathbf{X}^{-1}+\mathbf{Y}^{-1})\mathbf{X}^{-1}$, the matrix inversion can be done as

$$\begin{aligned}&\left(\widetilde{\mathbf{S}}^H_{biased}\widetilde{\mathbf{S}}_{biased} + v_n\mathbf{R}_h^{-1}\right)^{-1} \\ &= (\underbrace{N_d\left(E_s+\sigma_s^2\right)\mathbf{I}_{Nt} + v_n\mathbf{R}_h^{-1}}_{=\mathbf{\Psi}} + N_d\mathbf{\Phi}_{Nt})^{-1} \\ &= \mathbf{\Psi}^{-1} - \underbrace{\mathbf{\Psi}^{-1}\left(\tfrac{1}{N_d}\mathbf{\Phi}_{N_t}^{-1} + \mathbf{\Psi}^{-1}\right)^{-1}\mathbf{\Psi}^{-1}}_{=\mathbf{\Lambda}}.\end{aligned} \tag{3.40}$$

Using (3.40) and the facts $\mathbf{tr}\left(\mathbf{\Psi}^{-1}\mathbf{\Phi}_{Nt}\mathbf{R}_h\right) = 0$ and $\mathbf{tr}\left(\mathbf{\Phi}_{Nt}\mathbf{R}_h\right) = 0$, the MSE of the

LMMSE estimator suffering from correlated decision errors is finally expressed as

$$\begin{aligned}\varepsilon^2_{biased} &= \sum_{r=1}^{N_r} \mathbf{tr}\left\{\mathbf{R}_h^{(r)} - \widehat{\mathbf{h}}^{(r)}_{unbiased}\mathbf{h}^{(r)H}\right\} \\ &\quad +\mathbf{tr}\left\{\left(N_d\left(E_s+\sigma_s^2\right)\mathbf{\Lambda}^{(r)}\mathbf{R}_h^{(r)}\right)\right\} \qquad (3.41)\\ &= \varepsilon^2_{unbiased} + \sum_{r=1}^{N_r}\mathbf{tr}\left\{\left(N_d\left(E_s+\sigma_s^2\right)\mathbf{\Lambda}^{(r)}\mathbf{R}_h^{(r)}\right)\right\}.\end{aligned}$$

Note that $\mathbf{\Lambda R}_h$ is a semi-positive definite matrix, and therefore $\varepsilon^2_{biased} > \varepsilon^2_{unbiased}$ when $|m| \neq 0$. This confirms the loss due to correlated decision errors, even if the error power is the same. In effectively whitening the correlated decision error, the constant c is a crucial parameter that determines the number of selected symbols N_d and thus controls the trade-off between the observation sample size and the amount of error correlation in the channel estimator. The existence of an optimum value for c is also shown through the MSE simulation results of Fig. 3.5. Based on Fig. 3.5, we set $c = 2$ for the 3×3 and 4×4 SM-MIMO-OFDM systems, and $c = 2.5$ for the 2×2 SM-MIMO-OFDM system.

Even with unbiased decision errors, the LMMSE estimator suffers performance degradation when the noise variance is mismatched. Let us quantify the MSE penalty associated with not accounting for the uncertainty inherent in the soft decisions in the form of increased noise variance. The LMMSE estimator failing to consider the soft decision error can be described as

$$\hat{\mathbf{w}}_n^{(r)} = \mathbf{W}_n^{(r)}\mathbf{z}_n^{(r)} \qquad (3.42)$$

$$\begin{aligned}\mathbf{W}_n^{(r)} &= \mathbf{R}_h^{(r)}\widetilde{\mathbf{S}}_n^H\left(\widetilde{\mathbf{S}}_n\mathbf{R}_h^{(r)}\widetilde{\mathbf{S}}_n^H + \mathcal{N}_o\mathbf{I}_{N_d}\right)^{-1} \\ &= \left(\widetilde{\mathbf{S}}_n^H\widetilde{\mathbf{S}}_n + \mathcal{N}_o\mathbf{R}_h^{(r)-1}\right)^{-1}\widetilde{\mathbf{S}}_n^H. \qquad (3.43)\end{aligned}$$

Utilizing (3.38) and denoting $\mathbf{\Delta}_n^{(r)} \triangleq \hat{\mathbf{h}}_n^{(r)} - \hat{\mathbf{w}}_n^{(r)}$, the estimation error variance ε_w^2 of the

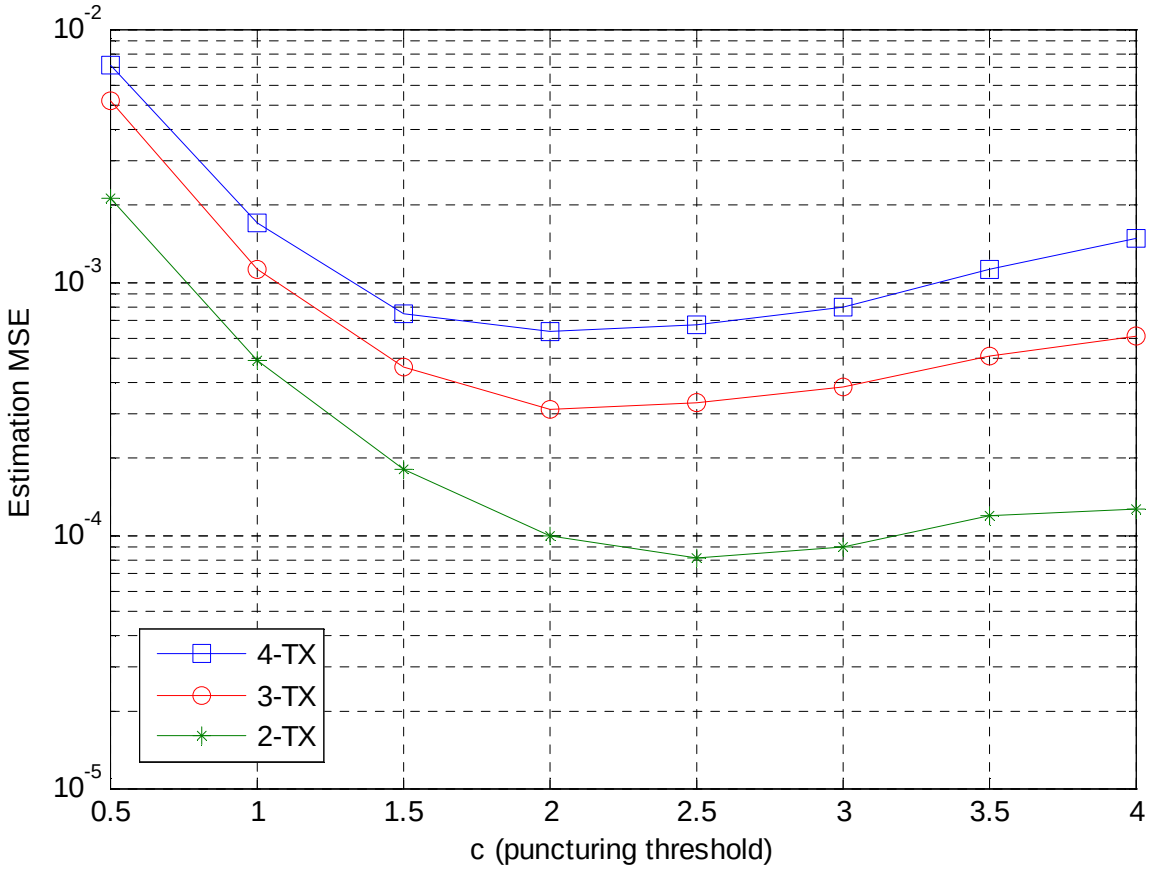

Figure 3.5: Threshold parameter c optimization for the optimal Kalman-based channel estimator

estimator (3.43) can be shown to be

$$\begin{aligned}
\varepsilon_w^2[n] &= \sum_{r=1}^{N_r} E\left\{\|\mathbf{h}_n^{(r)} - \hat{\mathbf{w}}_n^{(r)}\|^2\right\} \\
&= \sum_{r=1}^{N_r} \mathbf{tr} E\left\{\|\mathbf{h}_n^{(r)} - \left(\hat{\mathbf{h}}_n^{(r)} - \boldsymbol{\Delta}_n^{(r)}\right)\|^2\right\} \\
&= \varepsilon_{opt}^2[n] + \sum_{r=1}^{N_r} \mathbf{tr}\left\{E\left\{\hat{\mathbf{h}}_n^{(r)}\left(\mathbf{h}^{(r)} - \hat{\mathbf{h}}_n^{(r)}\right)^H + \hat{\mathbf{w}}_n^{(r)}\left(\mathbf{h}^{(r)} - \hat{\mathbf{w}}_n^{(r)}\right)^H \right.\right. \\
&\qquad \left.\left. + \mathbf{h}^{(r)}\left(\hat{\mathbf{h}}_n^{(r)} - \hat{\mathbf{w}}_n^{(r)}\right)^H\right\}\right\} \\
&= \varepsilon_{opt}^2[n] + \sum_{r=1}^{N_r} \mathbf{tr}\left\{E\left\{\mathbf{h}_n^{(r)}\hat{\mathbf{h}}_n^{(r)H} - \hat{\mathbf{w}}_n^{(r)}\hat{\mathbf{w}}_n^{(r)H} + \hat{\mathbf{w}}_n^{(r)}\mathbf{h}_n^{(r)H} - \mathbf{h}_n^{(r)}\hat{\mathbf{w}}_n^{(r)H}\right\}\right\}.
\end{aligned} \tag{3.44}$$

.

To simplify notation, the indices r and n are temporally dropped. As the number of iteration increases, the matrix inversions in (3.36) and (3.43) can be simplified as

$$\left(\widetilde{\mathbf{S}}^H\widetilde{\mathbf{S}} + v\mathbf{R}_h^{-1}\right)^{-1} = \mathrm{diag}[\rho_1/\left(\rho_1 N_d(E_s+\sigma_s^2)+v\right), ..., \rho_{N_t}/\left(\rho_{N_t} N_d(E_s+\sigma_s^2)+v\right)], \tag{3.45}$$

and

$$\left(\widetilde{\mathbf{S}}^H\widetilde{\mathbf{S}} + \mathcal{N}_o\mathbf{R}_h^{-1}\right)^{-1} = \mathrm{diag}[\rho_1/\left(\rho_1 N_d(E_s+\sigma_s^2)+\mathcal{N}_o\right), ..., \rho_{N_t}/\left(\rho_{N_t} N_d(E_s+\sigma_s^2)+\mathcal{N}_o\right)], \tag{3.46}$$

where the subscript for ρ for the time being indicates the TX antenna. Also, noting $E\{\hat{\mathbf{h}}(\mathbf{h}-\hat{\mathbf{h}})^H\} = 0$ by the orthogonality principle, it can be shown that

$$\begin{aligned}
E\{\mathbf{h}\hat{\mathbf{h}}^H\} &= \mathbf{R}_h\mathbf{S}^H\widetilde{\mathbf{S}}\left(\widetilde{\mathbf{S}}^H\widetilde{\mathbf{S}} + v\mathbf{R}_h^{-1}\right)^{-H} \\
&= \mathrm{diag}\left[\frac{\rho_1^2 N_d E_s}{\rho_1 N_d\left(E_s+\sigma_s^2\right)+v}, ..., \frac{\rho_{N_t}^2 N_d E_s}{\rho_{N_t} N_d\left(E_s+\sigma_s^2\right)+v}\right]_{N_t\times N_t}.
\end{aligned} \tag{3.47}$$

We also write

$$
\begin{aligned}
&E\{\hat{\mathbf{w}}\hat{\mathbf{w}}^H\} \\
&= \left(\widetilde{\mathbf{S}}^H\widetilde{\mathbf{S}} + \mathcal{N}_o\mathbf{R}_h^{-1}\right)^{-1}\widetilde{\mathbf{S}}^H\left(\mathbf{S}\mathbf{R}_h\mathbf{S}^H + \mathcal{N}_o\mathbf{I}_{N_d}\right)\widetilde{\mathbf{S}}\left(\widetilde{\mathbf{S}}^H\widetilde{\mathbf{S}} + \mathcal{N}_o\mathbf{R}_h^{-1}\right)^{-H} \\
&= \mathrm{diag}\left[\frac{\rho_1^2 N_d\left(\rho_1 N_d E_s^2 + \rho_\Sigma\sigma_s^2 E_s + \mathcal{N}_o\left(E_s+\sigma_s^2\right)\right)}{\left(\rho_1 N_d\left(E_s+\sigma_s^2\right)+\mathcal{N}_o\right)^2}, \ldots\right. \\
&\quad \left., \frac{\rho_{N_t}^2 N_d\left(\rho_{N_t} N_d E_s^2 + \rho_\Sigma\sigma_s^2 E_s + \mathcal{N}_o\left(E_s+\sigma_s^2\right)\right)}{\left(\rho_{N_t} N_d\left(E_s+\sigma_s^2\right)+\mathcal{N}_o\right)^2}\right]_{N_t\times N_t}
\end{aligned}
\tag{3.48}
$$

where $\rho_\Sigma = \sum_{t=1}^{N_t}\rho_t$. Finally, substituting (3.47) and (3.48) in (3.44) and also noting $E\{\hat{\mathbf{w}}\mathbf{h}^H\} = E\{\mathbf{h}\hat{\mathbf{w}}^H\}$, the MSE convergence behavior of the estimator (3.44) can be shown to be

$$
\lim_{N_d\to\infty}\varepsilon_w^2[n] = \varepsilon_{opt}^2[n] + \sum_{r=1}^{N_r}\frac{\rho_\Sigma^{(r)}E_s}{E_s+\sigma_s^2[n]}\left(1-\frac{E_s}{E_s+\sigma_s^2[n]}\right), \tag{3.49}
$$

from which it is easy to see that the mismatched MSE is an increasing function of the soft decision error variance σ_s^2.

To develop insights into the performance sensitivity off the sequentially updated channel estimator against the variations of the parameters σ_s^2 and N_d, we resort to an open-loop investigation. For this, the decision-feedback channel estimator is modified in such a way that unbiased soft decisions with various σ_s^2 and N_d combinations are artificially generated for the channel estimator. A 7-iteration IDD receiver for the 2×2 16-QAM MIMO-OFDM system is used for this test, but instead of using actual feedback from the demappers and decoders, artificially generated soft-decisions are provided to the channel estimator of (3.24)-(3.27). Fig. 3.6 and Fig. 3.7 show the MSE performance depending on the decision quality σ_s^2 and the number of feedback decisions N_d with an assumption of uncorrelated feedback decisions. The signal power is fixed at $E_s = 1$ and the channel SNR at 14 dB. With $N_d = 12$, the packet error rate (PER) due to imperfect CSI became negligible when $\sigma_s^2 \approx 0.1$. In Fig. 3.7, it is seen that reducing the number of feedback decisions, N_d, while fixing the decision quality causes the MSE to increase.

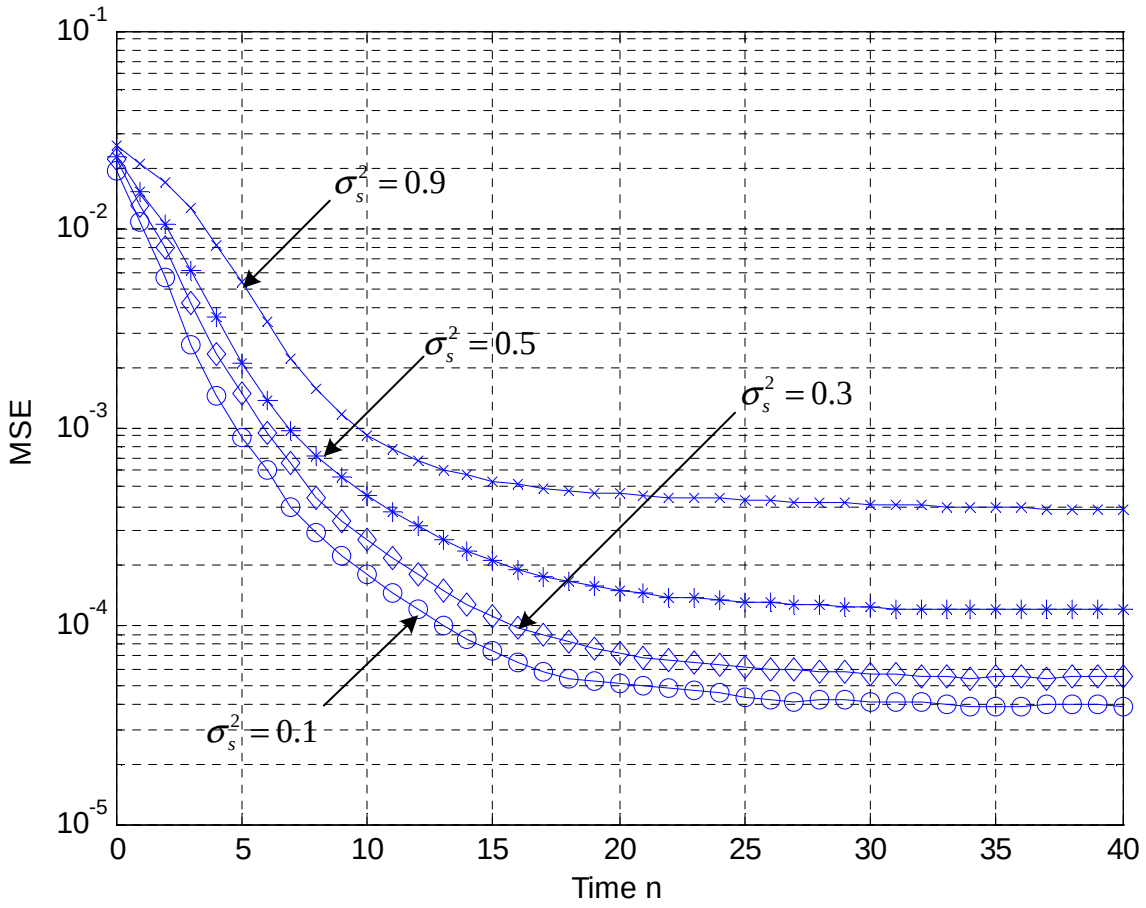

Figure 3.6: Open-loop channel estimation MSE for different values of σ_s^2 ($N_d = 12$)

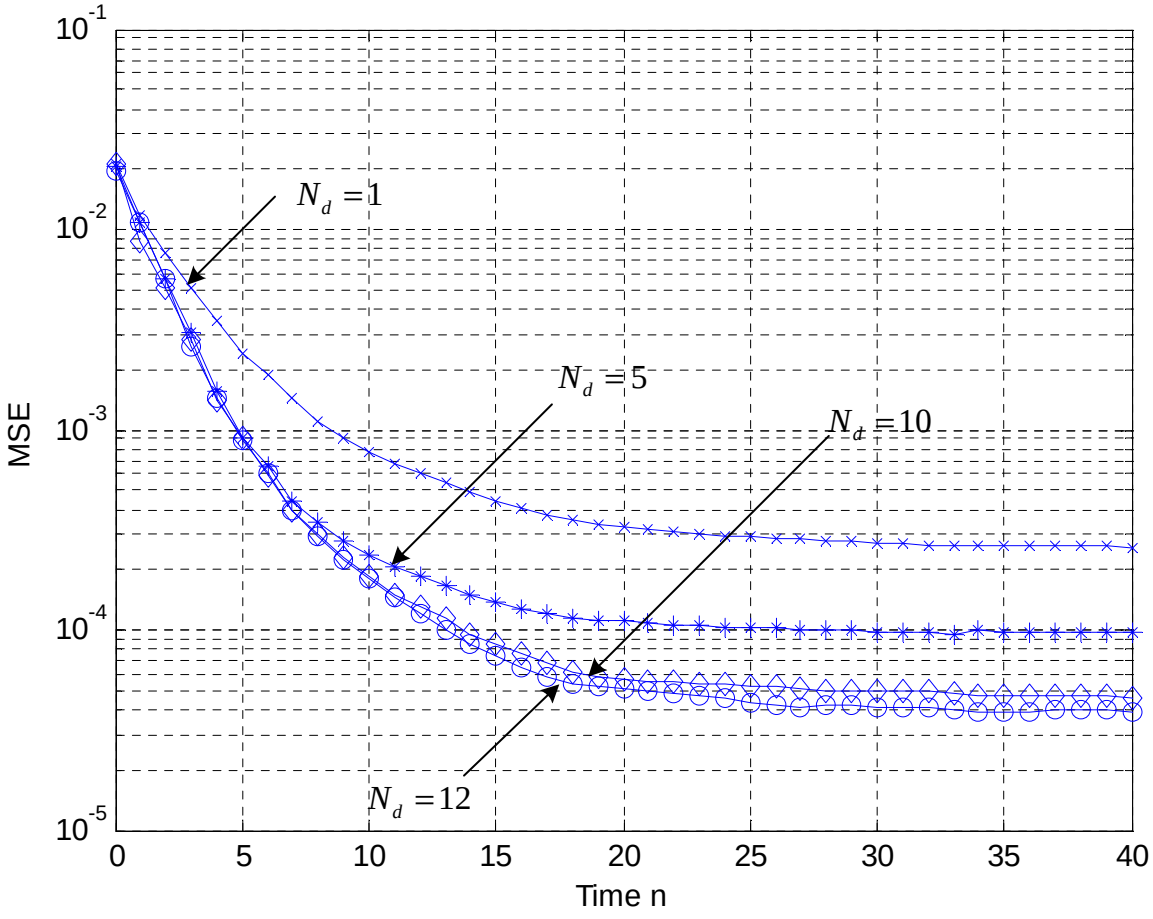

Figure 3.7: Open-loop channel estimation MSE depending on different values of N_d ($\sigma_s^2 = 0.1$)

3.5 Performance Evaluation

The proposed algorithm is investigated through an extrinsic information transfer (EXIT) chart analysis and packet error rate (PER) simulation. Performances are evaluated for 2×2, 3×3 and 4×4 16-QAM SM-MIMO-OFDM systems. The transmitter sends a packet with 1000 bytes of information. The SISO MAP-demapper is used for the 2×2 SM-MIMO-OFDM system, whereas the SISO MMSE-demapper is used for the 3×3 and 4×4 SM-MIMO-OFDM system [18] due to complexity. A rate-$1/2$ convolutional code is used with generator polynomials $g_o = 133_8$ and $g_1 = 171_8$, complying with the IEEE 802.11n specifications [27]. The SOVA is used for the decoding. The MIMO multi-path channel is modeled with an exponentially-decaying power profile with $T_{rms} = 50ns$ uncorrelated across the TX-RX links established.

3.5.1 EXIT and PER Performance Comparisons

The EXIT chart is a well-established tool that allows the understanding of the average convergence behavior of the mutual information (MI) in iterative soft-information processing systems [29]. Fig. 3.8 shows the results of an EXIT chart analysis on various competing schemes. A 2×2 SM-MIMO-OFDM system is used for this, and an SNR of 14 dB is chosen. I_{A_1} and I_{E_1} measure the MI at the input and output of the demapper, respectively, whereas I_{A_2} and I_{E_2} are the respective MI at the input and output of the decoder. At the next iteration stage, I_{E_1} becomes I_{A_2} and I_{E_2} turns to I_{A_1}. In the figure, the top-most curve indicates the average transfer function of MI through the demapper and the bottom-most curve is the same function for the decoder. Both the demapper and decoder EXIT chart curves correspond to Gaussian-distributed input LLRs, and the demapper EXIT curve is also based on the assumption of perfect channel estimation. The stair-case MI plots represent actual MI measured during IDD simulation runs and shows how the MI improves through the iterative process for three different channel estimation schemes. The gap between each

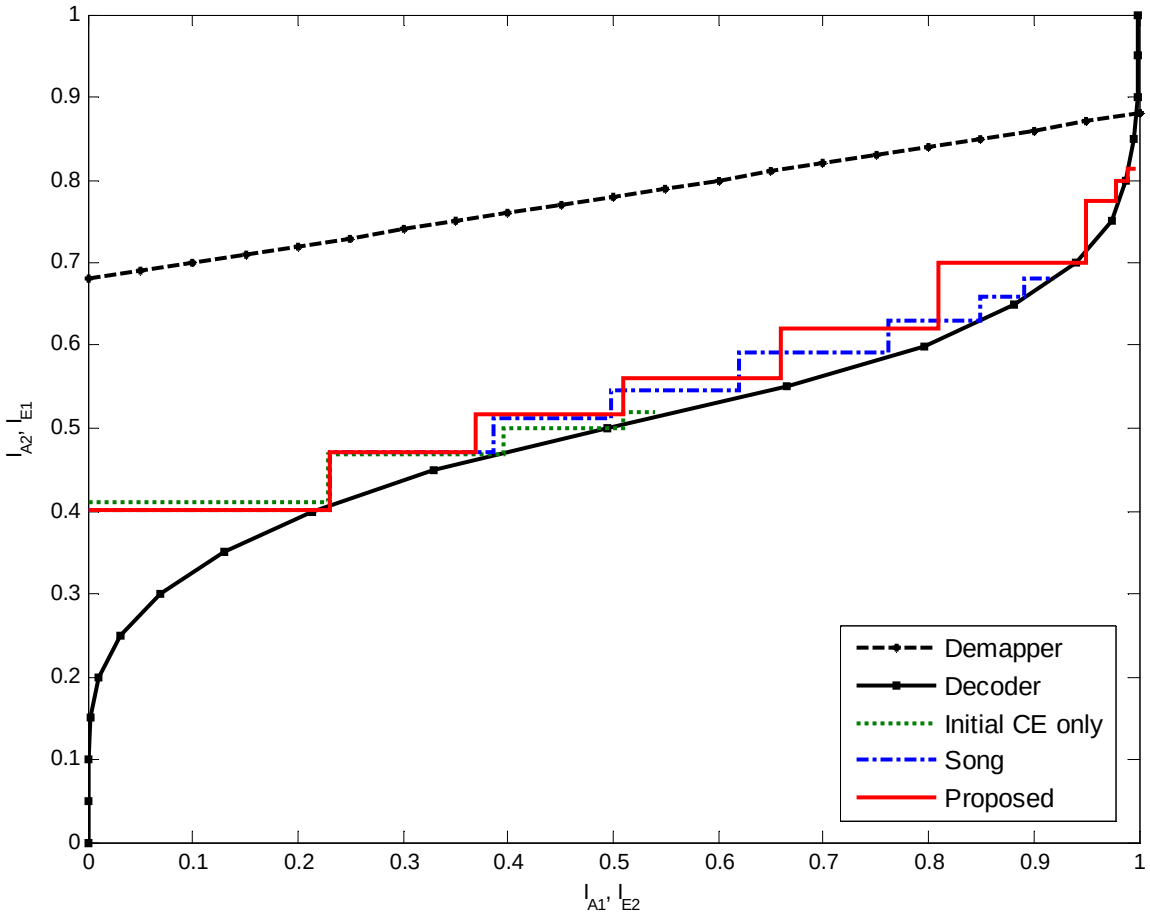

Figure 3.8: EXIT chart analysis on the proposed Kalman-based CE and conventional CEs in the 2×2 SM-MIMO-OFDM turbo receiver

stair-case MI trajectory and the demapper EXIT curve represents the performance loss due to imperfect-CSI. The solid stair-case line represents the proposed channel estimation algorithm. The dashed-line (labeled "Song") corresponds to the Kalman channel estimator of [23] applied to the conventional-IDD setting (non-pipelined IDD with a demapper utilizing the noise-variance update of (3.29) with channel estimation using only the decoder output decision). The dotted line is for the demapper utilizing only the preamble-based initial channel estimation (following the IEEE 802.11n format, where a fixed number of initial preamble symbols in the high-throughput long training field is utilized). For the proposed scheme, the MI trajectory measurement is taken from the last demapper in the pipeline, as the last demapper block best reflects the quality of the final decisions. It is clear that the proposed punctured-feedback Kalman estimation with pipelined-IDD shows superior MI convergence characteristics. The scheme of [23] fails to improve MI beyond nine iterations. With the demapper utilizing only initial channel estimation, the trajectory fails to advance earlier in the iteration.

Fig. 3.9 shows PER performances of the receivers with different channel estimators in the 2×2 SM-MIMO-OFDM system. Seven iterations are applied beyond which the iteration gain is plateaued. The performance gap between perfect CSI and preamble-based initial CE only is nearly 3 dB at low PERs. It can be seen that at low PER the proposed estimator almost compensates for the loss due to imperfect-CSI when the threshold parameter is set at $c = 2.5$. Although the performance with small c has inferior performance at low SNRs, the proposed Kalman CE curve with $c = 2.5$ crosses the $c = 4$ curve as SNR gets higher. The large c is effective in averaging noise in low SNR, but allows relatively large correlated errors. As expected from the EXIT chart analysis results, the Kalman estimator of [23] that utilizes only the decoder output in a non-pipelined setting does not perform as well. As one of competitive algorithms, the decision-directed EM estimator (referred to as EM-DD here) introduced as a variant of the EM estimator in [19] is applied with $\hat{\mathbf{h}}_{o,n}^{(r)} = \left(\widetilde{\mathbf{S}}_n^H \widetilde{\mathbf{S}}_n\right)^{-1} \widetilde{\mathbf{S}}_n^H \mathbf{z}_n^{(r)}$. In addition, the EM esti-

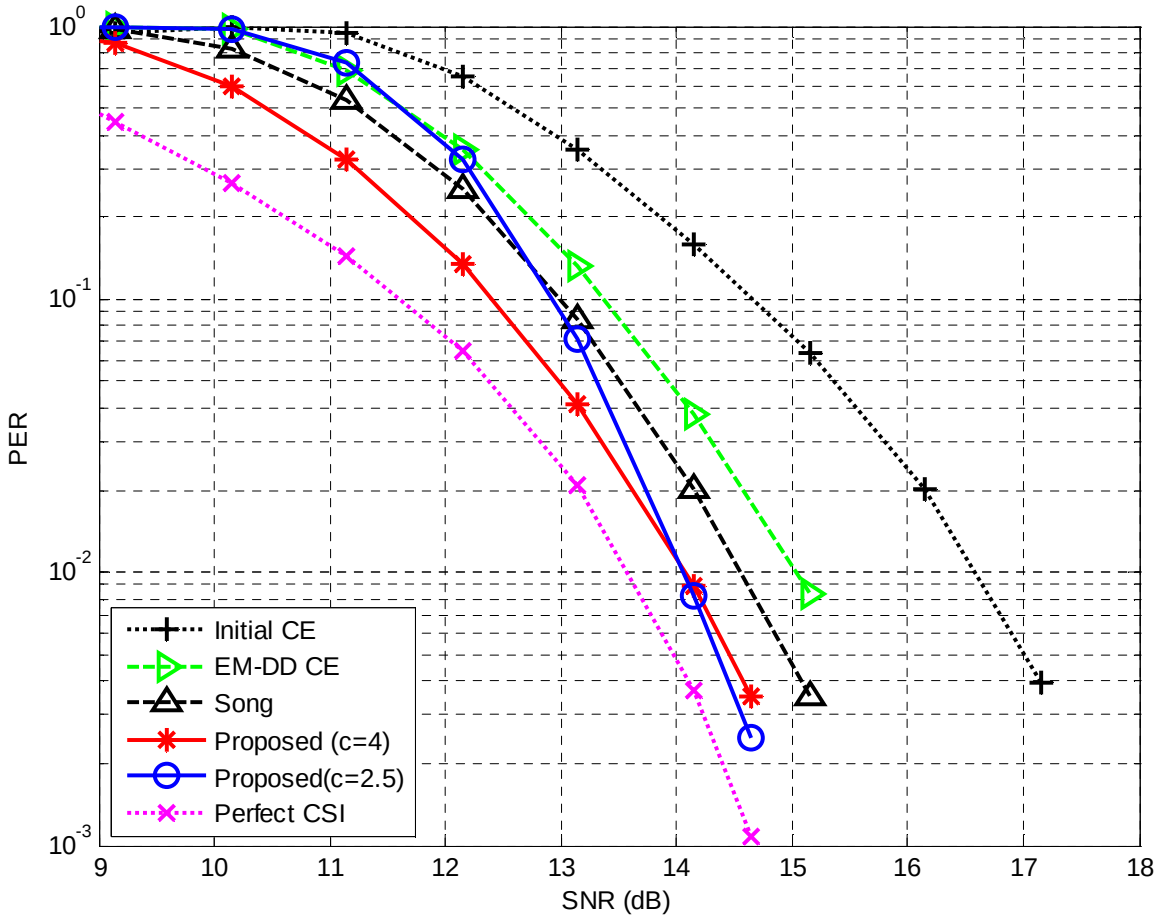

Figure 3.9: PER simulations of the proposed Kalman-based CE and conventional CEs in the 2x2 SM-MIMO-OFDM system(7 iterations)

mate is blended with the preamble-based channel estimate by a combining method (i.e., $\hat{h}_n^{(t,r)} = a_n \hat{h}_{preamble}^{(t,r)} + b_n \hat{h}_o^{(t,r)}[n]$) [20]. A method to find the combining coefficients a_n and b_n is discussed in [20]. The EM noise variance update method is presented in [19] as $\widehat{\mathcal{N}}_o[n] = 1/N_r N_d \sum_{r=1}^{N_r} \sum_{d=0}^{N_d-1} \left(z_n^{(r)} - \widetilde{\mathbf{S}}_n \hat{\mathbf{h}}_n^{(r)}\right)^* \left(z_n^{(r)} - \widetilde{\mathbf{S}}_n \hat{\mathbf{h}}_n^{(r)}\right)$. As can be seen, this scheme also does not perform as well as the proposed algorithm.

Fig. 3.10 and Fig. 3.11 show PER curves for 3×3 SM-OFDM-OFDM and 4×4 SM-OFDM-OFDM systems, respectively. These figures tell a consistent story. Namely, the initial-CE-only scheme suffers about a 3dB SNR loss relative to the perfect CSI case. The proposed schemes close this gap significantly, outperforming both the Kalman-based algorithm of [23] and the EM-based algorithm of [19]. As for the proposed channel estimation scheme, a more aggressive puncturing (corresponding to a lower c value) tends to give a lower PER as SNR increases. Before finishing this section, we compare computation complexity of the tested channel estimator. For all considered channel estimation schemes - the proposed, the Song method and the EM-DD - implementation complexity largely arises from the matrix inversion operation. Table 3.1 shows the number of a multiplier used to compute the MIMO channel estimates of each algorithm, and Fig. 3.12 illustrates its plot. Consequently, the proposed method and the Song method require complexity that roughly grows as $2N_r \times O(N_t^3)$ whereas the EM-DD requires complexity proportional to just $O(N_t^3)$. This is due to the consequence that both our method and the Song method require matrix inversion for each receive antenna, whereas the EM-DD method needs matrix inversion just once and can be used for all receive antennas. The factor 2 accounts for the fact that two matrix inversions are required for each update of the Kalman gain in the proposed and Song methods.

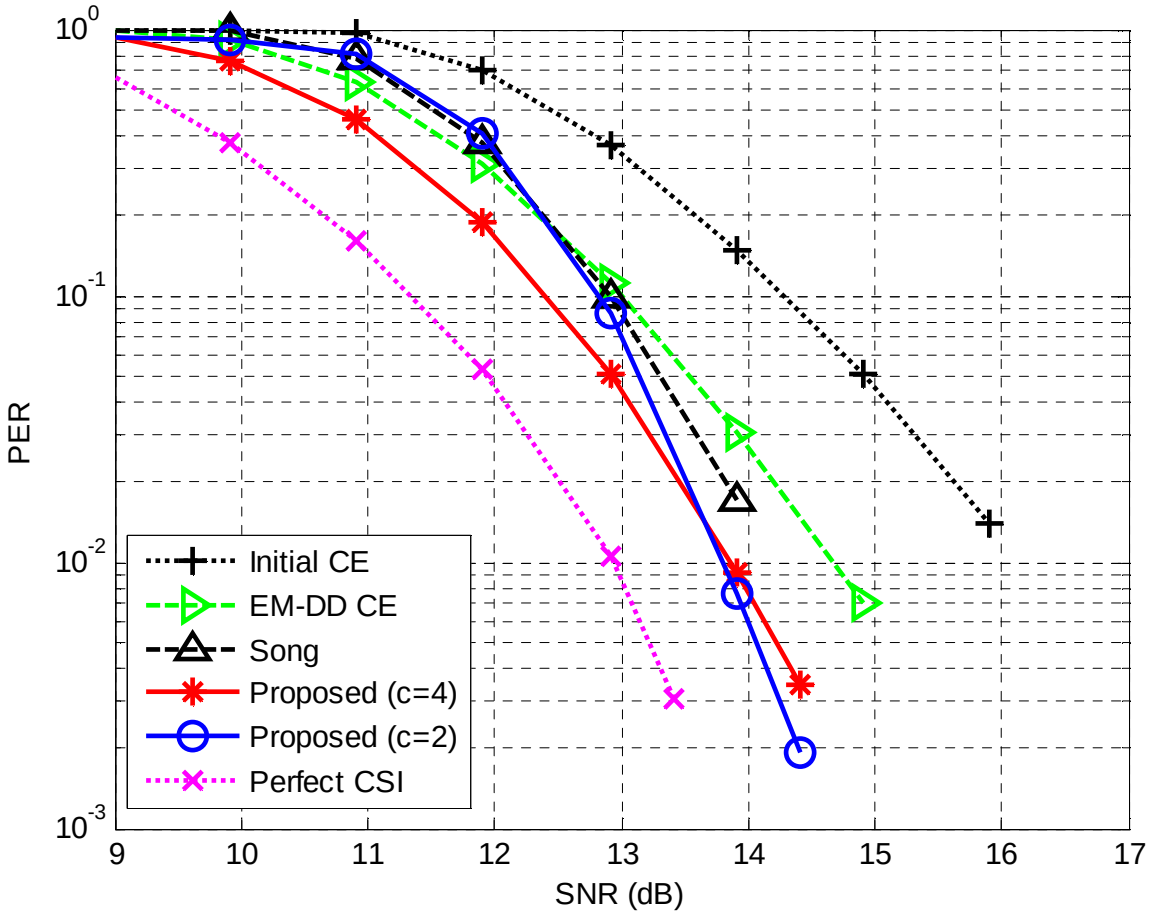

Figure 3.10: PER simulations of the proposed Kalman-based CE and conventional CEs in the 3x3 SM-MIMO-OFDM system(9 iterations)

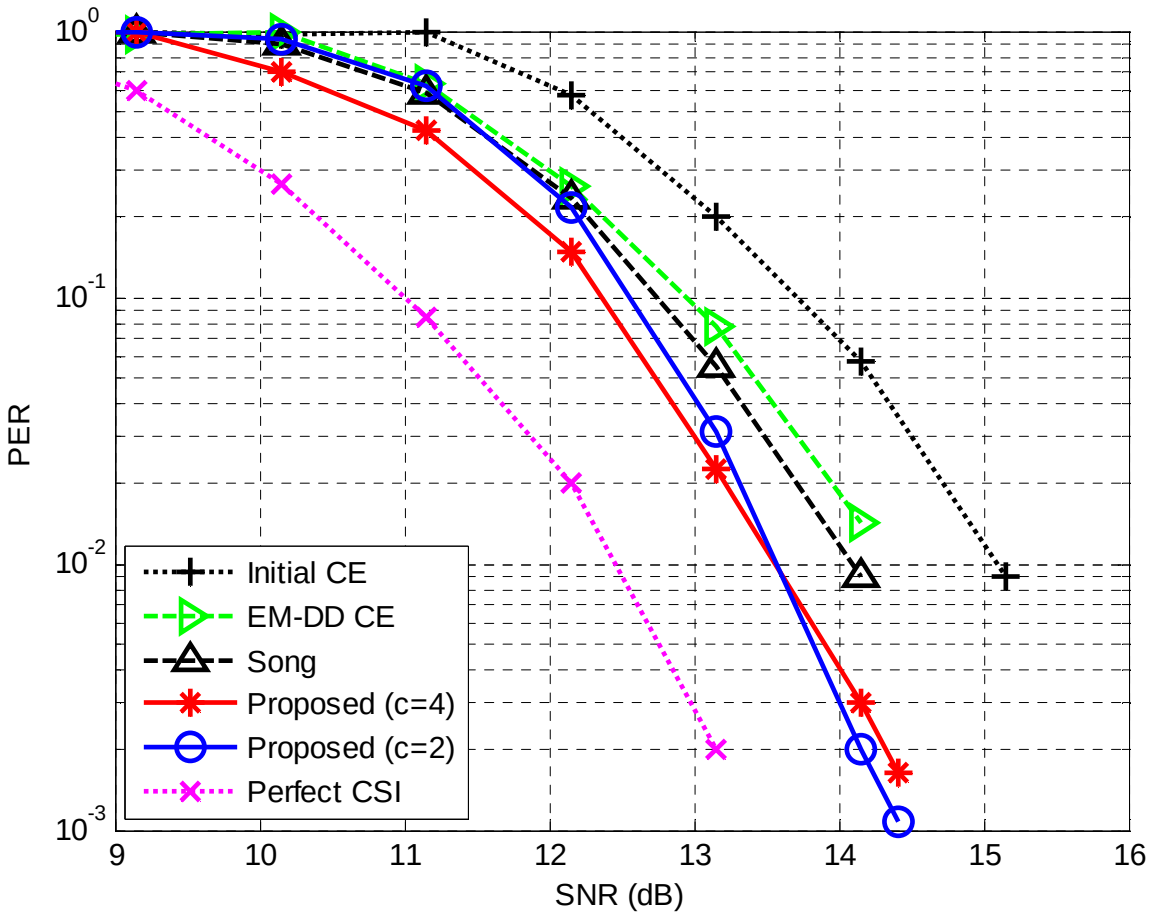

Figure 3.11: PER simulations of the proposed Kalman-based CE and conventional CEs in the 4x4 SM-MIMO-OFDM system (9 iterations)

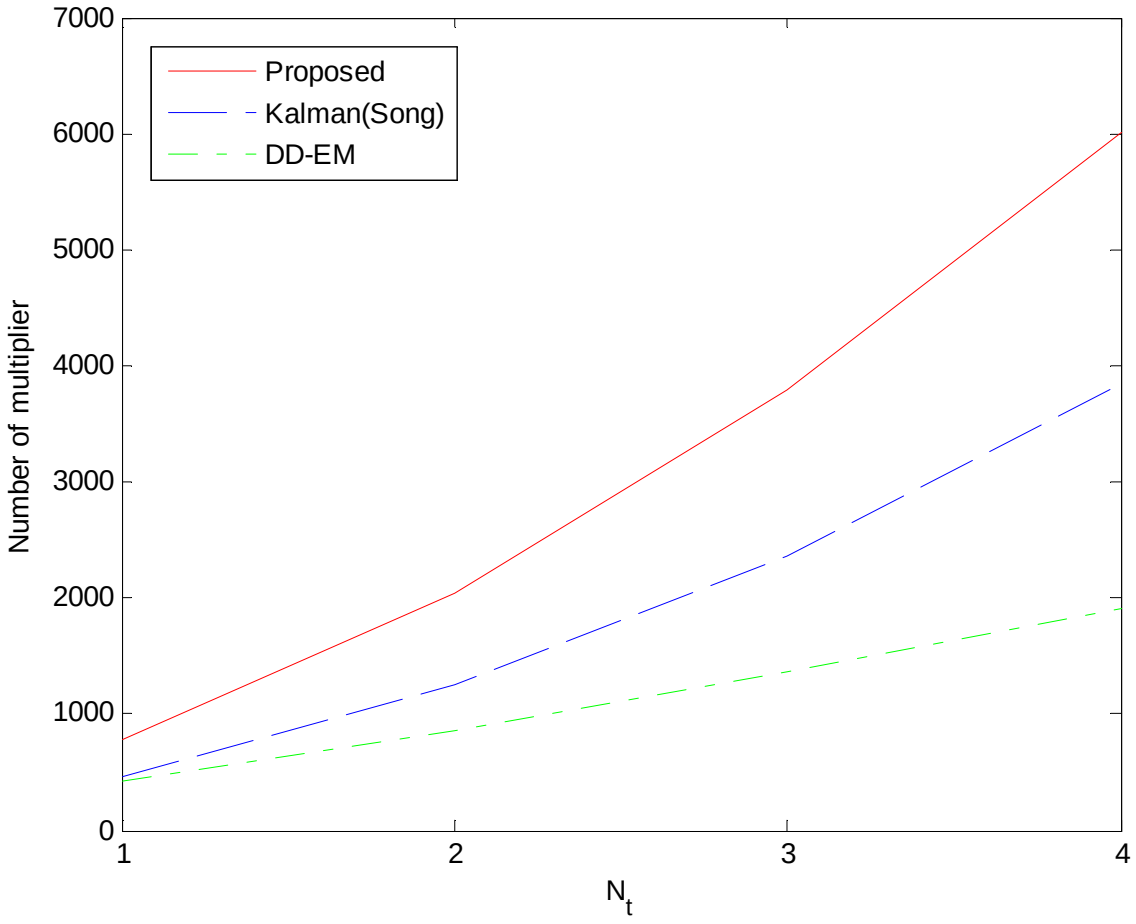

Figure 3.12: Complexity comparison : the number of multipliers used in the proposed Kalman-based CE, Song's CE and the EM-DD CE

Algorithm	Number of multiplication
Proposed CE	$N_tN_rN_d(10+8N_t+N_d)+2N_tN_r(2N_t+N_f+2)+3N_tN_d+2N_r+2N_r\mathbf{O}(N_t^3)$
Song's CE	$2N_r\mathbf{O}(N_t^3)+4N_t^2(N_r+2N_bN_r)+N_t(10N_bN_r+N_b^2N_r+4N_r+3N_b)$
DD-EM CE	$\mathbf{O}(N_t^3)+4N_t^2N_b+4N_t(3N_bN_r+N_r)+N_bN_r+4N_b^3$

Table 3.1: Complexity comparison : the number of multipliers used in the proposed Kalman-based CE, Song's CE and the EM-DD CE

3.6 Discussions

A sequential soft-decision-directed channel estimation algorithm for MIMO-OFDM systems has been proposed for the specific pipelined turbo-receiver architecture. The algorithm deals with observation sample sets with varying levels of reliability. In coping with decision errors that propagate in the pipeline, we have introduced a novel method of innovating a correlated observation sequence via puncturing. Based on the refined innovation sequence, a Kalman-based estimator has been constructed. The proposed algorithm establishes improved Kalman-based channel estimation where the traditional innovations approach cannot create a true innovation sequence due to soft-decision error propagation. The EXIT chart, MSE analysis and PER simulation results have been used to validate the performance advantage of the proposed channel estimator.

Chapter 4

Low-Complexity Iterative Channel Estimation for Turbo Receivers

4.1 Overview

This chapter discusses a receiver-side channel estimation algorithm well-suited to turbo equalizers for MIMO-OFDM systems. The proposed technique is a Kalman-based channel estimator that runs on parallel single-input single-output channels. Soft-decision-feedback interference cancellation is utilized to reduce the MIMO channel estimation problem into multiple SISO channel estimation problems. Unlike existing methods, however, the inherent correlation that exists among successive inputs of the Kalman estimator is suppressed via careful puncturing of observation samples. The quality of soft decisions and channel estimates are also continuously monitored and incorporated in the Kalman filter update process. This chapter is written based on the published paper [36].

4.2 Low-Complexity Kalman-Based Channel Estimation

We assume the SM-MIMO-OFDM transmitter in Fig.2.2 and use the turbo receiver introduced in in Chapter 2.1. In the research, we utilize the general IDD structure without the pipeline in order to make a general application of the proposed low-complexity channel estimator. The M-QAM symbol sequence from is sent through a wireless channel by an OFDM TX. The received signal on a particular frequency tone can be written as

$$\mathbf{z}_n = \mathbf{H}_n \mathbf{s}_n + \mathbf{n}_n, \tag{4.1}$$

where $\mathbf{z_n} = [z_n^{(1)}, z_n^{(2)}, \cdots, z_n^{(N_r)}]^T$ denotes the signal samples received at the N_r receiver (RX) antennas, $\mathbf{H}_n$ is the channel response matrix corresponding to all TX-RX antenna links with its $(r,t)^{th}$ element representing the link between the t^{th} TX antenna and the r^{th} RX antenna, $\mathbf{s_n} = [s_n^{(1)}, s_n^{(2)}, \cdots, s_n^{(N_t)}]^T$ are the transmitted symbols from the N_t TX antennas, and $\mathbf{n}_n$ is an $N_r \times 1$ vector of additive white Gaussian noise (AWGN) samples with zero mean and variance $\mathcal{N}_0$. An IEEE 802.11n packet is also provided with a special training sequence for initial channel estimation [27]. The initial channel estimation is performed by the least square (LS) estimator introduced in Chapter 3.3.1.

The turbo-equalization strategy can be applied to the MIMO-OFDM communication receiver [6, 18]. The turbo equalizer or IDD modules consist of the soft-input soft-output (SISO) decoder and the SISO demapper, as shown in Fig. 3.1. In our simulator, the soft MMSE-demapping algorithm is used for the SISO demapper [6], and the soft-output Viterbi algorithm (SOVA) is used for the SISO decoder implementation [30].

4.2.1 Linear Successive Interference Cancellation Based on Soft Decisions

The transmitted signal through a given TX-RX antenna link is affected by interferences coming from other TX antennas. One way to remove interference is to linearly cancel it out

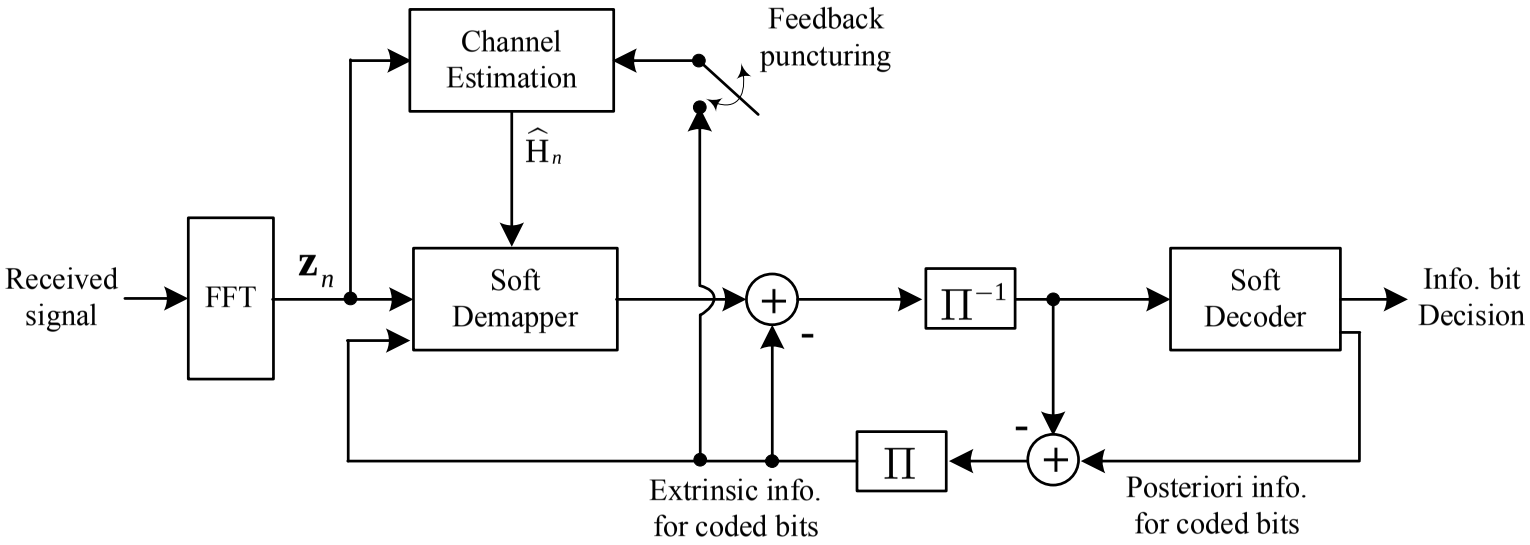

Figure 4.1: Block diagram of the turbo receiver and the soft-decision-directed channel estimator

using soft-decision feedback and the most recent channel estimate [35]. The iterative detection algorithm with successive interference cancellation (SIC) in [35] makes soft decisions while including the effect of soft-decision errors within the noise variance estimate. Monitoring the potential decision errors is effective in mitigating error propagation observed in decision-feedback schemes. The channel estimation error and the feedback decision error affect each other and cause error propagation. Our previous work in [33] also discussed potential interference from the channel estimation error and the soft-decision error and a strategy to handle it in optimal decision-feedback estimator design. In this work, we focus on a low-complexity technique that avoids matrix inversion during channel estimation. The proposed channel estimator utilizes SIC to resolve complex MIMO estimation into a single-input single-output setup. While applying SIC, the potential impact of the channel estimation and feedback soft-decision errors is monitored by estimating and tracking the interference variance.

The MIMO channel interference is cancelled using the soft decisions fed back from the soft decoder. The soft symbol decision $\tilde{s}$ is defined as the average of the constellation symbols with the averaging based on the estimated symbol probabilities, i.e., $\tilde{s} = \sum_{s_j \in \mathcal{A}} s_j P(s_j)$ where $P(s_j)$ can be taken as the "extrinsic probability" obtained from conversion of the available extrinsic LLR.

We notice that not all symbols in the M-QAM constellation has significant probabilities. Accordingly, only those QAM symbols associated with high extrinsic probabilities are considered. For example, the soft symbol decision is approximated as

$$\tilde{s} = \sum\nolimits_{s_j \in A^{\{4\}}} s_j P_4(s_j), \tag{4.2}$$

where $P_4(s_j)$ is defined as the normalized probability $P_4(s_j) = P(s_j) / \left(\sum_{s_j \in A^{\{4\}}} P(s_j) \right)$, and $A^{\{4\}}$ indicates an M-QAM sub-constellation containing only four highly probable symbols. This approximation leads to a reduced computational load with little performance

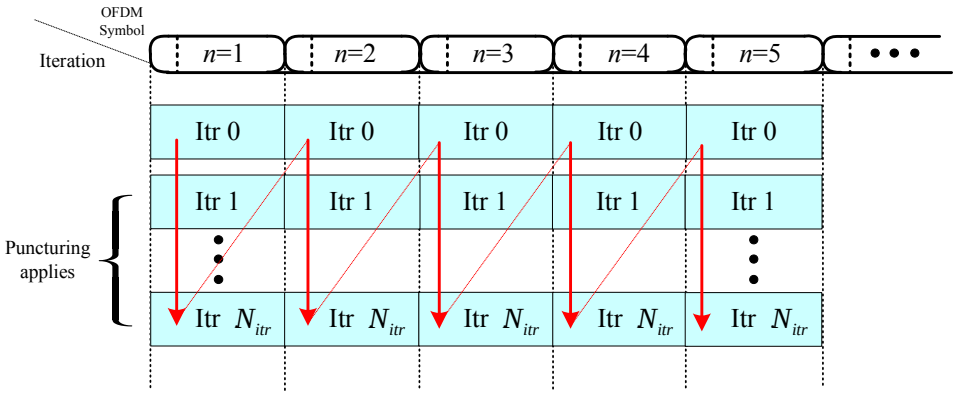

Figure 4.2: OFDM-symbol processing procedure in IDD

loss. The SIC scheme using soft decision feedback can be summarized as

$$\tilde{z}_n^{(r,t)}[i] = z_n^{(r)} - \sum_{\substack{j=1 \\ j\neq t}}^{N_t} \hat{h}_n^{(j,r)}[i-1]\tilde{s}_n^{(j,r)}[i] = h^{(r,t)}\tilde{s}_n^{(r,t)}[i] + u_n^{(r,t)}[i], \tag{4.3}$$

where $\tilde{z}^{(r,t)}$ denotes the received signal associated with the t^{th} TX– r^{th} RX channel link. Subscript n corresponds to the received OFDM symbol time index, and variable i points to the IDD iteration number $(0 \leq i \leq N_{itr})$, where N_{itr} denotes the number of the IDD iterations required to achieve satisfactory error rate performance. IDD iterations are applied sequentially to each OFDM symbol; for each n value, index i increases from 0 to N_{itr}, as illustrated like in Fig.4.2. The estimate $\hat{h}_n^{(r,t)}[i-1]$ is the available up-to-date channel estimate, whether from the initial channel estimation process or from the previous channel estimation cycle, and $u_n^{(r,t)}[i]$ represents noise plus any potential remaining interference after SIC is attempted at the i^{th} IDD iteration.

The estimate for each TX-RX channel link is obtained assuming all parallel channel responses are independent. In developing a Kalman-based channel estimation algorithm, one would naturally try to set up an innovation sequence using the observation signal $\tilde{z}$, but as discussed below, significant caution is in order.

4.2.2 Soft-Decision-Directed Kalman Channel Estimator

An innovation sequence is a white sequence that is a causal and casually invertible linear transformation of the observation sequence [28]. Unfortunately, the observation signal $\tilde{z}$ cannot lead to a reliable innovation sequence to develop a Kalman filter. In an attempt to derive a scalar version of the Kalman channel estimator, one would set up an innovation sequence as

$$\begin{aligned} x_n^{(r,t)}[i] &\triangleq \tilde{z}_n^{(r)}[i] - \hat{h}_n^{(r,t)}[i-1]\tilde{s}_n^{(t)}[i] \\ &= \sum_{j=1}^{N_t} \varepsilon_n^{(r,j)}[i-1]s_n^{(t)} - \sum_{j=1}^{N_t} h^{(r,j)}e_n^{(j)}[i] + n_n^{(r)} \ . \end{aligned} \tag{4.4}$$

where $e_n[i]$ and $\varepsilon_n^{(r,j)}[i]$ are defined as $e_n[i] \triangleq s_n - \tilde{s}_n[i]$ and $\varepsilon_n^{(r,j)}[i] \triangleq h^{(r,j)} - \hat{h}_n^{(r,j)}[i]$ respectively. With an understanding that we focus on a specific channel link, the TX–RX antenna indices t and r are dropped from (5.3) to reduce notational cluttering. The sequence $[\, x_0[0], .., x_0[N_{itr}], x_1[0], ..., x_1[N_{itr}], x_2[0], ..., x_n[N_{itr}]\,]$ would set up an innovation sequence, if the $\varepsilon_n[i]$ and $e_n[i]$ in (5.3) are proven uncorrelated over time n and iteration i. However, it is not difficult to see $x_n[i]$ is a correlated sequence. First, the AWGN noise component cannot be innovated during iterations, because the noise sample n_n is fixed for $i = 1, .., N_{itr}$. At least, the sequence x_n has correlation as $E\left[x_n[i-k]x_n^*[i]\right] \geq \mathcal{N}_o$ $(k > 0)$. Secondly, when the IDD makes erroneous decisions, $\varepsilon_n[i]$ and $e_n[i]$ are correlated with $\varepsilon_n[i-k]$ and $e_n[i-k]$ respectively, then correlated errors circulate among IDD blocks as well as the channel estimator during iterations [33].

In an effort to whiten the channel estimator input sequence, an useful insight is obtained from the well-known Gram-Schmidt procedure. Write $x_n^{'}[i] = x_n[i] - \frac{\langle x_n[i], x_n[i-k]\rangle}{|x_n[i-k]|^2} x_n[i-k], (k > 0)$, where $< a, b >$ denotes the inner product: $< a, b >= Re(a)Re(b) + Im(a)Im(b)$. Assuming there is no correlation between $Re(x_n)$ and $Im(x_n)$, we can write $E\left[x_n[i]\, x_n^*[i-k]\right] = E\left[x_n^{'}[i]\, x_n^*[i-k]\right] + E\left[|x_n[i-k]\,|^2 \frac{\langle x_n[i],\, x_n[i-k]\,\rangle}{|x_n[i-k]|^2}\right] = E\left[\langle x_n[i], x_n^*[i-k]\rangle\right]$. For the current input $x_n[i]$, the highest correlation exists with $x_n[i-1]$. So, define $\beta_n[i] \triangleq \langle x_n[i], x_n[i-1]\,\rangle$, which is used to monitor the amount

of correlation. The main idea is to filter out the samples with correlated errors, i.e., drop the samples with $\mid \beta_n[i] \mid > c\mathcal{N}_o$. The positive constant c is an adjustable parameter that controls the threshold level. In this way, the samples with high correlated errors are blocked from entering the channel estimator; this is done by defining the switching function:

$$\begin{aligned} &w_n[i] = 1, \quad when \;\; i = 1 \;\; or \;\; |\beta_n[i]| \;\leq\; c\mathcal{N}_o \;\; for \;\; 2 \leq i \leq N_{itr} \\ &w_n[i] = 0, \quad otherwise. \end{aligned} \tag{4.5}$$

The Kalma filter halts the channel update process when $w_n[i] = 0$. The decision from the initial iteration $(i \neq 0)$ is not utilized in estimation as it is typically not reliable enough, whereas the decision at $i = 1$ is always used.

A sequential linear MMSE-based channel estimator is given as follows:

$$\begin{aligned} \hat{h}_n[i] &\triangleq \widehat{E}\left[h|x_n[i]\right] + \widehat{E}\left[h|x_n[i-1], .., x_n[1], x_{n-1}[N_{itr}], ..., x_0[1]\right] \\ &= K_n[i]x_n[i] + \hat{h}_n[i-1], \end{aligned} \tag{4.6}$$

where $K_n[i]$ is the Kalman-filter gain, which can be derived from the orthogonality principle. Start with $\overline{\left(h - K_n[i]x_n[i]\right)x_n^*[i]} = 0$ or $\overline{hx_n^*[i]} = \overline{\left(K_n[i]x_n[i]\right)x_n^*[i]}$. Since $\overline{hx_n^*[i]} = \overline{|\varepsilon_n[i-1]|^2\tilde{s}_n^*[i]}$ and $\overline{x_n[i]x_n^*[i]} = \overline{|\tilde{s}_n[i]\varepsilon_n[i-1]|^2} + \overline{|u_n[i]|^2}$, we can write

$$\begin{aligned} K_n[i] &= \left(\overline{x_n[i]x_n^*[i]}\right)^{-1}\overline{hx_n^*[i]} \\ &= \frac{M_n[i-1]\tilde{s}_n^*[i]}{M_n[i-1]\left|\tilde{s}_n[i]\right|^2 + \sigma_u^2[i]}, \end{aligned} \tag{4.7}$$

where $M_n[i]$ is the channel estimation error variance given as $M_n[i] \triangleq \overline{|h - \widehat{h}_n[i]|^2}$, and $\sigma_u^2[i]$ is the noise-plus-interference variance of $u_n[i]$. Utilizing (4.6), we can express $M_n[i]$ recursively as $M_n[i] = (1 - K_n[i]\tilde{s}_n[i])M_n[i-1]$. Finally, the sequential Kalman-based estimator incorporating the puncturing scheme of (4.5) can be summarized as

$$K_n^{'}[i] = \frac{w_n[i]\;M_n[i-1]}{M_n[i-1] + \sigma_u^2[i]/\left|\tilde{s}_n[i]\right|^2}, \tag{4.8}$$

$$M_n[i] = (1 - K_n^{'}[i])M_n[i-1] \tag{4.9}$$

$$\hat{h}_n[i] = K_n^{'}[i]\check{h}_n[i] + (1 - K_n^{'}[i])\hat{h}_n[i-1], \tag{4.10}$$

where $K_n^{'}[i]$ is a modified form of the Kalman-filter gain with puncturing, and $\check{h}_n[i]$ denotes the channel estimate based on the current observation. The initial estimate $\hat{h}_{-1}$ is obtained from the initial preamble-based channel estimator. Also, the initial error variance M_{-1} is derived from the mean square error (MSE) analysis in [31] as $M_{-1} = |\hat{h}_{-1}|^2/\{|\hat{h}_{-1}|^2 E_s/(N_t\mathcal{N}_o)+1\}$ where E_s is the signal power of the training symbol. Finally, in order to complete the estimator (5.4)-(5.6), we need to find : (i) the noise-plus-interference variance $\sigma_u^2[i]$ and (ii) the channel estimate $\check{h}_n[i]$.

The soft feedback decisions have different levels of reliability, and this needs be taken into account. From (4.3), the variance of the noise-plus-interference can be written as

$$\begin{aligned}\sigma_u^2[i] &= \mathcal{N}_o + \sum_{\substack{j=1\\ i\neq t}}^{N_t}\left(|h^{(j)}|^2\overline{|s_n^{(j)}-\tilde{s}_n^{(j)}[i]|^2} + \overline{|h^{(j)}-\hat{h}_n^{(j)}[i-1]|^2}\;|\tilde{s}_n^{(j)}[i]|^2\right)\\ &\approx \mathcal{N}_o + \sum_{\substack{j=1\\ j\neq t}}^{N_t}\left(M_n^{(j)}[i-1] + \overline{|\hat{h}_n^{(j)}[i-1]|^2}\right)\overline{|s_n^{(j)}-\tilde{s}_n^{(j)}[i]|^2} + M_n^{(j)}[i-1]\;|\tilde{s}_n^{(j)}[i]|^2 .\end{aligned} \tag{4.11}$$

Note $\overline{|h^{(j)}-\hat{h}_n^{(j)}[i-1]|^2}$ can be provided by the Kalman filter parameter $M_n[i]$, which indicates the quality of the estimate. The soft decision variance is evaluated as $\overline{|s-\tilde{s}|^2} = \sum_{s_j\in A^{\{4\}}}|s_j-\tilde{s}|^2 P_4(s_j)$, and an approximation $|h|^2 \approx \overline{|\hat{h}_n[i-1]+\varepsilon_n[i-1]|^2}$ is used in solving (4.11).

Next, using the extrinsic probabilities of M-QAM symbols, $\check{h}_n[i]$ can be found as

$$\check{h}_n[i] = \sum_{s_j\in\mathcal{A}^{\{4\}}}\frac{s_j^*\tilde{z}_n[i]}{|s_j|^2+\sigma_u^2[i]/|\hat{h}_n[i-1]|^2}P_4(s_j). \tag{4.12}$$

Note that (4.12) is the linear MMSE estimator derived for a fixed QAM symbol s averaged according to $P(s)$, which can be considered as an optimal estimator given $\tilde{z}_n[i]$ and the extrinsic probabilities, $(i.e., \check{h}_n = \sum_{s_j\in\mathcal{A}^{\{4\}}} E(h_n|\tilde{z}_n, s_j)P(s_j))$. Another possible variation for the estimator is

$$\check{h}_n[i] = \sum_{s_j\in\mathcal{A}^{\{4\}}}\frac{\tilde{z}_n[i]}{s_j}P_4(s_j)\;, \tag{4.13}$$

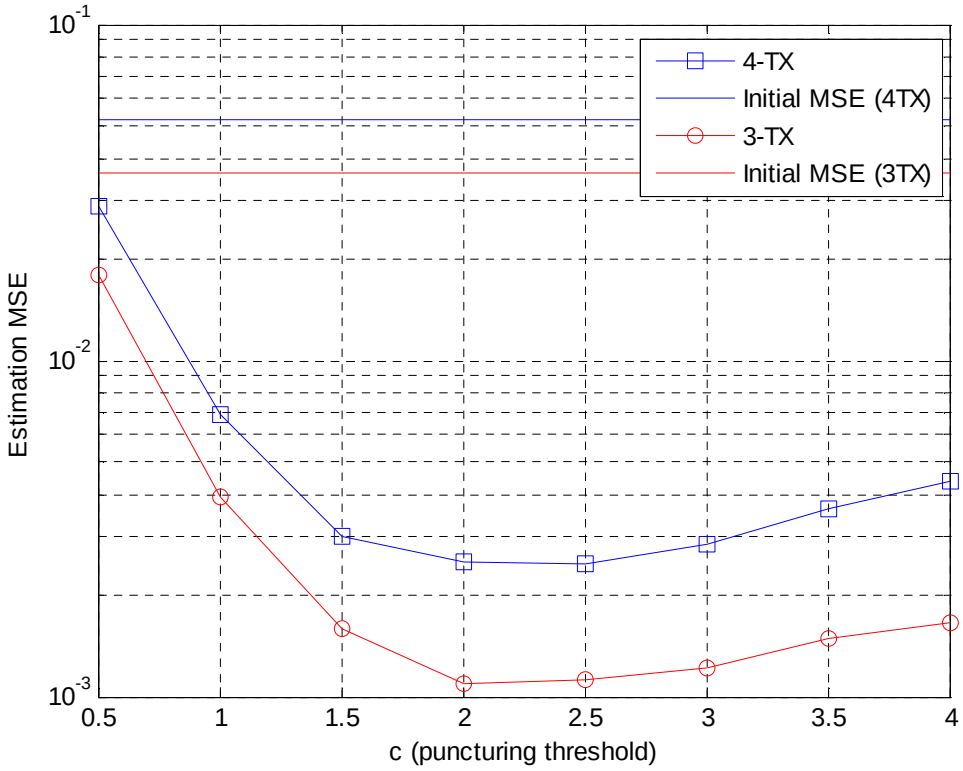

Figure 4.3: Threshold parameter c optimization for the low-complexity Kalman-based channel estimator

which is basically a weighted sum of the zero-forcing estimators. In the sequel, the estimator (4.13) is used in executing the recursive estimator of (5.4)-(5.6) and generating simulation results, as it was seen to be equally effective during our investigation.

We notice that the noise-interference variance σ_u^2 plays a key role in the Kalman update process. Based on the soft-decision reliability, the Kalman-filter solution is adaptively controlled by σ_u^2. Also, note that the constant c controls the estimation convergence speed and the amount of correlated errors, which can be traded in our channel estimator design. The existence of the optimum value for c is demonstrated with the initial channel estimation error by the MSE simulation results in Fig. 4.3. Our MSE simulation results in 3×3 and 4×4 systems show that the optimal c value is at 2 and 2.5, respectively.

4.3 Performance evaluation

The Kalman-based channel estimator [22] and the EM channel estimator [19] are compared to the proposed low-complexity channel estimator in terms of computation complexity and PER performance.

4.3.1 Complexity Comparison with Existing Channel Estimators

For performance comparison, the EM-based decision-directed (DD) estimator introduced in [19] as a variant of the EM estimator is set up as $\check{\mathbf{h}}_n^{(r)} = (\widetilde{\mathbf{S}}_n^H \widetilde{\mathbf{S}}_n)^{-1} \widetilde{\mathbf{S}}_n^H \mathbf{z}_n^{(r)}$, where $\mathbf{z}_n^{(r)}$ is an $N_b \times 1$ received signal vector buffering N_b OFDM symbols at the r^{th} RX, $\widetilde{\mathbf{S}}_n$ is a $N_b \times N_t$ matrix consisting of decoder-feedback soft symbols, $\mathbf{h}^{(r)}$ is a $N_t \times 1$ channel vector. This estimate is blended with the training-based channel estimate by the combining method of [20].

The iterative Kalman estimator using soft-decision feedback has been introduced in [22]. The proposed algorithm is compared with two versions of Kalman-based algorithms: a conventional scalar Kalman estimator and an optimum Kalman MIMO (matrix/vector version) channel estimator. The same SIC step is applied to the conventional scalar Kalman estimator, but the estimator only assumes additive random noise with variance $\mathcal{N}_o$ without considering the residual interference power. So, in the compared conventional scalar Kalman scheme, the gain update equation of (5.4) is replaced with $K_n'[i] = \frac{M_n[i-1]}{M_n[i-1]+\mathcal{N}_o/|\tilde{s}_n[i]|^2}$, while (4.10) and (5.6) remain the same. Also, the mean-symbol-based zero-forcing method [16] with $\check{h}_n[i] = \frac{\tilde{z}_n[i]}{\tilde{s}_n[i]}$ is employed instead of (4.13).

As for the comparison with the optimum MIMO Kalman-based estimator with full matrix operations, the Kalman estimator of [22] is modified. The scheme of [22] is designed to handle soft decisions with varying qualities by adjusting the effective noise variance but is unaware of the effect of correlation among successive estimator input samples caused by channel estimation errors. Also, since the scheme of [22] was introduced in the context

Algorithm	Number of multiplication
Proposed CE	$23N_tN_r + 18N_t$
Song's CE	$2N_r\mathbf{O}(N_t^3) + 4N_t^2(N_r + 2N_bN_r) + N_t(10N_bN_r + N_b^2N_r + 4N_r + 3N_b)$
DD-EM CE	$\mathbf{O}(N_t^3) + 4N_t^2N_b + 4N_t(3N_bN_r + N_r) + N_bN_r + 4N_b^3$

Table 4.1: Complexity comparison ; the number of a multiplier used in the proposed low-complexity CE, the optimal Kalman-based CE and EM-based CE.

of the intersymbol interference (ISI) channel, we modify it here to handle the multi-input-single-output (MISO) channel by setting up (i) the noise-interference variance update matrix $\mathbf{Q}_n^{(r)} = \text{diag}[\sum_{t=1}^{N_t}(p_n(t,t) + |\hat{h}_t[n-1]|^2)\sigma_s^2(n,i,t)]$, $i = 1,..,N_b$, (ii) the MMSE estimator $\mathbf{A}_n^{(r)} = (\widetilde{\mathbf{S}}_n^H(\mathbf{Q}_n^{(r)} + \mathcal{N}_o\mathbf{I}_{N_b})^{-1}\widetilde{\mathbf{S}}_n + \mathbf{P}_{n-1}^{(r)-1})^{-1}\widetilde{\mathbf{S}}_n^H(\mathbf{Q}_n^{(r)} + \mathcal{N}_o\mathbf{I}_{N_b})^{-1}$, (iii) the estimation error covariance matrix $\mathbf{P}_n^{(r)} = (\mathbf{I}_{N_t} - \mathbf{A}_n^{(r)}\widetilde{\mathbf{S}}_n)\mathbf{P}_{n-1}^{(r)}$, and (vi) the Kalman sequential update equation $\hat{\mathbf{h}}_n^{(r)} = \mathbf{A}_n^{(r)}\mathbf{z}_n^{(r)} + (\mathbf{I} - \mathbf{A}_n^{(r)}\widetilde{\mathbf{S}}_n)\hat{\mathbf{h}}_{n-1}$. To extend the matrix-version Kalman MISO estimator to the the case of MIMO channel estimation, we repeat the four steps above for each RX antenna signal vector. Existing channel estimators for MIMO channel links are designed based on matrix operations, and the computation load is largely caused by the corresponding multiplication operations. Assuming $N_r = 4$ RXs and $N_b = 4$ (buffer size), the total number of real multipliers versus the number of TX is presented in Table. 4.1 and Fig. 4.4. In the complexity computation, we assume the number of real multipliers for a matrix inversion goes as $\mathbf{O}(N_t^3)$ (as in the Gauss-Jordan elimination method). Overall, the matrix inversion causes a major computation load proportional to N_t^3. Fig. 4.4 shows that with $N_t = 4$, the proposed algorithm can operate with $1/7$ and $1/3$ computation load of the optimal Kalman estimator and of the EM estimator, respectively.

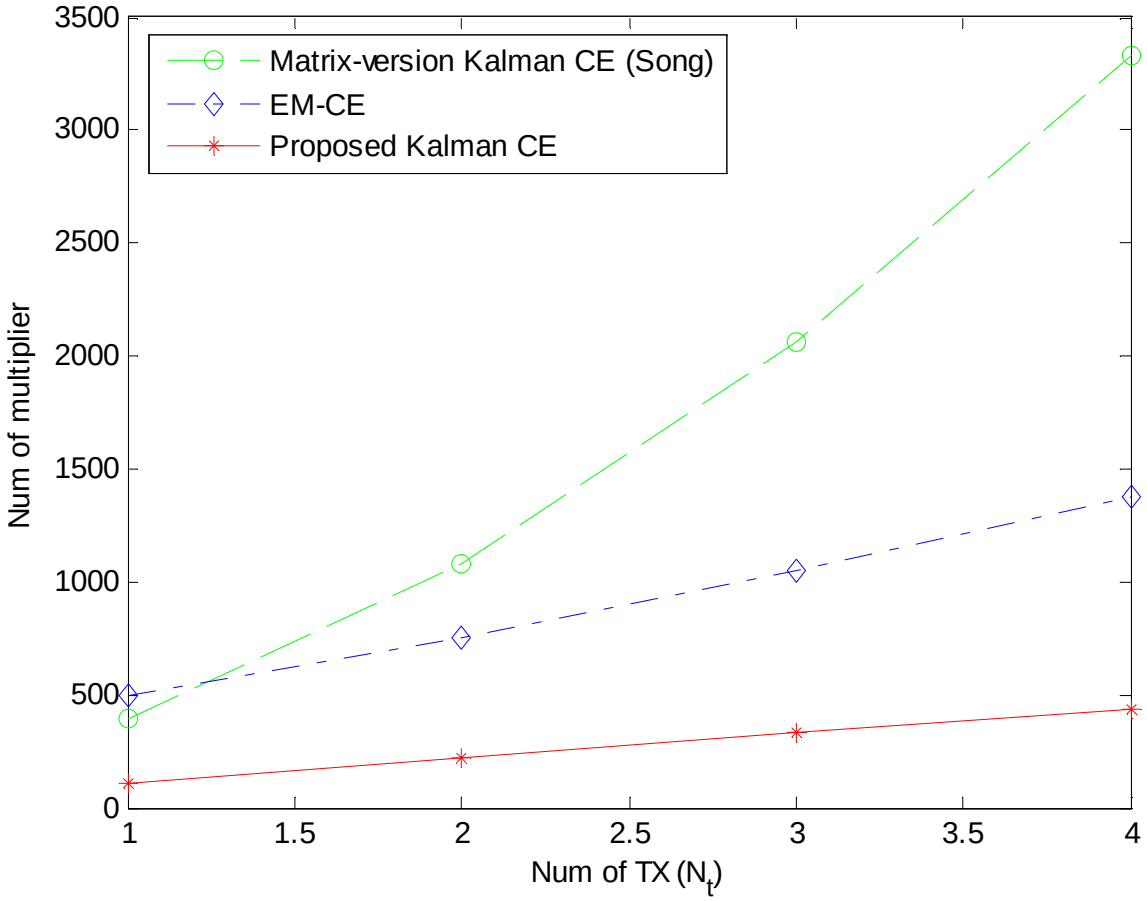

Figure 4.4: Complexity comparison ; the number of a multiplier used in the proposed low-complexity CE, the optimal Kalman-based CE and EM-based CE.($N_r = 4, N_b = 4$)

4.3.2 PER Simulation Results

In this section, we compare the receiver performance using the different channel estimation methods described in Section 4.3.1. The performance comparison is made in terms of PER versus SNR curves. Performance is evaluated for 3×3 and 4×4 16-QAM SM-OFDM systems. A rate 1/2 convolutional code is used complying with the IEEE 802.11n spec [27]. The transmitter sends packets that contain 1000 bytes of information. Required SNRs are compared with at the 1% PER level, at which practical WLAN systems reasonably operate. The simulated MIMO multi-path channel was modelled as a quasi-static multi-path channel with an exponential power profile with a root-mean-square (rms) delay of 50 ns. The channel responses are assumed uncorrelated across different antenna links.

For the sake of comparison, we also present PER curves for the cases of perfect CSI and perfect decision (PD) feedback knowledge respectively. In Fig. 4.5, the 3×3 SM-MIMO-OFDM system using only initial channel estimation (labelled 'initial CE') shows a 3 dB SNR degradation at a 10^{-2} PER relative to the perfect CSI curve. Considering computation complexity, the proposed algorithm shows competitive performance. The proposed estimator recovers a 1.2 dB of the 3 dB loss incurred by the initial estimation only. As compared to algorithms using full-matrix operation, the proposed algorithm achieves similar PER performance but with less computational load. Fig. 4.6 shows that the proposed algorithm shows slight performance degradation of 0.5 dB and 0.2 dB relative to the Kalman MIMO estimator (labelled 'Song') and the EM-DD MIMO estimator(labelled 'EM-DD'), respectively. Fig. 4.6 shows PER performance in the 4×4 SM-MIMO-OFDM system. The four TX antennas are the maximum number of antennas supported in the IEEE 802.11n standard. The proposed algorithm has a 0.8 dB advantage compared to the initial CE-only curve. Considering that the full-matrix Kalman MIMO channel estimator gets only 1 dB gain against the same scheme, it is safe to say that the proposed algorithm enjoys favorable complexity/performance tradeoff. Meanwhile, the mean-symbol-based algorithm (labelled 'Mean-symbol CE') lags behind noticeably in its performance relative to the proposed al-

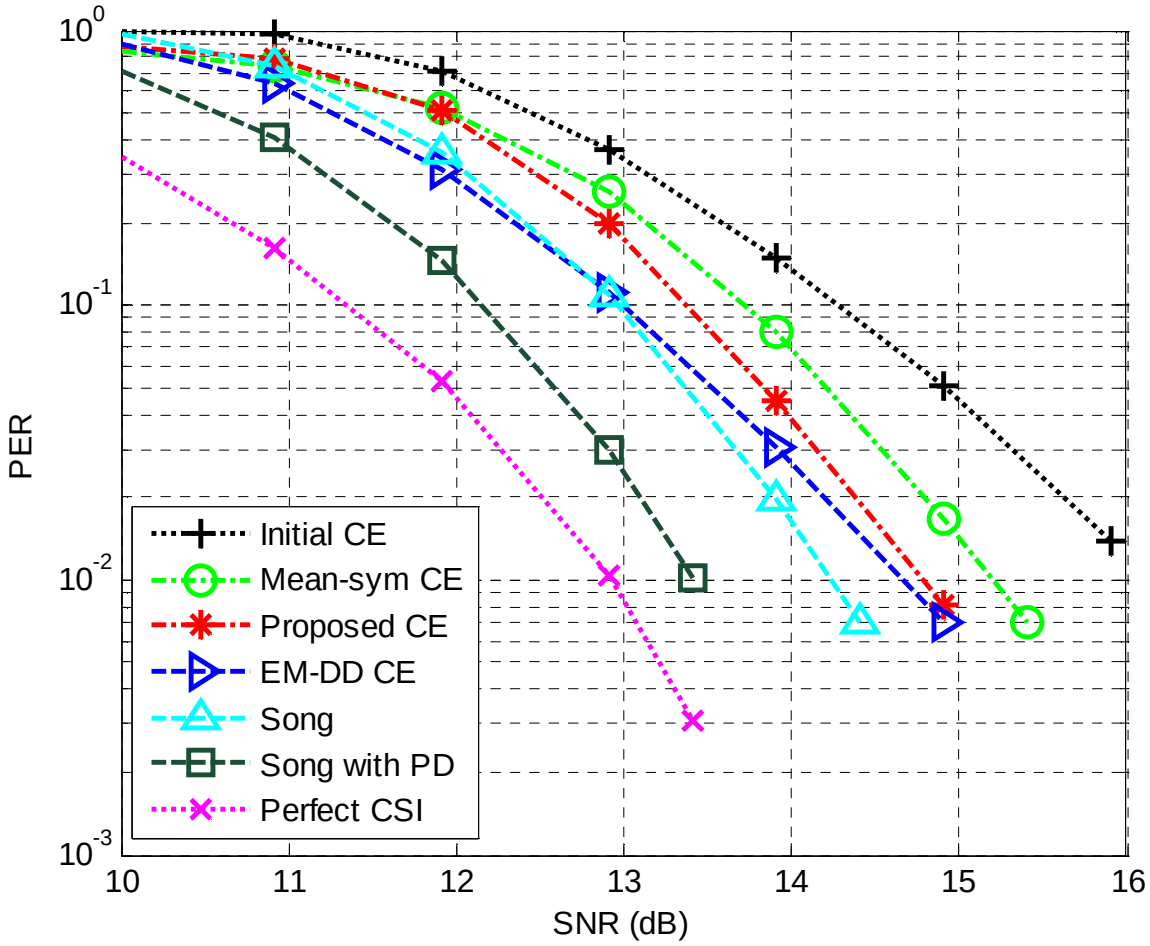

Figure 4.5: PER simulations of the low-complexity CE and the conventional CEs in the 3×3 SM-MIMO-OFDM turbo receiver (7 iterations, $c = 2$)

gorithm.

4.4 Discussions

A low-complexity Kalman-based channel estimation algorithm geared to turbo equalizers for MIMO-OFDM systems has been proposed. As shown in the performance evaluation results, MIMO receivers suffer significant performance loss due to imperfect CSI. It is desired to recover this loss, but existing MIMO channel estimation algorithms are computationally intensive. The proposed low-complexity algorithm resolves the MIMO channel estimation problem into multiple SISO channel estimation problems using SIC. The proposed channel estimator then tracks the combined power of noise and residual interference due to potential miss-cancellation in an effort to minimize the effect of error propagation. The scheme also utilizes a puncturing technique that drops correlated observation samples at the channel estimator input. Kalman-based channel estimators typically operate on the premise that the estimator input is an innovation sequence, a fallacy whenever channel estimation errors exist. Thus, puncturing has a tendency to correct this erroneous and harmful assumption. The proposed algorithm is well suited to iterative receivers, providing robust performance with a low computation load. The robust performance has been demonstrated via PER comparison with existing Kalman-based estimators as well as a representative EM-based estimator.

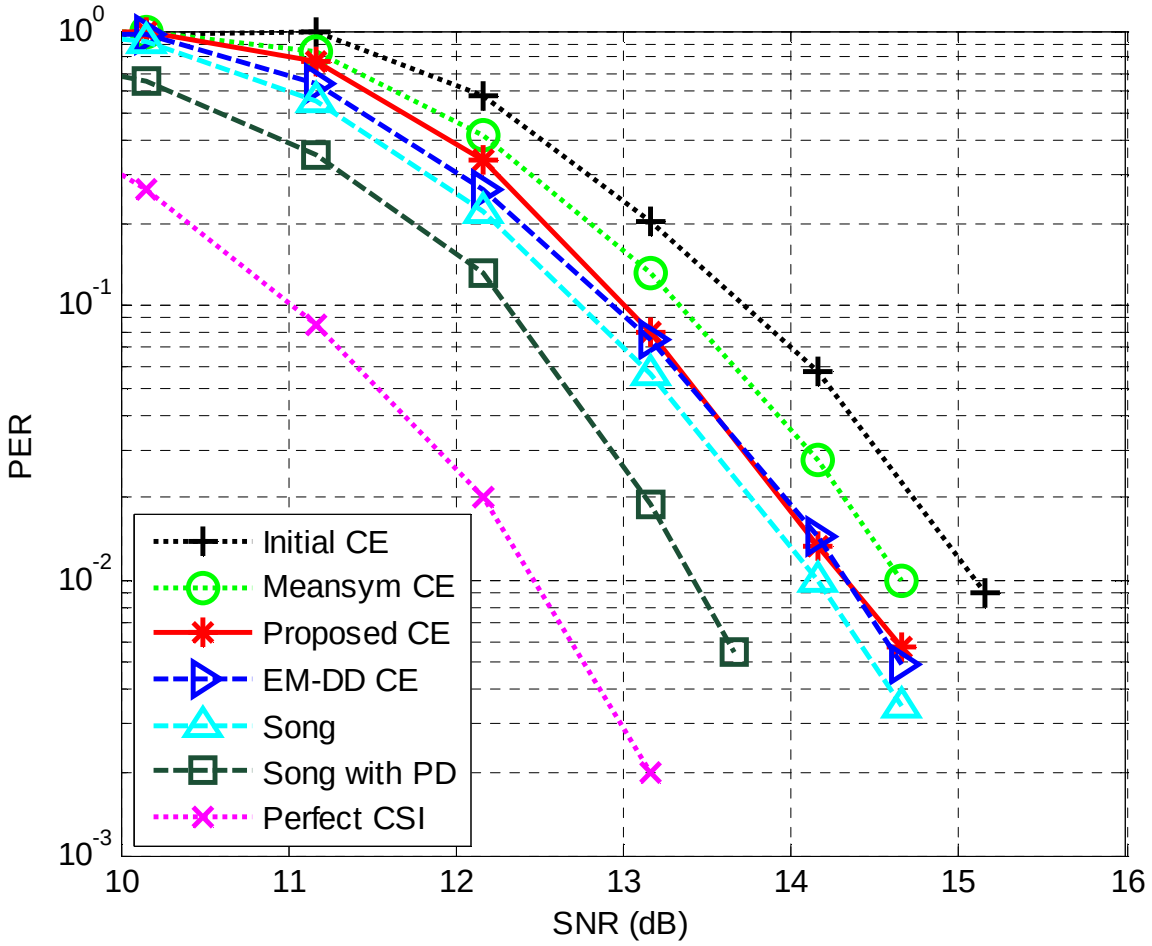

Figure 4.6: PER simulations of the low-complexity CE and the conventional CEs in the 4×4 SM-MIMO-OFDM turbo receiver (9 iterations, $c = 2.5$)

Chapter 5

Packet Recovery Algorithm using Turbo Equalization

5.1 Overview

A packet recovery scheme for the WLAN system is proposed. When a packet transmission fails, the identical packet is retransmitted using an acquisition (ACQ) procedure. However, frequent packet losses cause increased network loads as a result of packet retransmissions. Therefore, an effort to recover failed packets has the benefit of reducing redundant transmission loads in packet-based wireless communication systems. In this chapter, we develop a packet recovery method that enhances the receiving performance without causing increased network loads or using redundant parity information. The proposed algorithm performs error detection and correction using statistic decision information from IDD blocks. A new error detection scheme is proposed that screens out potential erroneous OFDM symbols by comparing the quality of soft decisions from IDD. Error OFDM symbols are corrected using additional IDD iterations. We note that correlated errors circulating between the IDD and a channel estimator are a major impediment that degrades turbo receiver performance. Our recovery scheme recovers a failed packet by whitening

the correlated error during the additional iterations.

5.2 System Model

We assume the SM-MIMO-OFDM transmitter in Fig.2.2 and use the turbo receiver introduced in in Chapter 2.1. In a transmitter, a data bit sequence is encoded by a convolutional channel encoder, and the encoded bit stream is divided to N_t spatial streams by a serial-to-parallel demultiplexer. Each spatial stream is interleaved separately, and the interleaved streams are modulated using an M-QAM symbol set $\mathcal{A}$. Since Q binary bits are mapped to an M-QAM symbol, a binary vector $\mathbf{b} = [b_0, b_1, \cdots, b_{QN_t-1}]^T$ is mapped to a transmitted symbol vector $\mathbf{s} = [s_1, s_2, \cdots, s_{N_t}]^T, (s_i \in \mathcal{A})$ is given from a set of $\mathcal{A}^{Nt}$, where $\mathcal{A}^{Nt}$ is the Cartesian product of M-QAM constellations. The M-QAM symbol sequence is allocated over 52 data frequency subcarriers in each spatial stream and transmitted by an OFDM TX, and let the number of data subcarriers $N_f = 52$. For a particular f^{th} subcarrier at the DFT output, the received signal of the n^{th} OFDM symbol can be written as

$$\mathbf{z}_n^{(f)} = \mathbf{H}\mathbf{s}_n^{(f)} + \mathbf{n}_n^{(f)} \ , \tag{5.1}$$

where $\mathbf{z}_n^{(f,r)} = [z_n^{(f,1)}, z_n^{(f,2)}, \cdots, z_n^{(f,N_r)}]^T$ is the received signal vector observed at N_r receive antennas, and, $\mathbf{H}$ is the channel response matrix associated with all wireless links connecting N_t transmitter antennas with N_r receiver antennas antennas, and each channel link is assumed to be a quasi-static within a packet. Also, $\mathbf{s}_n^{(f)}$ is the $N_t \times 1$ transmitted symbol vector, and $\mathbf{n}$ is a $N_r \times 1$ vector of uncorrelated, zero-mean AWGN samples with equal variance set to $\mathcal{N}_o$. The superscription indices is used for the frequency tone index and the TX-RX antenna index. In the receiver side, the IDD technique described in [6] that performs turbo equalization for MIMO systems is assumed. The extrinsic information on the coded-bit stream is exchanged in the form of LLR between the SISO decoder and the SISO demapper as shown in Fig. 5.1. A SOVA is used for a convolutional code [30]. Each data packet contains total N_s OFDM symbols, and each OFDM symbol in a packet

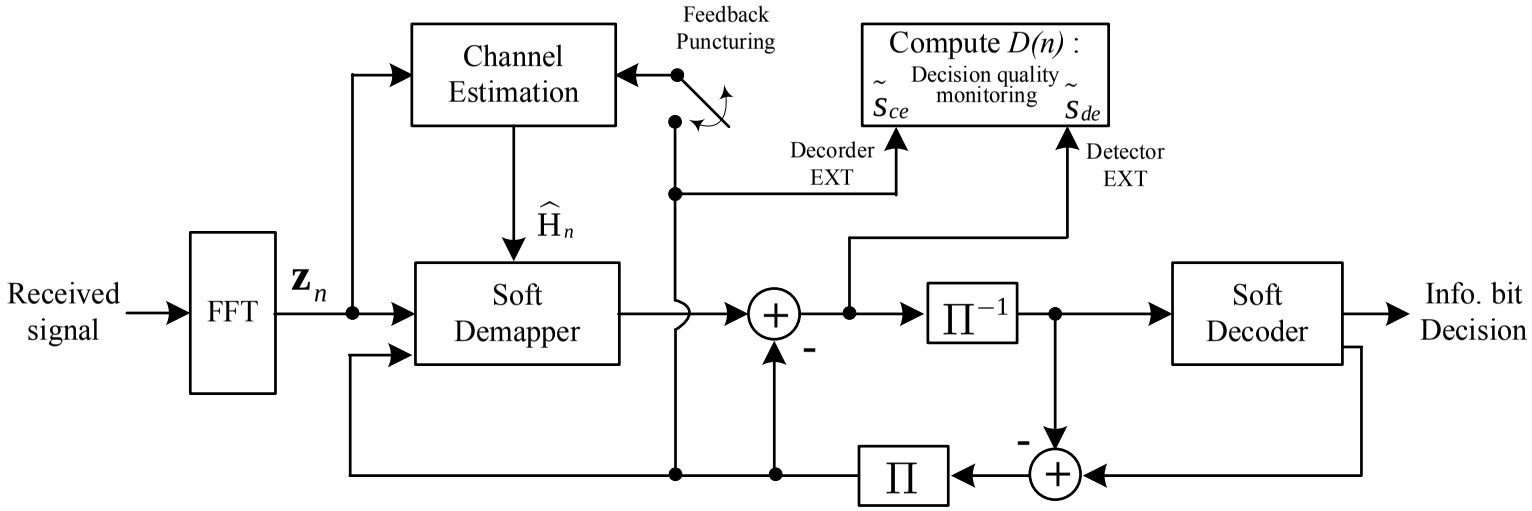

Figure 5.1: Turbo equalizer block diagram with the error monitoring scheme

is processed sequentially by the SISO demapper and the SISO decoder as they arrive at the receiver. Basically, N_i turbo iterations are applied sequentially to each OFDM symbol over a packet, that we set as a default receiving process. After finishing the default process, the receiver can check a packet validation using the CRC as in Fig.5.2. Assuming the OFDM symbols at $n = 2$ and $n = 3$ have error decisions in Fig.5.3, the packet is declared failed by the CRC check and additional IDD iterations are applied only to the OFDM symbols flagged by the decision-quality monitoring block. The monitoring method is discussed in the next session.

During the IDD iterations, the iterative channel estimation is applied to each frequency tone. Our previous research of [36] has proposed an iterative Kalman-based channel estimation for a practical receiver design. The channel estimator utilizes a SIC using the SISO decoder output, and it converts the MIMO channel estimation setup to the single-input-single-output channel setup. The SIC for the t^{th} TX – r^{th} RX link is performed as (temporarily drop index f)

$$\begin{aligned} \tilde{z}_n^{(r,t)}[i] &= z_n^{(r)} - \sum_{\substack{j=1 \\ j\neq t}}^{N_t} \hat{h}_n^{(j,r)}[i-1]\tilde{s}_n^{(j)}[i] \\ &= h\tilde{s}_n^{(t)}[i] + u_n^{(r,t)}[i], \end{aligned} \tag{5.2}$$

where $u_n^{(r,t)}[i]$ is a residual interference and noise after applying SIC to the t^{th} TX – r^{th} RX channel link. In order to set up the Kalman-filter-based channel estimator, we check the conditions of an innovation sequence at the filter input. A possible innovation sequence setup for $\tilde{z}_n^{(r,t)}[i]$ can be written as

$$\begin{aligned} x_n^{(r)}[i] &\triangleq \tilde{z}_n^{(r)}[i] - \hat{h}_n^{(r,t)}[i-1]\tilde{s}_n^{(t)}[i] \\ &= \sum_{j=1}^{N_t} \varepsilon_n^{(r,j)}[i-1]\tilde{s}_n^{(t)}[i] + \sum_{j=1}^{N_t} h^{(r,j)} e_n^{(j)}[i] + n_n^{(r)} \end{aligned} \tag{5.3}$$

where $e_n[i]$ and $\varepsilon_n^{(r,j)}[i]$ are defined as $e_n[i] \triangleq s_n - \tilde{s}_n[i]$ and $\varepsilon_n^{(r,j)}[i] \triangleq h^{(r,j)} - \hat{h}_n^{(r,j)}[i]$ respectively. The sequence $x_n^{(r,t)}[i]$ over $1 \leq i \leq N_i$ and $0 \leq n \leq N_s - 1$ becomes

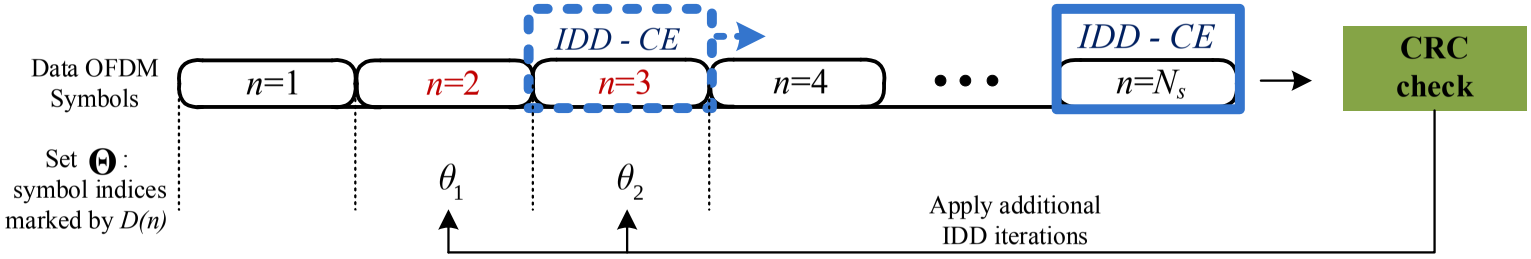

Figure 5.2: Block diagram of the packet recovery process

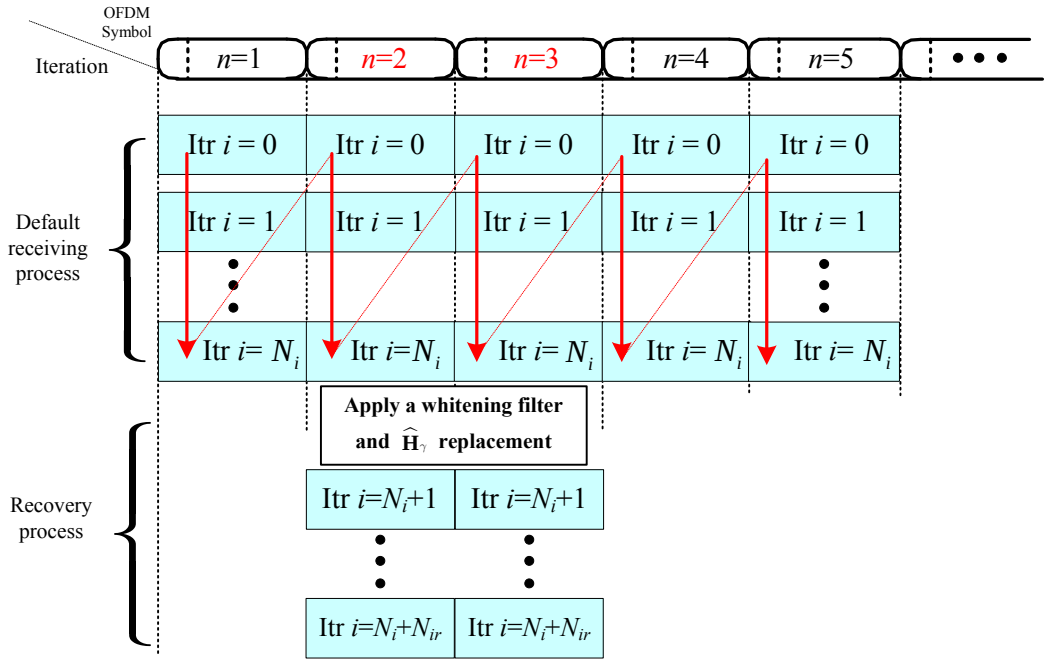

Figure 5.3: Packet processing timing diagram with the packet recovery

the residual interference and noise after SIC. In our previous work, we have discussed that the sequence $[x_0^{(r)}[1], x_0^{(r)}[2], .., x_0^{(r)}[N_i], ..., x_n^{(r)}[1], x_n^{(r)}[2], .., x_n^{(r)}[N_i]]$ is problematic to be used for the Kalman filter input because $\mathbf{x}_n$ is contaminated by correlated residual interference and noise [34]. In an effort to whiten the input sequence, we can investigate the correlation between the residual interference and noise samples. Our previous work in [34] has proposed a monitoring method : $E\,[\,x_n[i], x_n^*[i-1]] = E\,[\langle x_n[i], x_n[i-1]\,\rangle]$, where $< a, b >= Re(a)Re(b) + Im(a)Im(b)$. The samples with high correlated errors are blocked from entering the channel estimator by evaluating $\beta_n[i] \triangleq \langle x_n[i], x_n[i-1]\,\rangle$. The interface between the IDD blocks and the channel estimator is illustrated in Fig. 5.1. For a specific channel link at a subcarrier, the Kalman-based channel estimation is applied as

$$K_n[i] = \frac{w_n[i]\ M_n[i-1]}{M_n[i-1] + \sigma_u^2[i]/\,|\tilde{s}_n[i]|^2}, \tag{5.4}$$

$$M_n[i] = (1 - K_n[i])M_n[i-1] \tag{5.5}$$

$$\hat{h}_n[i] = K_n[i]\check{h}_n[i] + (1 - K_n[i])\hat{h}_n[i-1], \tag{5.6}$$

Note that $w_n[i]$ is a switching factor to puncture out the Kalman filter input with correlated error, where $w_n[i] = 1$ is set, when $\{i = 1\}$ or $\{|\beta_n[i]| \leq c\mathcal{N}_o$ for $2 \leq i \leq N_{itr}\}$. Otherwise $w_n[i] = 0$ is set. The constant c is a control parameter to evaluate the correlation amount in the filter input. Also, $\sigma_u^2[i]$ in (5.4) is a noise-plus-interference variance given as $\sigma_u^2[i] = \mathcal{N}_o + \sum_{\substack{j=1 \\ j \neq t}}^{N_t} \left(M_n^{(j)}[i-1] + \overline{|\hat{h}_n^{(j)}[i-1]|^2} \right) \overline{|s_n^{(j)} - \tilde{s}_n^{(j)}[i]|^2} + M_n^{(j)}[i-1] \left|\tilde{s}_n^{(j)}[i]\right|^2$, and $\check{h}_n[i]$ is given as

$$\check{h}_n[i] = \sum_{s_j \in \mathcal{A}} \frac{\tilde{z}_n[i]}{s_j} P(s_j). \tag{5.7}$$

The receiver performs the turbo equalization with the iterative channel estimation of 5.4 $\sim$ 5.6 in the default receiving procedure. After finishing it in the PHY layer, the CRC finally checks a packet validation in the MAC layer.

5.3 Packet Recovery Algorithm

5.3.1 Erroneous OFDM symbol detection

If either the channel estimates or feedback decisions are contaminated by significant errors, both the IDD blocks and the channel estimator are adversely affected. When this occurs, the soft-decisions and channel estimates diverge, and there is little that the receiver can do to fix it; it must declare an error packet for retransmission. In this case, the proposed algorithm starts the recovery mode to correct the major error upon completing the default receiving processes. The receiver can check the packet validation using CRC, however the CRC given by the IEEE.802.11n spec cannot make specific error correction information such as error-bit masks and error locations. The proposed scheme detects suspected error locations by comparing EXT information and marks error flags per an OFDM symbol. The flagged OFDM symbols are recovered through additional iterations with innovating channel estimates.

In order to compare soft-decision quality, define a soft decision based on the detector ELLR as

$$\tilde{s}_m^{(f,t)}(n) \triangleq \sum_{s_j \in A} s_j \; P_m^{(f,t)}(s_j) \tag{5.8}$$

where $\tilde{s}_m$ and P_m respectively indicates the detector ELLR-based soft symbol and probability of the last iteration ($i = N_i$) in the n^{th} OFDM symbol. Also, we define a soft decision of the SISO decoder as

$$\tilde{s}_c^{(f,t)}(n) \triangleq \sum_{s_j \in A} s_j \; P_c^{(f,t)}(s_j) \tag{5.9}$$

where $\tilde{s}_c$ and P_c indicates the decoder ELLR-based soft symbol and probabilities of the last iteration ($i = N_i$) in the n^{th} OFDM symbol. Using $\tilde{s}_m$ and $\tilde{s}_c$, soft-Euclidean distance is defined as

$$D(n) \triangleq \sum_{f=1}^{N_f} \sum_{t=1}^{N_t} \left| \tilde{s}_c^{(f,t)}(n) - \tilde{s}_m^{(f,t)}(n) \right|^2. \tag{5.10}$$

where $D(n)$ is a distance between soft decisions of the SISO detector and the SISO decoder per an OFDM symbol. During applying the default IDD iterations, $D(n)$ is saved in a buffer for the decision-quality monitoring block in Fig. 5.1. OFDM symbols with poor decision quality are marked based on $D(n)$. Intuitively, $D(n)$ measures a numerical amount of decision agreement between the SISO detector and SISO decoder. If the packet is declared invalid, the recovery scheme searches potential error locations based on $D(n)$. The rule for error-symbol marking is :

$$\boldsymbol{\Theta}_{N_b} = \left\{ \; n \; \mid \; [\max \; D(n)]_{N_b} \, , \quad n \in [0, .., N_s - 1] \; \right\} \tag{5.11}$$

where notation $[\max(\cdot)]_N$ is a set taking the maximum N elements, that gives a set $\boldsymbol{\Theta}_{N_b} = \{\theta_1, .., \theta_{N_b}\}$ consisting of OFDM-symbol indices having N_b largest elements of $D(n)$. Also, the IDD process selects one OFDM symbol index having the minimum distance $D(n)$ as

$$\gamma = \left\{ \; n \; \mid \; \min \; D(n) \, , \quad n \in [0, .., N_s - 1] \; \right\}, \tag{5.12}$$

which means that the decisions between the SISO detector and the SISO are the most well-matched in the selected OFDM symbol. The value of $D(n)$ is compared with the previous values during the default process, and an index γ is determined in the default receiving process. The channel estimates $\widehat{\mathbf{H}}_{\gamma}$ and the prediction error variances M_{γ} of the selected OFDM symbol are saved in a buffer for the recovery process.

While the SISO detector makes decisions based on the channel observations, the SISO decoder makes decisions based on the channel coding. These two kind of EXT decisions are generated based on different methods. If these decisions are not agreed, it is highly possible that either one of the decisions are error. Accordingly, the error distance can be an numerical indicator for error detection. We discuss details on the relation between the soft-symbol distance $D(n)$ and the decision quality in the chapter 5.4.

5.3.2 Error Recovery Scheme with IDD

Since the proposed recovery algorithm does not utilize redundant ECC parities at all, error information such as a error-bit mask or an error location is unknown. Instead, it relies on the IDD iteration power to find and correct error, but it does not simply run additional iterations over a whole broken packet. The proposed method corrects error by providing innovated channel information during the additional iterations. Basically, our innovation approaches in the recovery mode are proposed as : i) replacing the channel estimates with new estimates captured when decisions were reliable, ii) whitening correlated noise circulating the IDD blocks and the channel estimator. Mathematically speaking, an innovated sequence is defined as a white sequence providing unbiased information to an estimator. In a general sense, innovated information can also be understood as new information helping to escape from wrong convergence traps. We design the packet recovery algorithm based on these two concepts.

After finishing the default receiving process, a channel estimate $\widehat{\mathbf{H}}_{\gamma}$ and $\widehat{\mathbf{M}}_{\gamma}$ are obtained for the recovery mode. In the recovery mode, the SISO demapper starts with $\widehat{\mathbf{H}}_{\gamma}$,

additional N_{ir} iterations are applied to OFDM symbols marked in the set $\mathbf{\Theta}$. For the detection on marked OFDM symbols, the likelihood function in the recovery mode is given as

$$\begin{aligned} P\left[\mathbf{z}_\theta|\mathbf{s}_\theta\right] &= \prod_{r=1}^{N_r} \frac{1}{\sqrt{2\pi\widehat{\mathcal{N}}_o^{(r)}}} \exp\left(-\frac{|z_\theta^{(r)} - \widehat{\mathbf{h}}_\gamma^{(r)}\mathbf{s}_\theta|^2}{\widehat{\mathcal{N}}_o^{(r)}}\right) \\ &= \frac{1}{\left(\sqrt{2\pi}\right)^{N_r} \prod_{r=1}^{N_r} \widehat{\mathcal{N}}_o^{(r)}} \exp\left(-\sum_{r=1}^{N_r} \frac{|z_\theta^{(r)} - \widehat{\mathbf{h}}_\gamma^{(r)}\mathbf{s}_\theta|^2}{\widehat{\mathcal{N}}_o^{(r)}}\right), \end{aligned} \tag{5.13}$$

where the noise variance is given as $\widehat{\mathcal{N}}_o^{(r)} = |z_\theta^{(r)} - \sum_{t=1}^{N_t} \widehat{h}_\gamma^{(r,t)}[i]\ \tilde{s}_\theta^{(t)}[i]|^2$, ($\theta \in \mathbf{\Theta}$). With the given likelihood function, the soft MAP demapper directly gives out the posteriori LLR output L_P:

$$L_P\left(b_m\right) = \ln \frac{P\left(b_m = 1|\mathbf{z}_\theta\right)}{P\left(b_m = 0|\mathbf{z}_\theta\right)} \tag{5.14}$$

$$= \ln \frac{\sum\limits_{\mathbf{s}_\theta \in \mathcal{A}^{Nt}|b_m=1} P\left(\mathbf{z}_\theta|\mathbf{s}_\theta\right) \prod\limits_{j\neq i} P\left(b_j\right)}{\sum\limits_{\mathbf{s}_\theta \in \mathcal{A}^{Nt}|b_m=0} P\left(\mathbf{z}_\theta|\mathbf{s}_\theta\right) \prod\limits_{j\neq i} P\left(b_j\right)} + \ln \frac{P\left(b_m = 1\right)}{P\left(b_m = 0\right)}, \tag{5.15}$$

where $m = 0, ..., QN_t - 1$ for the individual bits in the transmitted symbol vector.

The MMSE demapper solution for the received signal in (5.1) is found as

$$\widehat{\mathbf{s}}_\theta = E[\mathbf{s}_\theta] + \mathbf{\Sigma}_\mathbf{s}\widehat{\mathbf{H}}_\gamma^H \left(\widehat{\mathbf{H}}_\gamma \mathbf{\Sigma}_\mathbf{s} \widehat{\mathbf{H}}_\gamma^H + \widehat{\mathcal{N}}_o \mathbf{I}\right)^{-1} \left(\mathbf{z}_\theta - \widehat{\mathbf{H}}_\gamma E[\mathbf{s}_\theta]\right), \tag{5.16}$$

where $E[\mathbf{s}]$ is a mean-symbol vector based on the $apriori$ probabilities, and $\mathbf{\Sigma}_\mathbf{s}$ is given as $\mathrm{diag}[\sigma_{s_0}^2, \ldots, \sigma_{s_{N_t-1}}^2]$, where $\sigma_s^2 = \sum_{s_j \in A} |s_j - \tilde{s}_j|^2\ P(s_j)$. In results, the SISO detector can be operated with the innovated channel estimate $\widehat{\mathbf{H}}_\gamma$.

As well as the channel estimate replacement, the whitening-filter approach is also effective to block the correlated error circulation. In decision-direct estimation manners, the error propagation is a critical problem inherent from wrong decision feedback or wrong estimation results [34]. However, it is very challenging for the receiver to completely remove the error propagation impact in the middle of the IDD process. Although the receiver can

attempt to monitor the signal quality, it is still unknown where error propagation specifically begins or how large tolerance the receiver has against error propagation. Therefore, we attempt to correct major errors upon completing the default receiving process.

In the recovery mode, a whiten filter is adopted to remove interference correlation at the channel estimator input. For a data subcarrier, SIC is applied using the decoder EXT as

$$\begin{aligned} \tilde{z}_{\theta}^{(r,t)}[i] &= z_{\theta}^{(r)} - \sum_{\substack{j=1 \\ j\neq t}}^{N_t} \hat{h}_{\gamma}^{(j,r)} \tilde{s}_{\theta}^{(j)}[i] \\ &= h\tilde{s}_{\theta}^{(t)}[i] + u_{\theta}^{(r,t)}[i], \end{aligned} \tag{5.17}$$

where $\theta \in \Theta$, and the residual interference and noise is obtained as $x_{\theta}^{(r)}[i] = z_{\theta}^{(r)} - \sum_{t=1}^{N_t} \hat{h}_{\gamma}^{(t)} \tilde{s}_{\theta}^{(t)}[i]$ after canceling out all TX signals.

First, we investigate correlation between $u_n^{(r)}[N_i]$ in (5.3) and $u_{\theta}^{(r)}[N_i+1]$ for the whitening filter design. Note that the variables with subscription θ indicates samples generating in the recovery mode, and the samples with subscription n are obtained from the default process. The additional iterations in the recovery mode are applied up to N_{ir} times. Using $u_n^{(r)}[N_i]$ and $u_{\theta}^{(r)}[N_i+1]$, we set up a received signal vector as (drop TX-RX antenna indices temporarily)

$$\underbrace{\begin{bmatrix} \widetilde{z}_n[N_i] \\ \widetilde{z}_{\theta}[N_i+1] \end{bmatrix}}_{\widetilde{\mathbf{z}}_{\theta}} = h \underbrace{\begin{bmatrix} \widetilde{s}_n[N_i] \\ \widetilde{s}_{\theta}[N_i+1] \end{bmatrix}}_{\widetilde{\mathbf{s}}_{\theta}} + \underbrace{\begin{bmatrix} u_n[N_i] \\ u_{\theta}[N_i+1] \end{bmatrix}}_{\mathbf{u}_{\theta}}. \tag{5.18}$$

The covariance matrix of sample $u_n^{(r)}[N_i]$ and $u_{\theta}^{(r)}[N_i+1]$ is approximately found as

$$\begin{aligned} \mathbf{V}_{\theta} &= E[\mathbf{u}_{\theta}\mathbf{u}_{\theta}^H] \\ &= \begin{bmatrix} E[|u_n[N_i]|^2] & E[\, u_n^*[N_i],\, u_{\theta}[N_i+1]\,] \\ E[\, u_n[N_i]u_{\theta}^*[N_i+1]\,] & E[|u_{\theta}[N_i+1]|^2] \end{bmatrix} \\ &\approx \begin{bmatrix} |x_n[N_i]|^2 & < x_n[N_i],\, x_{\theta}[N_i+1] > \\ < x_n[N_i],\, x_{\theta}[N_i+1] > & |x_{\theta}[N_i+1]|^2 \end{bmatrix}. \end{aligned} \tag{5.19}$$

The matrix $\mathbf{V}_\theta$ is a positive definite, so $\mathbf{V}_\theta^{-1}$ can be factorized using Cholesky decomposition as

$$\mathbf{V}_\theta^{-1} = \mathbf{F}\mathbf{F}^H, \tag{5.20}$$

then matrix $\mathbf{F}$ is a whitening filter to $\mathbf{u}_\theta$ since

$$E\left[(\mathbf{F}\mathbf{u}_\theta)\,(\mathbf{F}\mathbf{u}_\theta)^H\right] = \mathbf{F}\mathbf{V}_\theta\mathbf{F}^H = \mathbf{F}\mathbf{F}^{-1}\mathbf{F}^{-H}\mathbf{F}^H = \mathbf{I}. \tag{5.21}$$

Using the whitening filter $\mathbf{F}$, we define

$$\begin{aligned} \widetilde{\mathbf{z}}_\theta^{'} &\triangleq \mathbf{F}\widetilde{\mathbf{z}}_\theta \\ &= \mathbf{F}\widetilde{\mathbf{s}}_\theta h \;+\; \mathbf{F}\mathbf{u}_\theta, \end{aligned} \tag{5.22}$$

The innovated channel estimate $\check{h}$ can be found as

$$\begin{aligned} \check{h}_\theta &= \left\{ \left(\widetilde{\mathbf{s}}_\theta^H\,\mathbf{F}^H\right)\;(\mathbf{F}\;\widetilde{\mathbf{s}}_\theta) \right\}^{-1} \left(\widetilde{\mathbf{s}}_\theta^H\,\mathbf{F}^H\right)\,\widetilde{\mathbf{z}}_\theta^{'} \\ &= \left(\widetilde{\mathbf{s}}_\theta^H\,\mathbf{V}_\theta^{-1}\,\widetilde{\mathbf{s}}_\theta\right)^{-1} \widetilde{\mathbf{s}}_\theta^H\,\mathbf{V}_\theta^{-1}\;\widetilde{\mathbf{z}}_\theta. \end{aligned} \tag{5.23}$$

The only thing requiring caution is that if the determinant of $\mathbf{V}_\theta$ becomes numerically zero, the $\mathbf{V}_\theta$ is not invertible. Actually, it happens when $u_\theta \approx u_n$, which means the recovery scheme cannot obtain innovated information from the vector $\widetilde{\mathbf{z}}_\theta$. In this case, the whitening filter is not numerically available. Therefore, a threshold is set for a determinant of $\mathbf{V}_\theta$: applying the whitening filter only when $|det(\mathbf{V}_\theta)| > 10^{-3}$. If the whitening filter is available, the Kalman channel estimator in (5.4) $\sim$ (5.6) updates the channel estimates using $\check{h}_\theta$ and M_γ.

5.4 Analysis on soft-symbol distance

In this analysis, we try to understand behaviors of the soft information distance $D(n)$. The proposed algorithm utilizes $D(n)$ as an indicator of decision quality. We prove that the

$D(n)$ has correlation with mutual information variation per an OFDM symbol, so monitoring $D(n)$ is effective to screen out OFDM symbols with poor quality decisions.

The results from monitoring $D(n)$ are actually used only for broken packet recovery. For valid packets, there is no need to run the recovery scheme. Therefore, our analysis targets are also about invalid packets. Soft symbols from the demapper EXT information are modeled as

$$\tilde{\mathbf{s}}_m(n) = \mathbf{s}(n) + \mathbf{e}_m(n), \tag{5.24}$$

and soft symbols from the SISO decoder EXT information can be written as

$$\tilde{\mathbf{s}}_c(n) = \mathbf{s}(n) + \mathbf{e}_c(n), \tag{5.25}$$

where bold variables indicate $N_f \times 1$ size vectors loaded in OFDM subcarriers. Also, $\mathbf{e}_m(n)$ and $\mathbf{e}_c(n)$ denote the soft decision error of the SISO demapper and the SISO decoder respectively.

$$\begin{aligned} \mathbf{d}(n) &\stackrel{\Delta}{=} \tilde{\mathbf{s}}_m(n) - \tilde{\mathbf{s}}_c(n) \\ &= \mathbf{e}_m(n) - \mathbf{e}_c(n), \end{aligned} \tag{5.26}$$

where the decision error $\mathbf{e}_m(n)$ and $\mathbf{e}_c(n)$ have zero mean and diagonal decision-error covariance $\mathbf{V}_{em} = \sigma_{em}^2\mathbf{I}$ and $\mathbf{V}_{ec} = \sigma_{ec}^2\mathbf{I}$ respectively. Then, the covariance of $\mathbf{d}(n)$ can be written as $\mathbf{V}_d = \mathbf{V}_{em} + \mathbf{V}_{ec}$.

From (5.24), (5.25) and (5.26), a model can be set up for mutual information computation as

$$\tilde{s}_m(\, n, f\,) = \tilde{s}_c(n, f) + d(n, f), \tag{5.27}$$

where f is a subcarrier index ($1 \leq f \leq N_f$). Note that (5.27) is set up with an assumption that the decisions of the SISO demapper have significant error comparing to the decoder output. With this assumption, we can write a relation between the two error variances as $\sigma_{em}^2 >> \sigma_{ec}^2$.

It is also possible to assume the other case in (5.27) for this analysis; $\tilde{s}_c(\,n,f\,) = \tilde{s}_m(n,f) + d(n,f)$ that assumes the decoder output has significant error. Generally speaking, the decoder output has more accurate decisions than the demapper output, so (5.27) holds with the general assumption. In fact, the analysis result on both assumption cases is identical in consequence, since $\mathbf{d}(n)$ is a relative distance between the detector and decoder outputs. The bottom line is that there is no way for the receiver to know which SISO block output has significant error, so it is reasonable to investigate the both of the both assumptions. If investigating the case that the soft decoder EXT are erroneous, the soft symbol notation $\tilde{\mathbf{s}}_m$ and $\tilde{\mathbf{s}}_c$ are simply exchanged in (5.27), but the result of this analysis is same at the end.

In (5.26), the variable $d(n,f)$ has a gaussian distribution function as

$$f\left(\mathbf{d}[n]\right) = \frac{1}{(2\pi)^{N_f/2}\left[\det\left(\mathbf{V}_d\right)\right]^{1/2}} \exp\left(-\frac{1}{2}\mathbf{d}_n^H \mathbf{V}_d^{-1}\mathbf{d}_n\right). \tag{5.28}$$

For the model in (5.27), the mutual information is computed. The mutual information with discrete QAM symbols is found as

$$I(\tilde{\mathbf{s}}_m, \tilde{\mathbf{s}}_c) = \sum_{s_j \in A} P(s_j) \int_{\tilde{s}_m} \int_{\tilde{s}_c} f(\tilde{s}_m, \tilde{s}_c|s_j) \log \frac{f(\tilde{s}_m, \tilde{s}_c|s_j)}{f(\tilde{s}_m|s_j) f(\tilde{s}_c|s_j)}\, d\tilde{s}_c d\tilde{s}_m. \tag{5.29}$$

Since the relative distance between $\tilde{s}_c$ and $\tilde{s}_m$ is equal, the conditional distribution is given as

$$f\left(\tilde{\mathbf{s}}_m|\tilde{\mathbf{s}}_c\right) = \frac{1}{(2\pi)^{N_f/2}\left[\det\left(\mathbf{V}_d\right)\right]^{1/2}} \exp\left(-\frac{1}{2}\left(\tilde{\mathbf{s}}_m - \tilde{\mathbf{s}}_c\right)^H \mathbf{V}_d^{-1}\left(\tilde{\mathbf{s}}_m - \tilde{\mathbf{s}}_c\right)\right) \tag{5.30}$$

In (5.29), we define $i_m(\tilde{s}_m, \tilde{s}_c|s)$ as

$$\begin{aligned} i_m(\tilde{s}_m, \tilde{s}_c|s) &\triangleq \log \frac{f(\tilde{s}_m, \tilde{s}_c|s)}{f(\tilde{s}_m|s) f(\tilde{s}_c|s)} \\ &= \log\left(\frac{\det(\mathbf{V}_d)}{\det(\mathbf{V}_{ec})}\right) - \left(\tilde{\mathbf{s}}_m - \tilde{\mathbf{s}}_c\right)^H \mathbf{V}_d^{-1}\left(\tilde{\mathbf{s}}_m - \tilde{\mathbf{s}}_c\right) \\ &\quad + \left(\tilde{\mathbf{s}}_c - \mathbf{s}\right)^H \mathbf{V}_{ec}^{-1}\left(\tilde{\mathbf{s}}_c - \mathbf{s}\right). \end{aligned} \tag{5.31}$$

The average (ergodic) mutual information of (5.31) is solved as

$$\begin{aligned} I \quad & (\tilde{\mathbf{s}}_m, \tilde{\mathbf{s}}_c) = \sum_{s \in A} P(s) E\left[i_m \left(\tilde{s}_m, \tilde{s}_c | s \right) \right] \\ = \quad & \sum_{s \in A} P(s) \int_{\tilde{s}_m} \int_{\tilde{s}_c} f(\tilde{s}_m, \tilde{s}_c | s) \log \frac{f(\tilde{s}_m, \tilde{s}_c | s)}{f(\tilde{s}_m | s) f(\tilde{s}_c | s)} \, d\tilde{s}_c \, d\tilde{s}_m \\ = \quad & \log \frac{\det(\mathbf{V}_d)}{\det(\mathbf{V}_{ec})} - E\left[\left(\widetilde{\mathbf{s}}_m - \widetilde{\mathbf{s}}_c \right)^H \mathbf{V}_d^{-1} \left(\widetilde{\mathbf{s}}_m - \widetilde{\mathbf{s}}_c \right) \right] + \sum_{s \in A} P(s) E\left[\left(\widetilde{\mathbf{s}}_c - \mathbf{s} \right)^H \mathbf{V}_{ec}^{-1} \left(\widetilde{\mathbf{s}}_c - \mathbf{s} \right) \right] \\ = \quad & \log \frac{\det(\mathbf{V}_d)}{\det(\mathbf{V}_{ec})}, \end{aligned} \tag{5.32}$$

since $E[(\tilde{\mathbf{s}}_m - \tilde{\mathbf{s}}_c)^H \mathbf{V}_d^{-1} (\tilde{\mathbf{s}}_m - \tilde{\mathbf{s}}_c)] = 1$ and $E[(\tilde{\mathbf{s}}_c - \mathbf{s})^H \mathbf{V}_{ec}^{-1} (\tilde{\mathbf{s}}_c - \mathbf{s})] = 1$. The result in (5.32) is based on the ergodic hypothesis, our scheme attempt to measure and compare the mutual information per an OFDM symbol unit.

Meanwhile, $i\left(\tilde{s}_d, \tilde{s}_c | s \right)$ is a function of time n, the result in (5.32) can numerically obtained by time averaging. Numerically, $E\left[i\left(\tilde{s}_d, \tilde{s}_c | s \right) \right]$ can be calculated as

$$\begin{aligned} E \quad & [i\left(\widetilde{s}_c, \widetilde{s}_m | s \right)] = \frac{1}{N_s} \sum_{n=0}^{N_s - 1} i\left(\widetilde{s}_d[n], \widetilde{s}_c[n] | s \right) \\ = \quad & \log \frac{\det(\mathbf{V}_d)}{\det(\mathbf{V}_{ec})} - \frac{1}{N_s} \sum_{n=0}^{N_s - 1} \left(\widetilde{\mathbf{s}}_m[n] - \widetilde{\mathbf{s}}_c[n] \right)^H \mathbf{V}_d^{-1} \left(\widetilde{\mathbf{s}}_m[n] - \widetilde{\mathbf{s}}_c[n] \right) \\ & + \frac{1}{N_s} \sum_{n=0}^{N_s - 1} \left(\widetilde{\mathbf{s}}_c[n] - \mathbf{s} \right)^H \mathbf{V}_{ec}^{-1} \left(\widetilde{\mathbf{s}}_c[n] - \mathbf{s} \right) \end{aligned} \tag{5.33}$$

Our interest is the second and third terms because the first term becomes a constant over time n. The variation of the two terms are shown as a function of the time average and indicates the quality of the OFDM-symbol-unit decisions. The minimum mutual information

is determined by the second term and the third term as

$$\begin{aligned}
&\min_n \; i_m(\tilde{s}_m[n], \tilde{s}_c[n]|s) \\
&= \max_n \left\{ (\tilde{\mathbf{s}}_m[n] - \tilde{\mathbf{s}}_c[n])^H \mathbf{V}_d^{-1} (\tilde{\mathbf{s}}_m[n] - \tilde{\mathbf{s}}_c[n]) - (\tilde{\mathbf{s}}_c[n] - \mathbf{s})^H \mathbf{V}_{ec}^{-1} (\tilde{\mathbf{s}}_c[n] - \mathbf{s}) \right\} \\
&= \max_n \left\{ (\mathbf{e}_m[n] - \mathbf{e}_c[n])^H \mathbf{V}_d^{-1} (\mathbf{e}_m[n] - \mathbf{e}_c[n]) - \mathbf{e}_c^H[n] \mathbf{V}_{ec}^{-1} \mathbf{e}_c[n] \right\} \\
&\approx \max_n \left\{ \mathbf{e}_m^H[n] \mathbf{V}_d^{-1} \mathbf{e}_m^H[n] + \mathbf{e}_c^H[n] \mathbf{V}_d^{-1} \mathbf{e}_c[n] - \mathbf{e}_c^H[n] \mathbf{V}_{ec}^{-1} \mathbf{e}_c[n] \right\} \\
&= \max_n \left\{ \mathbf{e}_m^H[n] \mathbf{V}_d^{-1} \mathbf{e}_m^H[n] + \mathbf{e}_c^H[n] \mathbf{V}_{em}^{-1} \mathbf{e}_c[n] \right\} \qquad (5.34)
\end{aligned}$$

An approximation in the forth line is applied since ignoring the cross product of $\mathbf{e}_c$ and $\mathbf{e}_m$ (i.e. $\sum_{f=0}^{N_f-1} e_c^*(n,f)\, e_m(n,f) \approx 0$, and an approximation of $\mathbf{V}_d \approx \mathbf{V}_{em}$ is possible because of $\mathbf{V}_d = \mathbf{V}_{em} + \mathbf{V}_{ec}$ and $tr(\mathbf{V}_{em}) >> tr(\mathbf{V}_{ec})$. Also constant scalings do not affect the index selection of min and max values in (5.34). By removing the constant inverse of $\mathbf{V}_d$ from (5.34), we have

$$\begin{aligned}
&\max_n \left\{ \mathbf{e}_m^H[n] \mathbf{e}_m[n] + \mathbf{e}_c^H[n] \mathbf{e}_c[n] \right\} \\
&= \max_n \left\{ (\tilde{\mathbf{s}}_m[n] - \tilde{\mathbf{s}}_c[n])^H (\tilde{\mathbf{s}}_m[n] - \tilde{\mathbf{s}}_c[n]) \right\}. \qquad (5.35)
\end{aligned}$$

The conclusion in (5.34) $\sim$ (5.35) indicates that screening the soft symbol distance $\mathbf{d}(n)$ has direct relation with the mutual information variation in an OFDM symbol. For the other case (i.e. $\tilde{s}_c(\, n, f\,) = \tilde{s}_m(n,f) + d(n,f)$), the same analysis procedure in (5.27) $\sim$ (5.35) can be applied, at last, it reaches to the same conclusion of (5.35). Therefore, no matter that the decoder or the demapper outputs have error, monitoring $\mathbf{d}(n)$ provides a effective method to screen the mutual information variation and indicate decision quality of an OFDM symbol.

Fig.5.4 shows the 16-QAM constellation of EXT soft-decisions of invalid packets. As our assumption in the (5.24) model, soft decisions from the demapper has larger variance than the decoder outputs, but part of the decisions can be reversal. The block monitoring $D(n)$ computes the euclidian distance between soft decisions in the Fig.5.4 (a) and (b) constellations. Fig.5.5 shows $D(n)$ behavior with the channel estimate error variation in

invalid packets. Each curve is obtained by measuring channel estimation MSE. The circle-marked curve in Fig.5.5 illustrates the channel estimation MSE of a max $D(n)$ OFDM symbol in a packet, and the star-marked curve illustrates the MSE in a min $D(n)$ OFDM symbol. The actual quality of the channel estimates used during the default process exists between the min and the max curves. The proposed scheme utilizes the channel estimates with the min $D(n)$ to reprocess the OFDM symbols flagged in set Θ. Consequentially, the additional IDD iterations can be run with improved quality of channel estimates. Therefore, the method replacing the channel estimates based on min $D(n)$ and max $D(n)$ is effective to provide innovated information for the recovery mode process.

5.5 Performance Evaluation

Performance is evaluated for the 2×2 16-QAM SM-MIMO-OFDM system. A rate 1/2 convolutional code is used complying with the IEEE 802.11n specification [27]. The transmitter sends packets that contain 1000 bytes of information. Required SNRs are compared with below the PER 10^{-2} level, at which practical WLAN systems reasonably operate. The simulated MIMO multi-path channel was modeled as a quasi-static multi-path channel with an exponential power profile with a root-mean-square (rms) delay of 50ns. The channel responses are assumed uncorrelated across different antenna links. After applying four default iterations ($N_i = 4$) in the normal mode, three additional iterations are applied in the recovery mode ($N_{ri} = 3$). Also, the set Θ can select 20 indices of which OFDM symbols are suspected to have error decisions. First, we need to analyze the length of error due to error propagation. Obviously, if most of OFDM symbols in a packet have significantly propagated error, then the partially reprocessing approach may not be effective. Therefore, We need to investigate distributions of the number of error OFDM symbols. We capture 2000 error packets at SNR=15.2dB and analyze the histograms of the number of error symbols. Fig.(5.6)-(a) illustrates a histogram of the number of error OFDM symbols

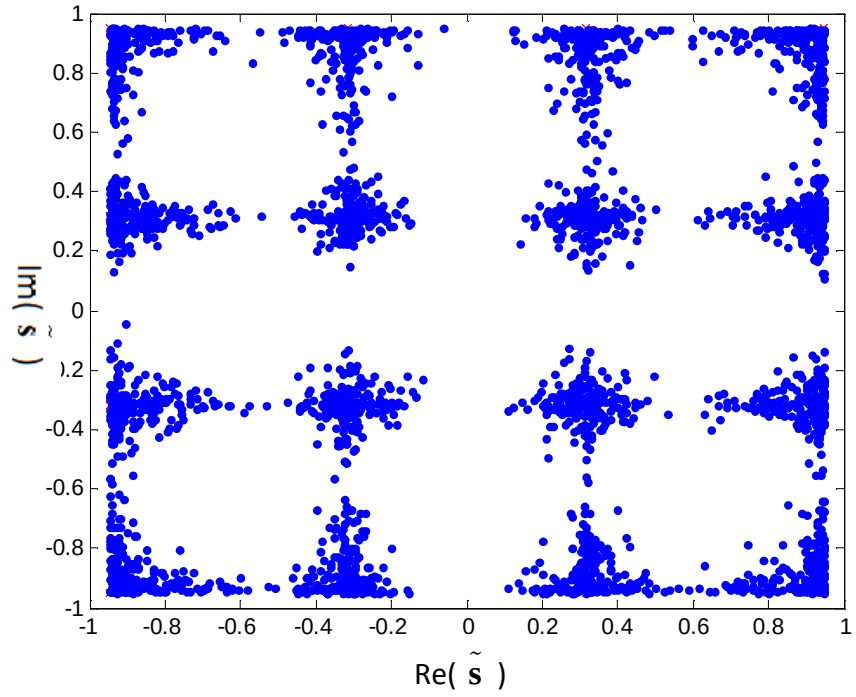

(a)

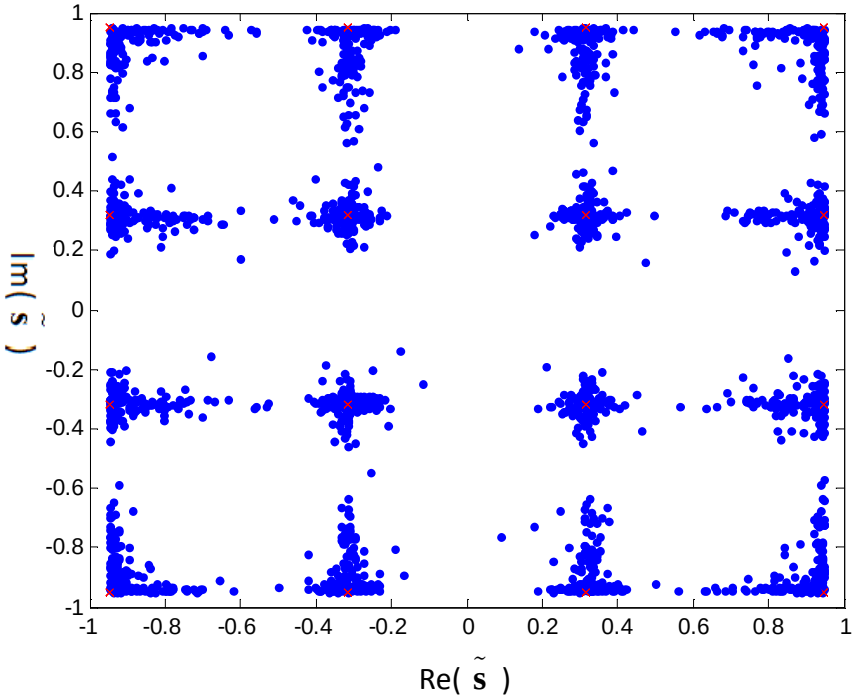

(b)

Figure 5.4: 16QAM constellation of soft symbols in error packets (a) SISO demapper EXT in (b) SISO decoder EXT

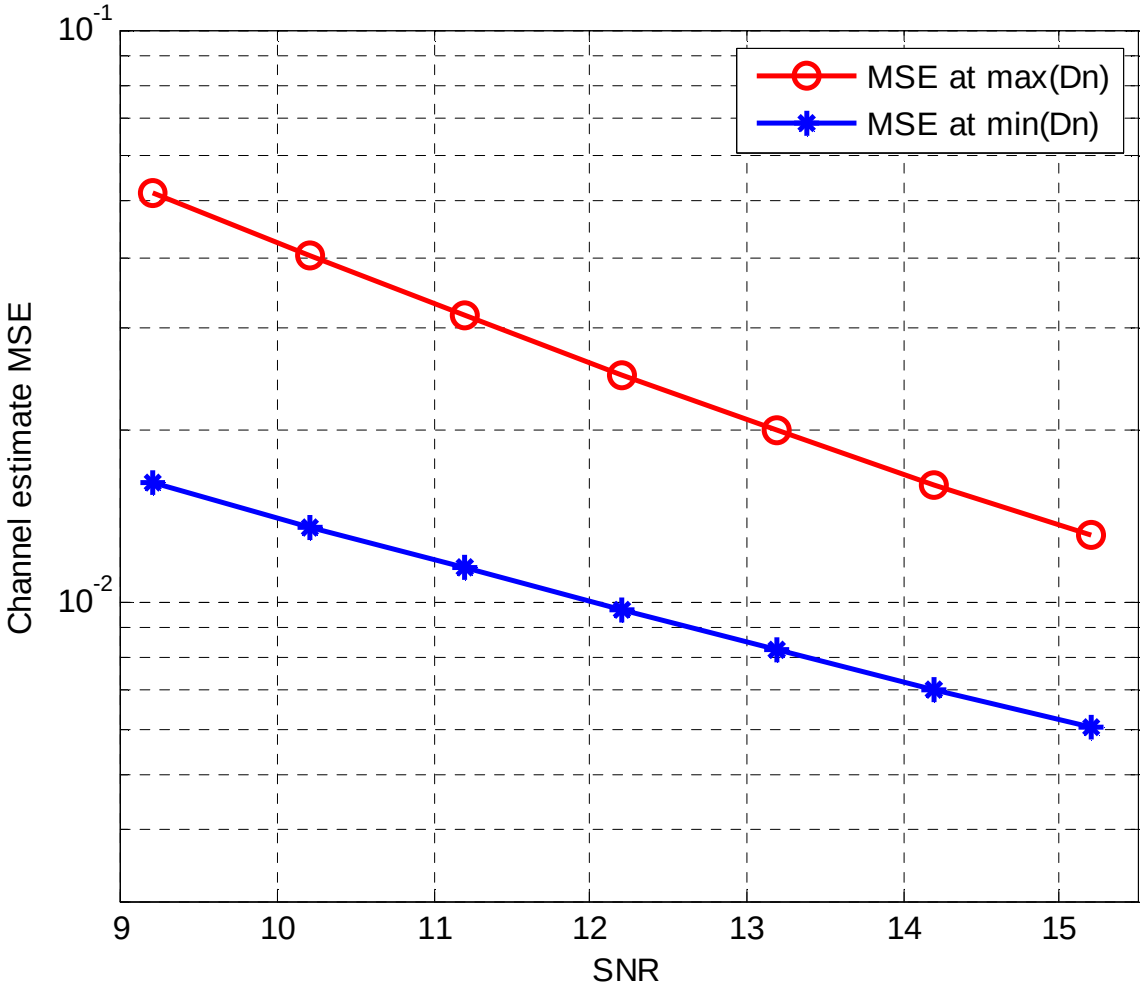

Figure 5.5: MSE analysis : channel estimate quality depending on min and max D_n

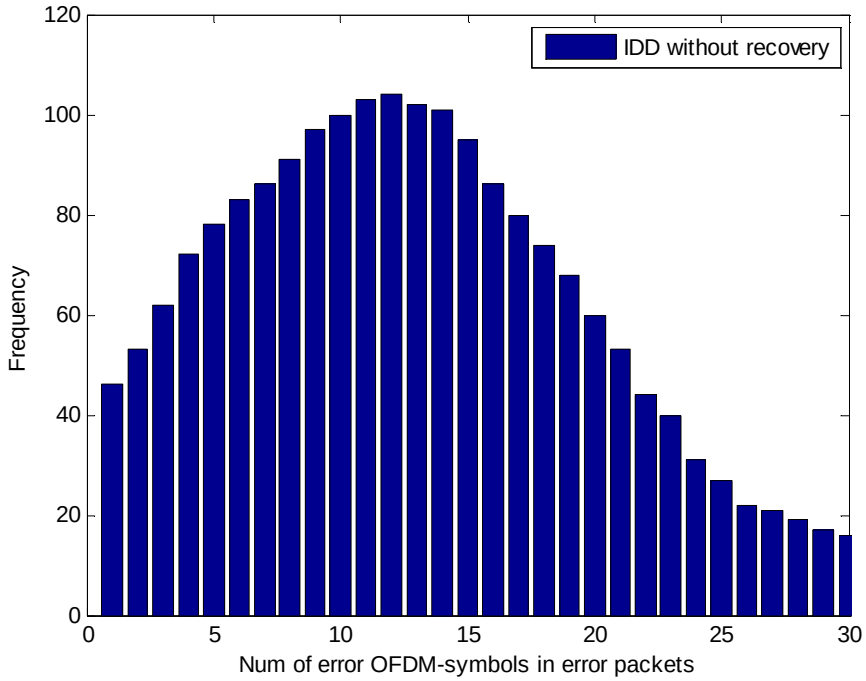

(a)

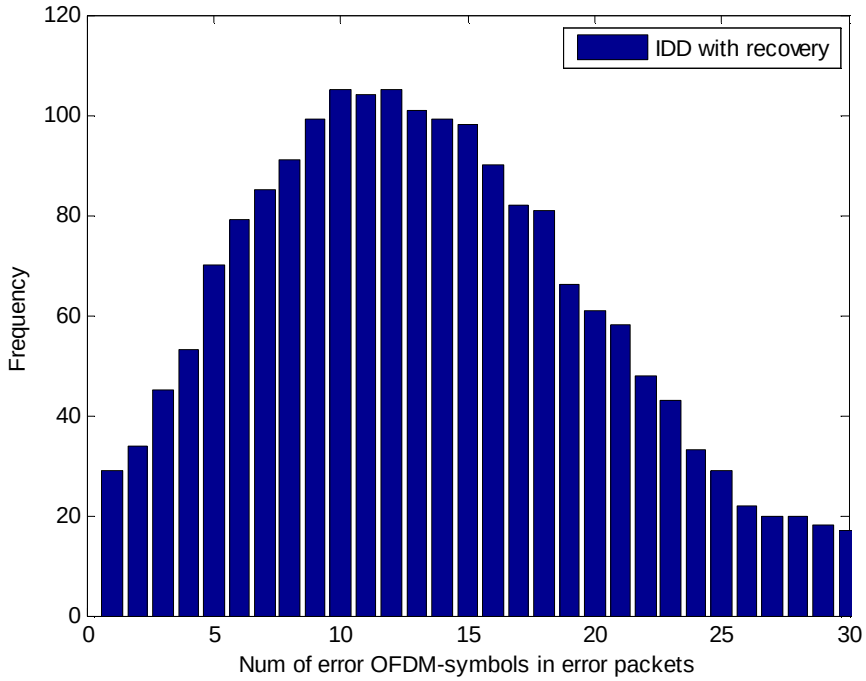

(b)

Figure 5.6: Histogram of the number of error OFDM-symbols in invalid packets (a) IDD without the recovery algorithm (b) IDD using the recovery algorithm

without applying the recovery scheme. Mostly, the number of error OFDM symbols are found around 12 error-symbols. Fig.(5.6)-(b) illustrates a histogram of the number of error OFDM symbols with the recovery scheme. Mostly, the number of error OFDM symbols are found around 12 error-symbols. Since the proposed algorithm captures and reprocess maximum 20 OFDM symbols, we can confirm that small numbers of error OFDM symbols (specifically $1 \sim 10$ error symbol range) are significantly reduced. It shows that 17% error packets are recovered in the $1 \sim 10$ error OFDM-symbols range. Fig. 5.7 compares PER performances. The default IDD iterations with the soft channel estimator makes 1.6dB SNR gain when compared with the IDD iteration case only using initial channel estimates at 10^{-2} PER level. The recovery scheme applies a limited number of IDD iterations to a part of OFDM symbols in a packet. When applying the recovery scheme, the proposed algorithm makes 0.2dB improvement from the default IDD iteration curve in Fig. 5.7.

5.6 Discussions

A error packet recovery scheme utilizing turbo equalization and iterative channel estimation has been proposed. Conventionally, transmitters rely on ECC or modulation techniques to improve channel throughput performance. The proposed algorithm is able to enhance the channel throughput utilizing the IDD iterations rather than the conventional methods. Since the IDD iteration is an important computation resource of a receiver, it does not simply apply many IDD iterations over packets. It selectively applies IDD iterations to potential erroneous OFDM symbols with updating channel estimates. We propose a novel scheme to monitor the soft-decision quality using the SISO demapper and the decoder extrinsic information. The error correction is performed within a limited IDD-iteration number. During the additional iterations, the channel estimates are updated using a whitening filter output to get the best Kalman filter performance. A significant merit of the proposed algorithm is that it can improve the receiving performance without extra aids from the transmitter

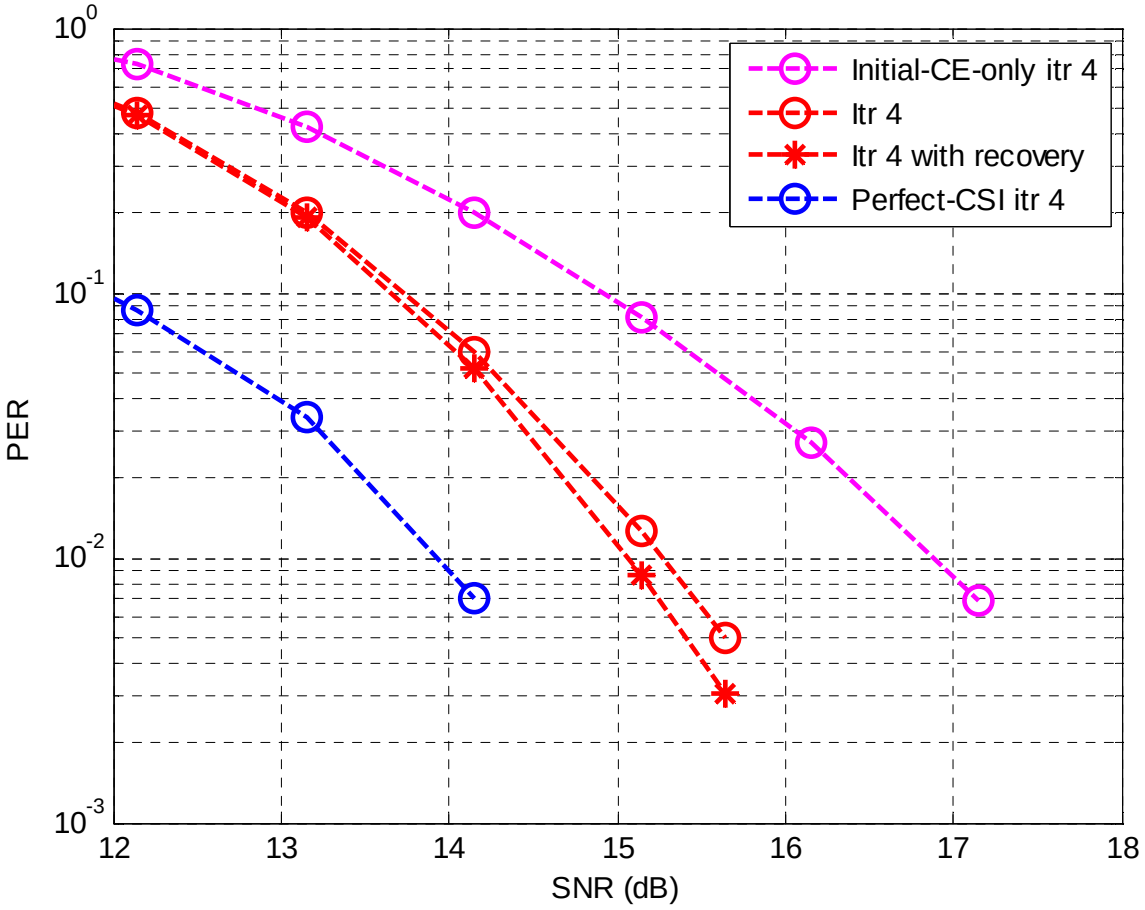

Figure 5.7: PER simulation with the recovery algorithm in the 2×2 MIMO-OFDM

or side information on channel and data. The proposed error monitoring method has been analyzed in term of mutual information and MSE analysis; also PER simulations have been used to validate the performance advantage of the proposed recovery algorithm.

Chapter 6

Conclusion and Future Work

6.1 Concluding Remarks

This thesis represents a study of the design of iterative channel estimators and a packet recovery algorithm for the SM-MIMO-OFDM communication system. This work is motivated by the fact that imperfect CSI degrades the MIMO receiver performance significantly, easily wiping out performance gains obtained via turbo equalization. We have proposed novel algorithms to recover the performance lost due to the imperfect CSI. Our main results can be summarized as follows:

- Statistical characteristics of soft decision errors and the channel estimation errors are analyzed, and their impacts to the iterative channel estimators are discussed. It is significant that decision errors from the turbo equalizer are correlated. The correlated errors can adversely impact optimality of the conventional Kalman-based estimation algorithms which use an innovation sequence input.

- An optimal Kalman-based iterative MIMO channel estimation algorithm has been proposed for the pipelined turbo equalizer. Since the decision error from the pipelined turbo equalizer is correlated, the puncturing process is used to innovate

the correlated error. The Kalman-based channel estimator has successfully been constructed based on the refined innovation sequence.

- A low-complexity Kalman-based channel estimator is proposed to reduce computational complexity of the optimum Kalman-based MIMO channel estimator. The complexity can be reduced using SIC resolving the MIMO channel outputs into single-input single-output channel outputs.

- A packet recovery algorithm using the turbo equalizer is proposed for reprocessing packets broken due to error propagation. The errorneous OFDM-symbols are detected and flagged by comparing EXT information in the turbo equalizer. Error recovery is performed by innovating on the CSI during additional IDD iterations.

We confirmed that the Kalman-based soft-decision-directed channel estimation algorithm effectively compensates performance loss due to imperfect CSI. The channel estimator interface with the pipelined turbo equalization is unique in that the estimator utilizes multiple feedback soft-decisions at a processing time. It effectively recovers the imperfect CSI loss using multiple soft-decisions, however, caution is required in setting up the Kalman-based channel estimation algorithm with the IDD decision feedback. Although both the IDD and the Kalman-based estimator are optimal, the combination of the two may not be optimal. We address constraints on the input sequence of the iterative Kalman-based estimator. The Innovation sequence is corrupted by correlation of the decision and estimator errors over time. Moreover the feedback soft-decisions have different levels of decision reliability at each IDD iteration, complicating the Kalman-filter design. To address this, the proposed algorithm evaluates the varying levels of reliability. For the Kalman-filter gain update, the combined noise and interface variance is calculated based on the reliability of the soft decision and the channel estimates. Also, we have introduced a novel method of innovating a correlated observation sequence via puncturing to deal with correlated errors that propagate in the pipelined turbo equalizer. The Kalman-based soft decision-directed

channel estimator has successfully been constructed based on the refined innovation sequence. The proposed channel estimator has shown impressive performance comparing to the conventional EM-based and Kalman-based algorithms.

In addition to the optimum form of the Kalman-based MIMO channel estimator, our research has included development of a practical algorithm. A low-complexity Kalman-based channel estimation algorithm adapted to turbo equalizers for MIMO-OFDM systems has been proposed. The proposed algorithm resolves the MIMO channel estimation problem into multiple SISO channel estimation problems using SIC. Although the computation load of the MIMO communication receiver can be reduced using SIC, residual interference significantly degrades the channel estimator performance due to soft-decision error or channel estimation error. The proposed channel estimator tracks the combined power of noise and residual interference due to potential cancellation errors in an effort to minimize the effect of error propagation. The scheme also utilizes the puncturing technique that rejects observation samples contaminated by correlated error at the SIC output. The proposed algorithm is well suited to the turbo receiver, providing robust performance with low computation loads.

If errors in the feedback decisions or noise in the observation samples exceed the tolerance of the DD-type estimators, the receiver inevitably declares an errorneous packet. In this case, the receiver requests retransmission of the packet; however, doing so increases network and transmitter channel throughput and power consumption loads. The proposed error recovery algorithm is able to enhance physical layer performance via IDD iterations. It selectively applies IDD iterations to potential erroneous OFDM symbols for error correction rather than simply iterating on broken packets again. In order to locate suspected errors, a novel scheme is proposed monitoring the soft-decision distance between the SISO demapper and the decoder extrinsic information. Error correction is performed within a limited number of IDD-iterations. During the additional iterations, the channel estimates are replaced with new CSI data buffered when decisions were reliable. A whitening filter is

incorporated to innovate the estimator input. The proposed algorithm has the demonstrated ability to improve receiving performance without extra aiding from externally provided statistical information on channel and data.

6.2 Future Research Directions

6.2.1 Detection algorithm to prevent error propagation

Error propagation remains a difficult problem in decision feedback estimation. When the decision error exceeds the tolerance level, the wrong decision feedback easily upsets the estimation process, causing the estimation outputs diverging. To address this, it is necessary to develop an accurate method of detecting the amount of propagated errors before the processing outputs diverge; the problem of assessing error propagation in DD feedback algorithms needs to be further investigated. In fact, error propagation is a chicken-and-egg problem between the decision error and the channel estimation error as illustrated in Fig.(6.1). An approach can be considered to measure the impact of propagated errors from both the IDD and channel estimator sides. In this thesis, we mainly sought to detect the error quantity and correlation characteristics from the IDD side. We have observed that the iterative channel estimator is particularly apt to be affected by biased error from IDD decisions. If the circulated error quantity and correlation can be monitored from both the IDD and channel estimator sides, this can be used to prevent the propagated errors. It is also possible for the MIMO detector to mitigate the error propagation based on the error propagation measurement. For example, the detector can try to subtract biased error estimates from the channel estimates, or a whitening filter approach can be explored to mitigate channel estimate error.

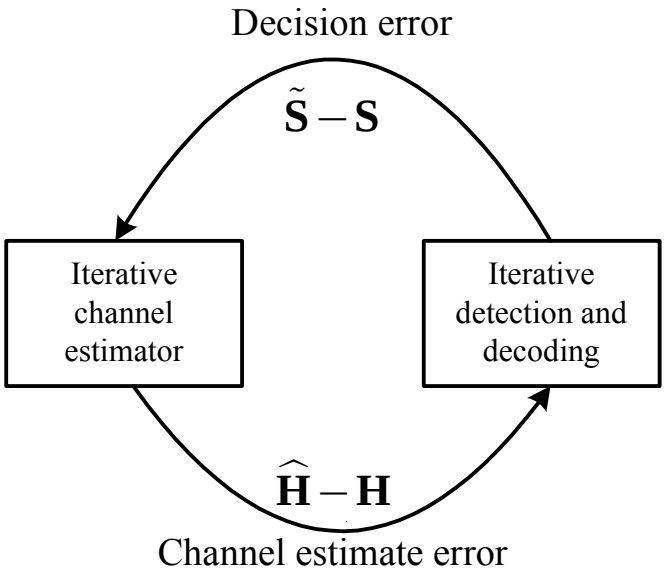

Figure 6.1: Conception diagram of error propagation problem in decision feedback estimation manners

6.2.2 Packet recovery algorithm using an inner ECC

We have discussed the error packet recovery algorithm using the turbo equalization in Chapter 5. Error packets can be recovered using the innovated channel estimates during additional IDD iterations. A strategy to maximize the effect of the additional iterations could be a valuable follow-on research topic. First, it is still challenging to locate accurate errors in a packet without error location codes. As a possible solution, the channel estimation error information at each frequency tone may prove useful for error location. For example, error-bit patterns dependent on the channel estimation error can be helpful for error correction in the MIMO detector, or bit-flipping similar to chase-decoding techniques can be applied based on analysis of channel estimation error.

In addition to error correction using channel estimation error analysis, an additional inner code can be inserted to the IDD to maximize the recovery performance. There are many published research results about CSI feedback from the RX to the TX, so we may assume that the receiver knows the deep channel fading information. Then, devising a

high code-rate inner code geared to channel fading may be effective in enhancing the turbo receiver performance, since the inner code can aid finding error location and boosting the IDD iteration power.

Bibliography

[1] G. Caire, G. Taricco, and E. Biglieri, "Bit-interleaved coded modulation," *IEEE Trans. Inform. Theory*, vol. 44, no. 3, pp. 927-946, May, 1998.

[2] A. Tonello, "Space-time bit-interleaved coded modulation with an iterative decoding strategy," *Proc. of IEEE Vehicular Technology Conference*, pp. 473-478, Boston, Sept., 2000.

[3] D. Park and B. Lee, "Design criteria and performance of space-frequency bit-interleaved coded modulations in frequencyselective Rayleigh fading channels," *Journal of Commun. and Networks*, vol. 5, no. 2, pp. 141-149, June, 2003.

[4] C. Douillard, M. Jezequel, C. Berrou, A. Picart, P. Didier, and A. Glavieux, "Iterative correction of intersymbol interference: Turbo-equalization," in *European Trans. Telecomm.*, vol. 6, pp. 507–511, September 1995.

[5] M. Tuchler, R. Otnes, and A. Schmidbauer, "Performance of soft iterative channel estimation in turbo equalizer," *Proc. IEEE ICC2002 Int. Conf.* vol. 3, pp. 1858-1862, New York, NY, Apr. 2002.

[6] R. Koetter, A. Singer, and M. Tuchler, "Turbo equalization : an iterative equalization and decoding technique for coded data transmission," *IEEE Signal Processing Mag.*, vol. 21, pp. 67-80, Jan. 2004.

[7] Y. Huang and J. Ritcey, "EXIT chart analysis of BICM-ID with imperfect channel state information," *IEEE Commun. Letters*, vol. 7, no. 9, pp. 434-436, Sept., 2003.

[8] Y. Huang and J. Ritcey, "16-QAM BICM-ID in fading channels with imperfect channel state information," *IEEE Trans. Wireless Commun.*, vol. 2, no. 5, pp. 1000-1007, Sept., 2003.

[9] Y. Li, N. Seshadri, and S. Ariyavisitakul, "Channel estimation for OFDM systems with transmitter diversity in mobile wireless channels," *IEEE J. Select Areas Commun.*, vol. 17, no. 3, pp. 461-471, Mar., 1999.

[10] Y. Li, L. Cimini, and N. Sollegberger, "Robust channels estimation for OFDM systems with rapid dispersive fading channels," *IEEE Trans. Commun.*, vol. 46, no. 7, pp. 902-915, Jul., 1998.

[11] Y. Li, "Simplified channel estimation for OFDM systems with multiple transmit antennas," *IEEE Trans. Wireless Commun.*, vol. 1, no. 1, pp. 67-75, Jan., 2002.

[12] X. Ma, L. Yang, and G. Giannakis, "Optimal training for MIMO frequency-selective fading channels," *IEEE Trans. Wireless Commun.*, vol. 4, no. 2, pp. 453-466, Mar., 2005.

[13] B. Hassibi and B. Hochwald, "Optimal training in space time systems," *Proc. 34th Asilomar Conf. on Signals, Systems and Computers*, pp. 743-747, Oct., 2000.

[14] X. Deng, A. Haimovich, and J. Garcia-Frias, "Decision directed iterative channel estimation for MIMO systems," *Proc. IEEE Int. Conf. Commun.*, vol. 4, pp. 2326-2329, Anchorage, AK, May, 2003.

[15] J. Gao and H. Liu, "Decision-directed estimation of MIMO time-varying Rayleigh fading channels," *IEEE Trans. Wireless Commun.*, vol. 4, no. 4, pp. 1412-1417, Jul., 2005.

[16] M. Loncar, R. Muller, J. Wehinger, and T. Abe, "Iterative joint detection, decoding, and channel estimation for dual antenna arrays in frequency selective fading," *Proc. Int. Symposium on Wireless Personal Multimedia Commun.*, Honolulu, HI, Oct., 2002.

[17] M. Sandell, C. Luschi, P. Strauch, and R. Yan, "Iterative channel estimation using soft decision feedback," *Proc. Globecom*, vol. 6, pp. 3728-3733, Sydney, Australia, Nov., 1998.

[18] M. Tuchler, A. Singer, and R. Koetter, "Minimum mean square error equalization using a prori information," *IEEE Trans. Signal Processing*, vol. 50, no. 3, pp. 673-683, Mar, 2002.

[19] X. Wautelet, C. Herzet, A. Dejonghe, J. Louveaux, and L. Vandendorpe, "Comparision of EM-based algorithms for MIMO channel estimation,"*IEEE Trans. Commun.*, vol. 55, no. 1, pp. 216-226, Jan., 2007.

[20] M. Kobayashi, J. Boutros, and G. Caire, "Successive interference cancellation with SISO decoding and EM channel estimation," *IEEE J. Select Areas Commun.*, vol. 19, no. 8, pp. 1450-1460, Aug., 2001.

[21] M. Khalighi and J. Boutros, "Semi-blind channel estimation using the EM algorithm in iterative MIMO APP detectors," *IEEE Wireless Commun.*, vol. 5, no. 11, pp. 3165-3173, Nov., 2006.

[22] S. Song, A. Singer, and K. Sung, "Soft input channel estimation for turbo equalization," *IEEE Trans. Sig. Processing*, vol. 52, no. 10, pp. 2885-2894, Oct., 2004.

[23] S. Song, A. Singer, and K. Sung, "Turbo equalization with unknown channel," *in Proc. IEEE Int. Conf. Acoustics, Speech, and Sig. Processing ICASSP*, vol. 3, pp. 2805-2808, Orlando, FL, May 2002.

[24] S. Abbasfar, "Turbo-like codes; design for high speed decoding," Springer, Netherlands, 2007.

[25] G. Strang, "Introduction to linear algebra," 3rd edition, Wellesley, MA, Wellesley-Cambridge press, 2003.

[26] S. Lee, N. Shanbhag, and A. Singer, "Area-efficient high-throughput VLSI architecture for MAP-based turbo equalizer," *Proc. IEEE signal procssing system: design and implementation* pp. 87-92, Aug. 2003, Seoul, Korea.

[27] *IEEE P802.11n/D1.0 : Draft Amendment to STANDARD FOR 2 Information Technology-Telecommunications and 3 information exchange between systems-Local and 4 Metropolitan networks-Specific requirements-Part 5 11: Wireless LAN Medium Access Control (MAC) 6 and Physical Layer (PHY) specifications: 7 Enhancements for Higher Throughput*.

[28] H. Stark and J. Woods, "Probability and random processes with applications to signal processing," USR, NJ, Prentice-Hall, 2002.

[29] S. Brink, "Designing iterative decoding schemes with the extrinsic information transfer chart," *Int. J. Electron. Commun.*, vol. 54, No. 6, pp. 389-398, Nov. 2000.

[30] J. Hagenauer and P. Hoeher, "A Viterbi Algorithm with Soft-Decision Outputs and its Applications," *Globecom 1989*, vol. 3, pp. 1680-1686, Dallas,TX, Nov., 1989

[31] S. Kay, "Fundamentals of statistical signal processing-estimation theory," Englewood Cliffs, NJ, Prentice-Hall, 1993.

[32] J. Proakis "Digital communication," 4rd edition, New York, NY, McGraw Hill, 2000.

[33] D. Yoon and J. Moon, "Soft-decision-driven estimator for pipelined turbo receivers," accepted in *IEEE Trans. Commun.*.

[34] D. Yoon and J. Moon, "Soft-decision-directed MIMO channel estimation geared to pipelined turbo receiver Architecture," *Proc. IEEE Int. Conf. Commun.*, Cape Town, South Africa, May, 2010.

[35] W. Choi, K. Cheong, and J. Cioffi, "Iterative soft interference cancellation for multiple antenna systems," *IEEE Wireless Commun. and Networking Conf.*, Chicago, Illinois, Sept., 2000.

[36] D. Yoon and J. Moon, "Low-Complexity Iterative Channel Estimation for Turbo Receivers,"submitted to *IEEE Trans. Commun. letter*.

[37] X. Dong and P. Varaiya, "Saturation Throughput Analysis of IEEE 802.11 Wireless LANs for a Lossy Channel," *IEEE Trans. Commun. letter*, vol. 9, no. 2, Feb., 2005.

[38] P. Wu and N. Jindal, "Coding Versus ARQ in Fading Channels: How reliable should the PHY be?" *Proc. IEEE Globecom* Honolulu, Hawaii, USA, 2009

[39] D. Baron, S. Sarvotham, and R. Baraniuk, "Coding vs. Packet Retransmission over Noisy Channels" *Proc. IEEE ISSC*, Princeton, New Jersey, USA, 2006

[40] G. Woo, P. Kheradpour, D. Shen, and D. Katabi, "Beyond the Bits: Cooperative Packet Recovery Using Physical Layer Information" *AMC Mobicom* Montreal, Canada, May, 2007.

[41] J. Barry, E. Lee, and D. Messerschmitt "Digital communication," 3rd edition, Norwell, MA, Kluwer Publishers, 2003.